大規模アンサンブルシミュレーションに基づく気候変動の不確実性を考慮した洪水リスクの評価

Muroran IT

Muroran Institute of Technology

DISSERTATION

Flood risk assessment considering uncertainty in climate change impacts using large-ensemble simulations

Nguyen Thanh Thu

FLOOD RISK ASSESSMENT CONSIDERING UNCERTAINTY IN CLIMATE CHANGE IMPACTS USING LARGE-ENSEMBLE SIMULATIONS

by

Nguyen Thanh Thu

A dissertation submitted in partial fulfillment of the requirements for the degree of Doctor of Engineering

Examination Committee: Prof. Makoto Nakatsugawa
Prof. Katsutoshi Kimura
Prof. Mikiharu Arimura

Muroran Institute of Technology
Division of Sustainable and Environmental Engineering
Japan

September 2021

Acknowledgements

This is my third cherry blossom season in the beautiful country, Japan. During three years, I had a great chance to meet friendly Japanese friends and explore Japanese culture and traditions. It was the most memorable time for me. Besides, I also learned a lot of valuable specialized knowledge. Now, I am so proud that the difficult research path has reached the final stage. I can look back on my study process, and write this dissertation book. It is my pleasure to acknowledge the roles of several individuals who supported me too much for the completion of my Ph.D. research.

At first, the most appreciation I would like to send to my supervisor, Professor. Makoto Nakatsugawa, for his excellent guidance, caring, patience, motivation, passion, and providing me with a great study environment for doing research. I could never finish my research without his kind direction and proper guidance.

I am also grateful to Associate Professor. Tomohito. J. Yamada, and Dr. Tsuyoshi Hoshino who provide important data to me, support me too much during three years of research, and have given helpful advice about my major. Without this precious support, it would not be possible to complete this research.

I would like to express my respect and great thank to Professor. Katsutoshi Kimura, and Professor. Mikiharu Arimura for their support and attendance as a member of the examination committee. Their insightful comments and constructive suggestions have helped me to improve the quality of my research.

I would like to express my special thank to Dr. Takehiro Oki, who support me too much, and encourages me to do my research. His patience, motivation, and encouragement helped me successfully carried out this assignment.

My sincere thanks to the laboratory members, who help me too much not only in my research but also in all the difficult things I faced when I have lived in Japan for three years. Especially thanks to Ms. Sakamoto Riko, Mr. Sakuma Kanzu, Mr. Junya Seki, and Mr. Tanaka Masato for their great kind support, and take care of me during my Ph.D. course.

Sincere gratitude is extended to the Japanese Government for providing the scholarship for my Ph.D. course. I would like to offer my special thank to the International Center for Relation of Muroran Institute of Technology for their great support while I am living in Japan.

I would like to offer my special thanks to my friend Dr. Try Sophal, who always helped me too much in my research, as well as gave me a lot of useful advice for my research. Without his kind support, this study would face many challenges. I will always remember his kindness and support.

I greatly appreciate my friends Mr. Doan Hoa Khiem, Mr. Le Manh Tien, Mr. Tran Nguyen Luong, who helps me too much when I have trouble with my research for three years. Besides, I greatly appreciate Dr. Pham Quang Vuong, Mr. Le Huy Sinh, Mr. Ta Quy Hung, Ms. Tanya, and other Vietnamese friends, who always help me too much and share even joy or stress when I live alone in Japan for three years.

Last but not least, I would like to send my special thank to my soulmate, who always beside me and support me too much, and willing to share every moment, stress, and happiness every day. Thank you too much for everything. One of the key factors that encourage me too much during my research, I would like to express my special thanks to my family. Although my family lives in Vietnam, I always feel that my family beside me. I am deeply grateful to my parents, my brother, my sister-in-law, my nephew, my niece for their encouragement all time. All of this work is for them. I think I would never have been able to finish my Ph.D. research without their support and encouragement.

Muroran, 2021
Nguyen Thanh Thu

Abstract

In recent decades, extreme weather events associated with climate changes have rapidly become one of the global concerns threatening natural environments and human life. Floods are the most frequent type of natural disaster on earth, causing massive damage all over the world. Flood disaster is considered to become more frequent and higher intensity in the future. In particular, people who live in floodplain areas, or lack early flood warning systems are the most affected by flooding. In Japan, flood inundation disasters due to short-term extreme rainfall have occurred frequently and caused considerable damage in recent years. Notable severe flood events in recent years in Japan can be mentioned as the large-scale flood event in August 2016 in Hokkaido, or severe flooding and landslides occurred in many river basins in central-northern parts of Japan in October 2019, causing great loss of life and property.

The northernmost Japanese island, Hokkaido has recorded severe floods and caused massive damage, such as the flood event in August 1981, and recently in August 2016. The Ishikari River basin plays a vital role in the socio-economic development of Hokkaido. The Ishikari Plain occupies most of the basin's area and is located around the central and downstream basin area, which is the most productive agricultural area not only in Hokkaido, but also entire Japan.

Therefore, this study aims to investigate the change in extreme rainfall and severe floods associated with climate change, choosing the Ishikari River basin, Hokkaido, Japan as a case study. Change in extreme rainfall and river floods in the Ishikari River basin, as well as in its main sub-basins is evaluated using the Integrated Flood Analysis System (IFAS) coupled with the large-ensemble rainfall dataset with a super high-resolution of 5 km as an input data to the model. In addition, change in flood inundation in the Chitose River basin, a tributary of the Ishikari River is also evaluated using the Rainfall–Runoff–Inundation (RRI) model and a large-ensemble rainfall dataset of 5 km (d4PDF). Owing to the topographical characteristics of its low-lying area, the Chitose River basin is frequent affected by backwater from the Ishikari River and experiences severe flood inundation. The remarkable point of this study is to use the large-ensemble and super high-resolution climate simulations for extreme rainfall and severe floods assessment. It could predict extreme rainfall and severe flood events with return periods equal to or larger than 100 years. Simulation with large ensemble members could properly verify the uncertainty in the estimation of the probability of extreme events. The results of this study are expected to provide useful information for river basin management, particularly for climate change adaptation and flood damage mitigation in floodplain areas.

概要

この数十年で、気候変動による異常気象とそれに起因する自然災害は、自然環境や私たちの生活に対する脅威の一つとして急速に関心を集めるようになった。こうした自然災害の中でも、洪水は世界的に頻発しており、世界各地で甚大な被害を引き起こしている。さらに、洪水による災害は、将来的により頻繁に発生し、より深刻な被害を発生させると考えられている。特に河川の氾濫原の住民や、早期の洪水警報システムが整備されていない地域で生活している人々は、洪水による影響を最も大きく受ける。日本では、近年、短時間での極端豪雨による洪水氾濫が頻発し、大きな被害をもたらしている。顕著な例として、2016 年 8 月には北海道で大規模な洪水が発生した。また 2019 年 10 月には日本の中部から東北地方にかけて多数の河川で深刻な洪水と地すべりが発生した。これらの被害により、尊い人命と資産が失われた。

日本の北端に位置する北海道では、過去には 1981 年 8 月、近年では 2016 年 8 月の洪水において、石狩川流域は甚大な被害を受けた。石狩川流域内は石狩平野が大部分を占め、その中流域から下流域にかけては北海道のみならず全国で最も生産性の高い農業地域となっていることから、北海道の社会経済的発展に重要な役割を果たしている。そのため、本研究では、北海道の石狩川流域を対象とし、気候変動による極端豪雨の降雨量の変化と、それに伴い大規模洪水を引き起こす河川流量の変化を推定することを目的としている。石狩川流域とその主要な支川における不確実性を考慮した極端豪雨のデータとして水平解像度 5km の大量アンサンブル降雨情報(d4PDF)を用いた。また、石狩川とその主要支川の河川流量の推定には統合洪水解析システム(IFAS)を用いた。さらに、千歳川流域の洪水氾濫の変化についても、d4PDF と降雨-流出-氾濫モデル(RRI)を用いることで、石狩川からの背水影響を考慮した氾濫計算を行った。本研究では、豪雨と洪水の評価に高解像度の大規模アンサンブル気候シミュレーションを使用したことが特徴である。これは、100 年に一度以上の低頻度で生起する極端豪雨と、それによって発生する深刻な洪水を予測することができる。さらに、大規模アンサンブル気候シミュレーションを用いることにより、極端豪雨時の降雨の不確実性を適切に評価することができる。

本研究において判明した結果は、河川流域管理、特に氾濫原における洪水被害の軽減といった気候変動への適応策に役立てることが期待される。

Contents

Title	Page
Acknowledgements………………………………………………………………..	i
Abstract…………………………………………………………………………	iii
Abstract (Japanese)……………………………………………………………..	iv
Contents………………………………………………………………………....	v
List of Figures…………………………………………………………………..	viii
List of Tables……………………………………………………………………	xii
List of Abbreviations……………………………………………………………	xiii

CHAPTER 1

Introduction…………………………………………………………………	1
1.1. Overview……………………………………………………………….	1
1.2. Purposes and objectives of the research…………………………………..	10
1.3. Thesis outline…………………………………………………………..	11
1.4. References……………………………………………………………....	14

CHAPTER 2

Uncertainty of rainfall patterns………………………………………………	18
2.1. Introduction……………………………………………………………...	18
2.2. Overview of database for Policy Decision making for Future climate change (d4PDF)………………………………………………………………	23
2.3. Summary………………………………………………………………....	27
2.4. References………………………………………………………………	28

CHAPTER 3

Assessing climate change impacts on extreme rainfall and severe flooding in the Ishikari River basin, Japan……………………………………………….	32
3.1. Introduction……………………………………………………………...	32
3.2. Methodology…………………………………………………………….	34
3.2.1. Overview of the Ishikari River basin………………………………….	34
3.2.2. d4PDF dataset………………………………………………………	36
3.2.3. Overview of the Integrated Flood Analysis System (IFAS) model……	38
3.2.4. Data inputs………………………………………………………….	43

Title	Page

3.2.5. Analytical procedure…………………………………………………….. 44
3.3. Results and Discussions………………………………………………………… 46
3.3.1. Hydrological model calibration and validation……………………….. 46
3.3.2. Future changes in extreme rainfall……………………………………. 49
3.3.3 Future changes in extreme rainfall between the top 20 and top 36 rainfall events………………………………………………………………………… 50
3.3.4. Future changes in severe river floods between the top 20 and top 36 rainfall events…………………………………………………………………… 56
3.3.5. Time difference prediction…………………………………………… 60
3.4. Conclusions…………………………………………………………………... 61
3.5. References…………………………………………………………………… 62

CHAPTER 4

Flood inundation assessment in the low-lying river basin considering extreme rainfall impacts and topographic vulnerability…………………… 67
4.1. Introduction…………………………………………………………………... 67
4.2. Materials and Methods……………………………………………………….. 71
4.2.1. Description of the study area…………………………………………. 71
4.2.2. d4PDF dataset………………………………………………………… 73
4.2.3. Overview of the Rainfall-Runoff-Inundation (RRI) model…………… 74
4.2.4. Data inputs…………………………………………………………….. 78
4.2.5. Analytical procedure…………………………………………………... 85
4.3. Results and Discussions………………………………………………………. 87
4.3.1. RRI model calibration and validation…………………………………. 87
4.3.2. Evaluation of climate change impacts on river flood in the Ishikari River basin………………………………………………………………………… 90
4.3.3. Evaluation of climate change impacts on flood inundation in the Chitose River basin…………………………………………………………... 91
4.3.4. Evaluation of time difference impacts on flood inundation in the Chitose River basin………………………………………………………….. 97
4.3.5. Discussions……………………………………………………………. 98
4.4. Conclusions…………………………………………………………………... 100
4.5. References…………………………………………………………………… 102

Title **Page**

CHAPTER 5

Conclusions and Suggestions………………………………………………………. 107

5.1. Introduction…………………………………………………………………... 107

5.2. Summarize of the study findings……………………………………….. 107

5.3. Proposing flood mitigation measures……………………………………… 109

5.4. Suggestions for future researches………………………………………. 113

Appendix………………………………………………………………………. 114

Published works…………………………………………………………... 114

List of Figures

List **Page**

Figure 1.1 Annual global average temperature from 1891 to 2017…………….. 1
Figure 1.2. Annual precipitation (over land area only) from 1901 to 2017 for the globe………………………………………………………………………. 2
Figure 1.3 Change in (a) globe average surface temperature and (b) globe average precipitation for 2081-2100 relative to 1986-2005 under the RCP 2.6 scenarios (left) and RCP 8.5 scenarios (right)………………………………. 3
Figure 1.4 The city of Hitoyoshi, Kumamoto Prefecture, is seen flooded in July, 2020 after the Kuma River overflowed due to torrential rainfall………………. 4
Figure 1.5 People using kayaks and paddle boards navigate a residential neighbourhood inundated with floodwaters as severe flooding affects the suburb of McGraths Hill in Sydney, Australia, March 24, 2021………………. 5
Figure 1.6 A flooded slum in Manila in August, 2012………………………….. 5
Figure 1.7 Annual surface temperature over Japan…………………………….. 6
Figure 1.8 Annual number of days with (a) precipitation ≥ 100 mm, and (b) precipitation ≥ 200 mm from 1901 to 2017…………………………………….. 7
Figure 1.9 Severe flood events in (a) August 2016 in Hokkaido, and (b) July 2018 in western Japan……………………………………………………….. 8
Figure 1.10 Climate change adaptation cycle………………………………….. 10
Figure 1.11 Research outline…………………………………………………… 14
Figure 2.1 Global mean temperature anomalies (°F) relative to 1976-2005 for four RCP scenarios, 2.6 (green), 4.5 (yellow), 6.0 (orange), and 8.5 (red)..……. 19
Figure 2.2 Coarse data from Global Climate Models (GCMs) forms the initial and boundary conditions necessary for Regional Climate Models (RCMs) to dynamically downscale to much finer resolution climate data………………….. 22
Figure 2.3 A schematic view of these research activities form an interdisciplinary community on global warming research……………………… 24
Figure 2.4 Descreption of d4PDF………………………………………………. 25
Figure 2.5 Experimental design of d4PDF……………………………………… 26
Figure 3.1 Ishikari River basin, Hokkaido, Japan and its main sub-basins…….. 35

List **Page**

Figure 3.2 +4K future climate simulation for the Tokachi River basin at Obihiro point station with the rainfall data of 20-km resolution (left) and 5-km resolution (right)………………………………………………………………………… 38
Figure 3.3 Functions of IFAS model……………………………………………. 39
Figure 3.4 Schematic of the IFAS model………………………………………. 41
Figure 3.5 Applicable/Outside the scope Phenomenon for IFAS……………….. 42
Figure 3.6 Flowchart of the procedure for flood simulation by the IFAS model… 43
Figure 3.7 Elevation data and Land-use data…………………………………… 44
Figure 3.8 Comparison of observed and simulated discharges at Ishikari Ohashi station for the (a) 1981 flood event, (b) 2001 flood event, (c) 2011 flood event, (d) 2016 flood event………………………………………………………… 48
Figure 3.9 Relative frequency of annual maximum rainfall (mm/ 72h) in the Ishikari River basin for the observed rainfall data, and the historical and future simulations……………………………………………………………...... 50
Figure 3.10 Boxplots of annual maximum rainfall (mm/ 72h) for the top 20 and top 36 rainfall events in the Ishikari River basin and in its main sub-basins…… 53
Figure 3.11 Percentage difference in the median of annual maximum rainfall (mm/ 72h) between the top 20 and top 36 rainfall events……………………… 54
Figure 3.12 Spatial distribution of annual maximum rainfall (mm/ 72h) averaged for the (a) top 20 rainfall events and (b) top 36 rainfall events; (c) percentage difference between the selected historical and future events………. 55
Figure 3.13 Boxplots of the peak runoff depth (mm/h) for the top 20 and top 36 rainfall events in the Ishikari River basin and in its main sub-basins………….. 58
Figure 3.14 Percentage difference in the median of peak runoff depth between the top 20 and top 36 rainfall events in the Ishikari River basin and in its main sub-basins………………………………………………………………………. 59
Figure 3.15 Time differnce averaged for the top 20 and top 36 rainfall events in each of the sub-basin……………………………………………………………. 60
Figure 4.1. Locations of the Ishikari River basin and Chitose River basin…….. 72

List **Page**

Figure 4.2. Severe flood inundation event in August 1981 in the Chitose River basin. Data source: Hokkaido Regional Development Bureau…………………. 73

Figure 4.3. Schematic of the rainfall-runoff-inundation (RRI) model………….. 78

Figure 4.4 Topographic data as inputs for the RRI model…………………….. 80

Figure 4.5 Land cover classification in the Ishikari River basin for (a) original Global Land Cover Characterization, and (b) reclassified land cover types……… 82

Figure 4.6 Plot of river width and river depth with contributing area for the Ishikari River basin………………………………………………………… 84

Figure 4.7 Plot of river width and river depth with contributing area for the Chitose River basin………………………………………………………… 84

Figure 4.8 Plot of river width and river depth future plan with contributing area for the Ishikari River basin…………………………………………………… 84

Figure 4.9 Comparison between the simulated and observed discharges at Ishikari Ohashi station for (a) the August 1981 flood event, (b) the September 2001 flood event, (c) the September 2011 flood event, and (d) the August 2016 flood event…………………………………………………………………… 88

Figure 4.10 Comparison between the simulated and observed inundation areas for the flood event of August 1981 in the Chitose River basin………………… 90

Figure 4.11 Inundation area averaged for the top 20 rainfall events (historical simulation) and top 36 rainfall events (future simulation) with (a) inundation depth ≥0.5 m, and (b) inundation depth ≥3.0 m……………………………… 92

Figure 4.12 Boxplots of (a) peak inundation depths, (b) inundation volumes with inundation depth ≥0.5 m, and (c) inundation volumes with inundation depth ≥3.0 m for the top 20 past and top 36 future rainfall events in the Chitose River basin……………………………………………………………………… 93

Figure 4.13. Spatial distribution of the inundation frequency averaged for (a) the top 20 rainfall events (historical simulation), (b) the top 36 rainfall events (future simulation), and (c) inundation frequency difference between the top 20 past and top 36 future rainfall events…………………………………………… 95

List **Page**

Figure 4.14. Spatial distribution of inundation durations averaged for (a) the top 20 rainfall events (historical simulation), (b) the top 36 rainfall events (future simulation), and (c) inundation duration differences between the top 20 past and top 36 future rainfall events……………………………………………………….. 96
Figure 4.15. Relative frequency of time difference in the Chitose River basin for the top 20 rainfall events (historical simulation) and top 36 rainfall events (future simulation)………………………………………………………………… 98
Figure 5.1. Land treatment for agricultural areas………………………………. 110
Figure 5.2. Structural measures for mitigation flood damage in public works combined to urban landscape…………………………………………………… 111
Figure 5.3. Dams in Hokkaido island………………………………………….. 112

List of Tables

List **Page**

Table 2.1 RCP scenarios description (Source: IPCC Fifth Assessment Report Summary for Policymakers)………………………………………………… 19
Table 2.2 18 Global climate models (GCMs)……………………………….. 20
Table 3.1 Characteristics of the Ishikari River basin and its main sub-basins and reference hydrological stations in each sub-basin……………………………… 36
Table 3.2. Model configuration……………………………………………… 41
Table 3.3. Parameter value settings in the IFAS model………………………… 47
Table 3.4 Performance of the IFAS model in the Ishikari River basin…………. 49
Table 3.5. Top 20 rainfall events in the Ishikari River basin and in its main sub-basins……………………………………………………………………… 51
Table 3.6 Top 36 rainfall events in the Ishikari River basin and in its main sub-basins……………………………………………………………………… 52
Table 3.7 Peak discharge results for the top 20 rainfall events in the Ishikari River basin and in its main sub-basins…………………………………………. 56
Table 3.8 Peak discharge results for the top 36 rainfall events in the Ishikari River basin and in its main sub-basins…………………………………………. 57
Table 4.1 Optimal parameter settings of the RRI model……………………….. 88
Table 4.2 Statistical indicators of the RRI model performance………………… 89
Table 4.3. Percentage difference of the mean values of the inundation area and inundation volume for inundation depths of ≥0.5 and ≥3.0 m between the top 20 rainfall events (historical simulation) and top 36 rainfall events (future simulation)……………………………………………………………… 92

List of Abbreviations

IPCC	Intergovernmental Panel on Climate Change
RCP	Representative Concentration Pathway
IFAS	Integrated Flood Analysis System
d4PDF	Database for Policy Decision making for Future Climate Change
RRI	Rainfall-Runoff-Inundation
CMIP5	Coupled Model Intercomparison Project Phase 5
GCMs	Global Climate Models
RCMs	Regional Climate Models
SST	Sea-surface temperature
SIC	Sea-ice concentration
NHRCM	Meteorological Research Institute Nonhydrostatic Regional Climate Model
AR4	Fourth assessment report
CMIP3	Coupled Model Intercomparison Project Phase 3
WHO	World Health Organization
ICHARM	International Centre for Water Hazard and Risk Management
PWRI	Public Works Research Institute
DHM	Distributed hydrological model
GUI	Graphical user interface
GTOPO30	Global digital elevation model
GLCC	Global land cover characterization
USGS	United States Geological Survey
MLIT	Ministry of Land, Infrastructure and Transport
DEM	Digital elevation model
DIR	Flow direction
ACC	Flow accumulation
SRTM	Shuttle Radar Topography Mission
HRDB	Hokkaido Regional Development Bureau
IFD	Inundation frequency difference
AGCM	Atmospheric general circulation model

Chapter 1

Introduction

Chapter 1

1.1 Overview

In the world:

In recent decades, human influence on the climate system is clear, and recent anthropogenic emissions of greenhouse gases are the highest in history. As a result, the atmosphere and ocean have warmed, which results in the amount of snow and ice have diminished, the sea level has risen, and the occurrence of some climate extremes. Since the 1950s, many observed changes are unprecedented over decades to millennia [1]. Extreme weather events have occurred frequently threatening the natural environment and human life in recent years. According to the IPCC Fifth Assessment Report [2], on a longer time scale, the global average surface temperature increased by 0.73°C per century. Figure 1.1 shows the annual global average temperature from 1891 to 2017. The annual global average surface temperature in 2017 was increased by 0.38°C compared to the 1981-2010 average, and the third-highest since 1891 [3].

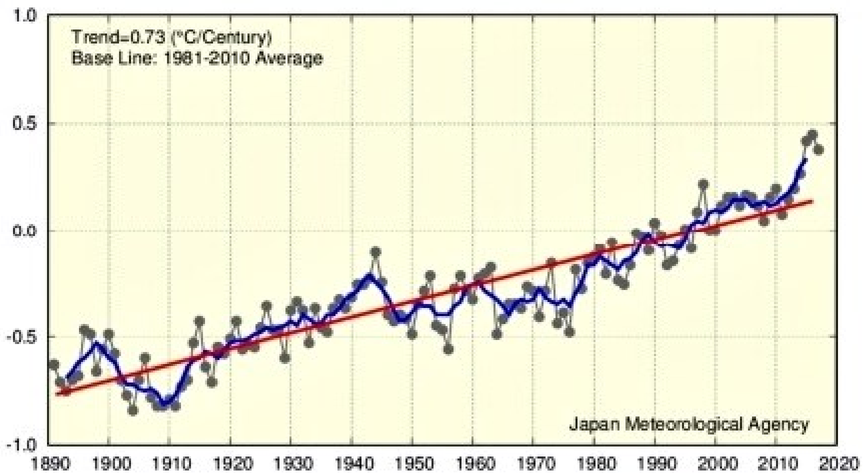

Figure 1.1. Annual global average temperature from 1891 to 2017 [3]

In addition, precipitation is one of the most critical and useful indicators reflecting changes in climate conditions [4]. Among many factors, precipitation is the main factor affecting runoff formation and flow regimes [4, 5]. According to the IPCC Fifth Assessment Report (2013 [2], precipitation is also predicted to increase significantly in the future, especially extreme rainfall. According to the Japan Meteorological Agency (2017) [3], annual precipitation (for land areas only) in 2017 was risen 49 mm compared to the 1981-2010 average (Figure 1.2). Long-term trends are not analyzed because the precipitation data for sea areas are not available [3].

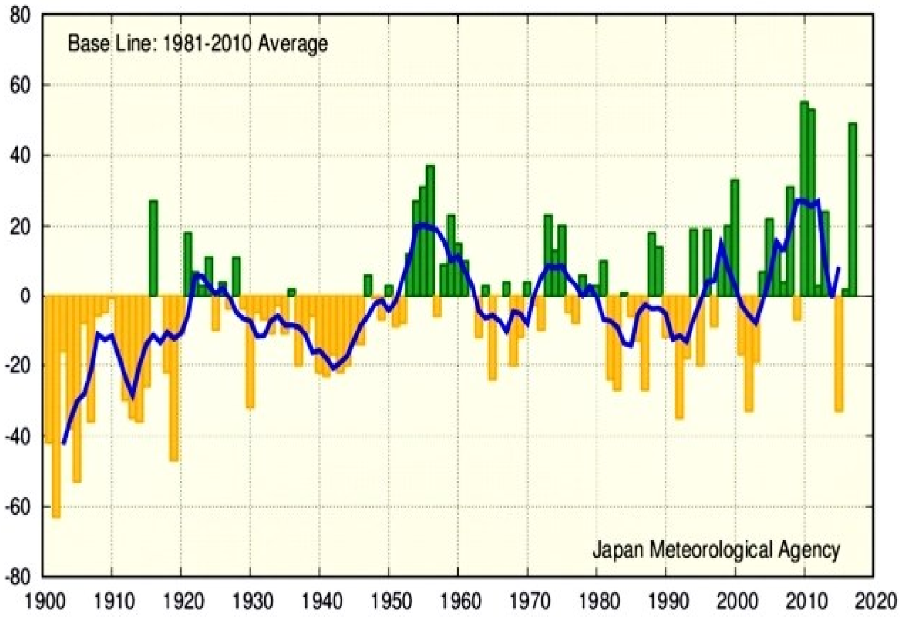

Figure 1.2. Annual precipitation (over land area only) from 1901 to 2017 for the globe [3]

Figure 1.3 shows the change in global average surface temperature and global average precipitation for 2081-2100 relative to 1986-2005 under the Representative Concentration Pathway (RCP) RCP 2.6 and RCP 8.5 was evaluated [1]. It can be clearly seen that, the average surface temperature and average precipitation is projected to increase remarkable in the future.

(a)

(b)

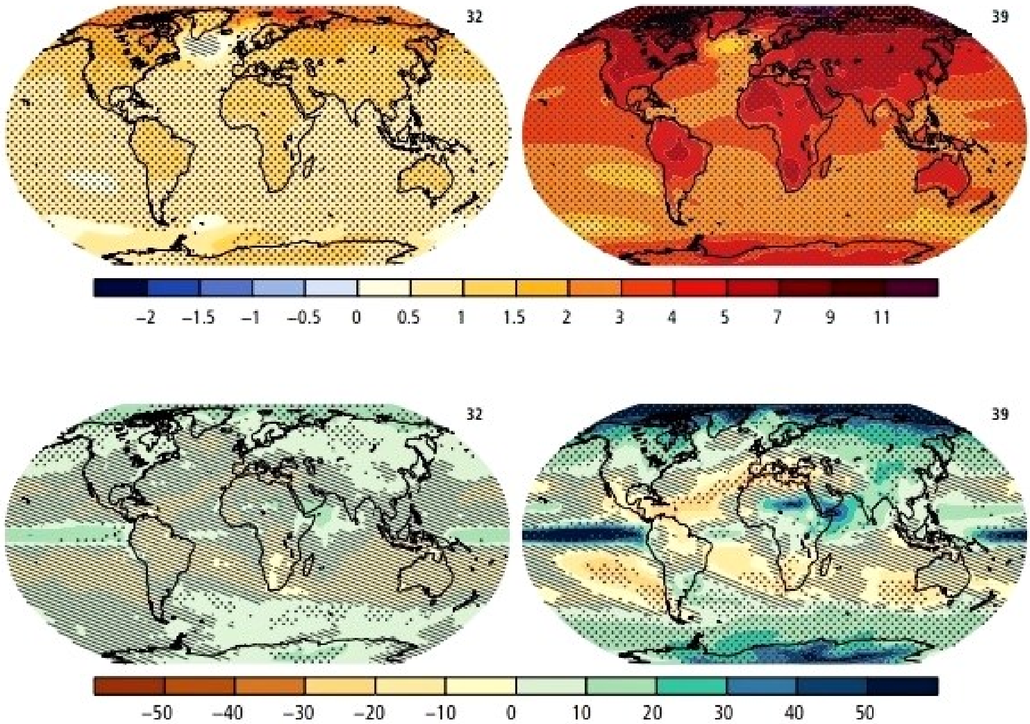

Figure 1.3. Change in (a) global average surface temperature and (b) global average precipitation for 2081-2100 relative to 1986-2005 under the RCP 2.6 scenarios (left) and RCP 8.5 scenarios (right) [1]

The effects of climate change are easily observed over the years. These impacts directly affect human life, the natural environment, and the ecosystem. In particular, changes to water resources can have a big impact on people's lives. In many regions, floods, drought problems are expected to be worse because of climate change. The risk of natural events, such as flood inundation, landslides, and sediment-related disasters caused by extreme rainfall, is likely to increase in the future [6,7]. Approximately 80-90% of all recorded disasters from natural hazards during the past 10 years have caused by floods, droughts, tropical cyclones, heatwaves, and severe storms [8]. Among these natural events, floods are the most frequent type of natural disaster on earth, causing massive damage all over the world. There are three common types of floods including flash floods, river floods, and coastal floods [8]. River floods are one of the most frequent natural hazards and causing enormous damage [9]. Climate change may increase the magnitude and frequency of flooding in the future [9,10,11,12]. Floods can cause widespread devastation, resulting in loss of life and property damages [8]. Floods accounted for 34% of global natural disasters, causing an annual economic loss of more than 2.5$ billion and 1254 deaths each year from 1960 to 2014 [13,14]. According to the World Health Organization floods affected directly more than 2 billion people worldwide from 1998 to 2017. People who live in floodplain areas, or non-resistant buildings, or lack early flood warning systems are the most affected by flooding. Drowning accounts for 75% of deaths in flood disasters. Flood disasters are becoming more frequent and higher intensity in the future [8]. Some pictures of the effects of climate change on flood risks in the world in recent years are shown in Figures 1.4, 1.5, and 1.6 below.

Figure 1.4. The city of Hitoyoshi, Kumamoto Prefecture, is seen flooded in July, 2020 after the Kuma River overflowed due to torrential rainfall (Source: Japantimes.co.jp)

Figure 1.5. People using kayaks and paddleboards navigate a residential neighborhood inundated with floodwaters as severe flooding affects the suburb of McGraths Hill in Sydney, Australia, March 24, 2021 (Source: usnews.com)

Figure 1.6. A flooded slum in Manila in August 2012 (Source: reliefweb.int/)

In Japan:

In Japan, a new record has been reached for temperature and precipitation almost every year in recent times [15]. According to the Japan Meteorological Agency (2017) [3], the annual mean surface temperature over Japan has increased by 1.19ºC on a longer time scale, which is higher than the global average surface temperature increase (0.73ºC) (Figure 1.7).

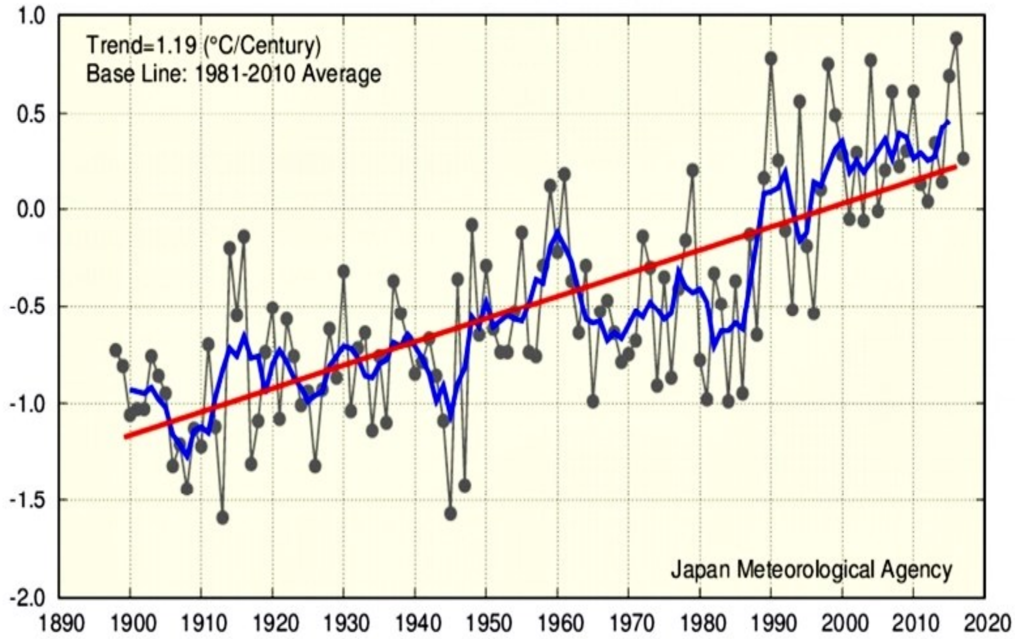

Figure 1.7. Annual surface temperature over Japan [3]

Additionally, the annual number of days when precipitation is equal to or greater than 100 mm and 200 mm has increased (statistically significant at a confidence level of 99%) during the period from 1901 to 2017 in Japan [3]. (Figure 1.8)

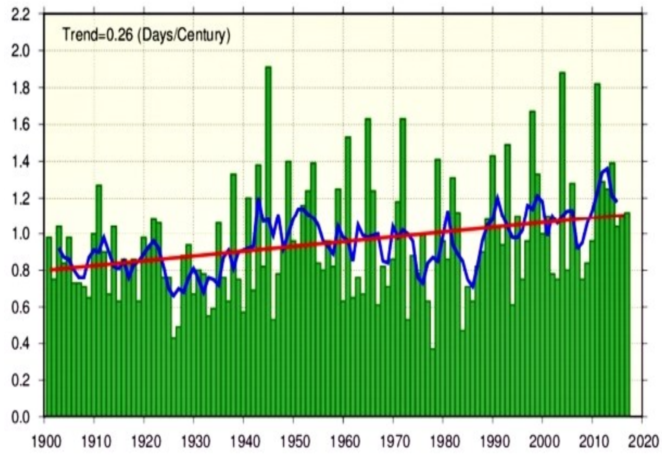

(a)

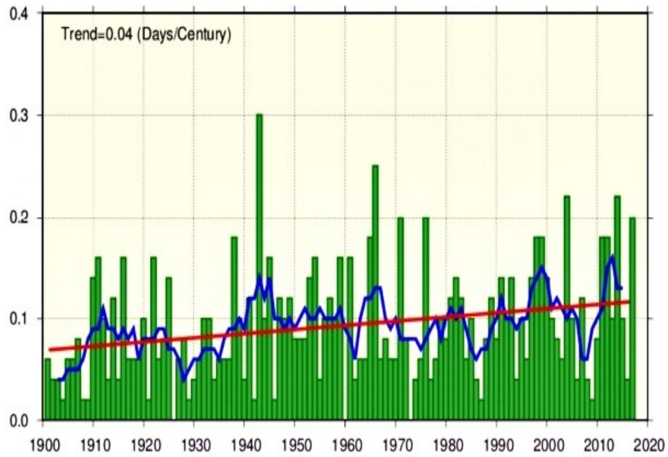

(b)

Figure 1.8. Annual number of days with (a) precipitation ≥ 100 mm, and (b) precipitation ≥ 200 mm from 1901 to 2017 [3]

Flood inundation disasters due to short-term heavy rainfall have occurred frequently in Japan and caused considerable damage in recent years. For example, an extreme rainfall event on 5-6 July 2017 caused severe floods in many parts of Kyushu, Japan, and resulted in extensive damage [16]. One year later, during 5-8 July 2018, severe flood due to extreme rainfall occurred in western Japan, and also caused the great loss of life and property damage [17]. In August, 2018 four typhoon attacked to Hokkaido island within two weeks, and caused the seveve flood in this area. This disaster reportedly caused approximately USD 260 million in damage, in addition to agricultural losses over 40,258 ha of land throughout Hokkaido [18]. In this context, the development of climate change adaptation measures to minimize flood damage should be considered in Japan.

Figure 1.9. Severe flood events in (a) August 2016 in Hokkaido, and (b) July 2018 in western Japan

Literature reviews:

In the context of complex unpredictable changes of extreme weather events, especially flood disasters caused by extreme rainfall around the world in recent years, assessment and prediction of their changes have become the most concern of water scientists, as well as hydrologists. Flood inundation risk assessment and prediction of extreme rainfall as well as severe river flooding caused by extreme rainfall have been carried out for many important river basins around the world [19,20,21,22,23]. These efforts could provide useful information for policymakers to take measures to adapt to climate change and minimize loss of life and property damage from floods in many important river basins. For example, Akter et al. (2018) [23] evaluated the change in peak flow due to urbanization under current and future climate scenarios of high summer and high winter rainfall for 20 sub-basins of the Schijn River, Belgium. The results indicated that the peak flow of high summer was significantly higher from 200% to 250% than that of the current climate conditions in this region. They concluded that climate change impacts contribute the most to producing peak discharge in the future. In a study by Shrestha et al. (2017) [19], the change in flood hazard under climate change scenarios was evaluated in the Yang River basin of Thailand. The results showed that in this basin, the temperature is expected to be warmer and wetter in the future. In addition, average annual rainfall is also predicted to increase in the future, higher in near future and lower in far future. Moreover, the intensity of annual floods is projected to increase for both RCP 4.5 and 8.5 scenarios. An additional 60 km^2 area of this basin is likely to be flooded with a return period of 100 years. Therefore, assessing climate change impacts on extreme rainfall as well as severe river flooding, and inundation for the important river basin in the world is an important task for environmental scientists. Special attention should be paid to the vulnerable area, low-lying areas with high potential flood inundation.

The information of change in extreme rainfall, as well as severe river floods would be additional references for water managers in adapting to climate change and making decisions to develop the flood early warning systems, the flood control constructions such as dam operations, and pump stations. In addition, it is necessary to raise public awareness of prevention and evacuation when necessary in order to mitigate the loss of life and property damage caused by flood inundation.

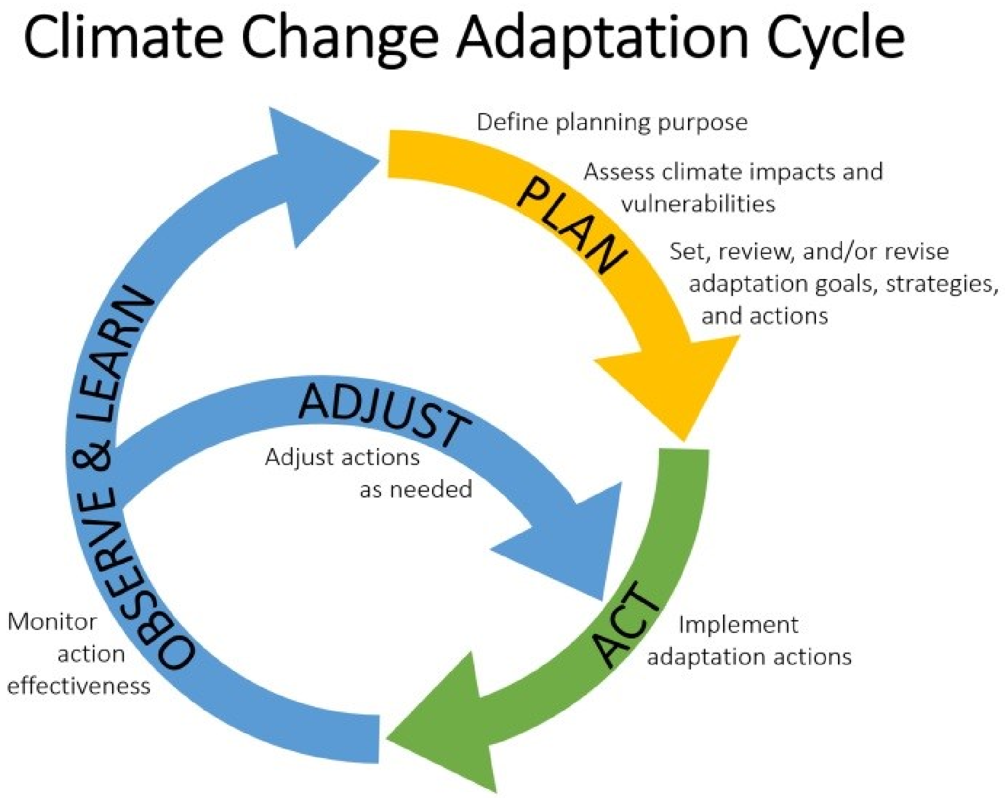

Figure 1.10. Climate change adaptation cycle
(Source: https://blackfeetclimatechange.com/our-environment/climate-change-adaptation-plan/)

1.2. Purposes and objectives of the research

Investigating the climate change impacts on extreme rainfall and severe flood inundation in vulnerable areas is an important mission in the current period. Therefore, this research was conducted to evaluate the changes in extreme rainfall as well as severe flood inundation considering climate change impacts, choosing the most important and largest river basin in Hokkaido, Japan is the Ishikari River basin as a case study. In addition, the change in flood inundation was evaluated comprehensively in the Chitose River basin, the downstream low-lying area of the Ishikari River.

This focus was chosen since new records have been reached for temperature and precipitation almost every year in recent times in Japan [15]. Moreover, the Ishikari River with a length of 268 km, which is the longest river in Hokkaido, and the third-longest river in Japan. Additionally, this river has the second largest basin area in Japan, with a drainage area of 14,330 km^2. The Ishikari Plain occupies most of the basin's area and is located around the central and downstream basin area, which is the most productive agricultural area in Hokkaido. This river basin plays a vital role in the socioeconomic development of Hokkaido. In addition, the Chitose River basin is one of the main tributaries of the Ishikari River. Owing to the topographical characteristics of its low-lying area, the Chitose River basin is frequently affected by backwater from the main river, causing severe flood inundation. As a result, the Chitose River basin is considered a vulnerable region in the Ishikari River basin. Finally, the most important reason motivating us to conduct this research is to the best of our knowledge, there have been no studies focusing on evaluating the impacts of climate changes on severe river floods in the entire Ishikari River basin, in particular in its main sub-basins comprehensively. Moreover, there have been no studies assessing the impacts of climate changes on flood inundation hazards in the Chitose River basin comprehensively. As a result, this study can be considered a pioneering work to evaluate the impacts of climate changes on severe flood inundation in the target basin.

To achieve the objective of this research, specific objectives need to be addressed as follow:

- Investigating the change in short-term extreme rainfall as well as its impact on severe river flooding in the Ishikari River basin, as well as in its main sub-basins comprehensively under various climate change scenarios.
- Assessing and investigating the change in flood inundation in the Chitose River basin considering the extreme rainfall impacts and topographical vulnerability.

1.3. Thesis outline

This research consists of five chapters, the results of the research will be presented in the next chapters of the study. The main contents of each chapter are presented as follows:

- **Chapter 2: Uncertainty of rainfall patterns**

This chapter was conducted to review the uncertainty of rainfall patterns from future projection climate methods. To evaluate the changes in climate variables to adapt to climate change impacts, the future projection climate dataset was established using various climate change scenarios. Prediction of changes in the flow regime is a challenge, as it demands climate variables such as rainfall and evapotranspiration from future projection climate models as input data. However, using future projection climate datasets have still uncertainties. The uncertainties in input data will lead to inaccurate prediction results from the hydrological models. In this chapter, we conducted to review of the future projection climate models and their limitations, especially for the rainfall value. In addition, we overview the database for Policy Decision making for Future climate change (d4PDF). It is a large-ensemble and high-resolution climate simulations for extreme rainfall as well as severe floods assessment. It could predict extreme rainfall as well as severe flood events with return periods equal to or larger than 100 years or more. Simulation with large ensemble members could reduce the uncertainty in the estimation of the probability of extreme events

- **Chapter 3: Assessing climate change impacts on extreme rainfall and severe flooding in the Ishikari River basin, Japan**

In this chapter, we conducted to evaluate climate change impacts on extreme rainfall and severe river flooding caused by extreme rainfall during the summer monsoon season. The Ishikari River basin located in Hokkaido, Japan is chosen as a case study. The changes in the short-term extreme rainfall and the risk of river flooding associated with climate change in the Ishikari River basin are evaluated. This is the first study to assess the changes in extreme short-term rainfall and extreme river flooding events during the summer monsoon season in the Ishikari River basin as well as in its main sub-basins using an Integrated Flood Analysis System (IFAS) coupled with a large-ensemble rainfall dataset (d4PDF) with a super high-resolution of 5 km. In addition, considering the dangers of the backwater phenomenon, the time differences between the time of peak discharge at the reference stations in each tributary and the time of peak water level at the confluence points in the main river were evaluated. The Student's t-test was used to find a significant difference between the two sets of samples (historical simulation and future simulation). The results from this chapter would indicate which areas should be special paid attention to mitigate the flood damage in the Ishikari River basin in the future.

- **Chapter 4: Flood inundation assessment in the low-lying river basin considering extreme rainfall impacts and topographic vulnerability**

From the result of chapter 3, we indicated that the effect of climate change is significant in the Chitose River basin, the downstream lowland area of the Ishikari River basin. This river basin is considered to be the most flood-prone in the Ishikari River basin. Therefore, in this chapter, we aim to focus on evaluating the change in flood inundation risk comprehensively (including inundation area, inundation volume, peak inundation depth, inundation frequency, and inundation duration) considering the extreme rainfall impacts and topographic vulnerability in the Chitose River basin using the Rainfall-Runoff-Inundation (RRI) model and rainfall data extracted from d4PDF with a super high-resolution of 5 km. Owing to the topographical characteristics of its low-lying area, the Chitose River basin is frequently affected by backwater from the Ishikari River and experiences severe flood inundation. Moreover, this chapter is conducted to improve the time difference prediction result considering the dangerous impacts of backwater phenomenon on flood inundation risk in the Chitose River basin using the RRI model, which uses a 2D distributed hydrodynamic model with diffusive wave models. The time difference is evaluated between the peak discharge at the reference station in the Chitose River basin and the peak water level at the confluence point intersecting the Ishikari River. In addition, the statistical Kolmogorov-Smirnov (K-S) test, which is a nonparametric test of two samples, was used to examine the variation in flood inundation between the historical and future simulations.

- **Chapter 5: Conclusions and suggestions**

This chapter summarizes the main results obtained in this research, discusses the research targets that have been met, limitations of the study. In addition, we propose some structural and non-structural measures to mitigate flood risk in vulnerable areas. Finally, suggestions for future research are also recommended in this chapter.

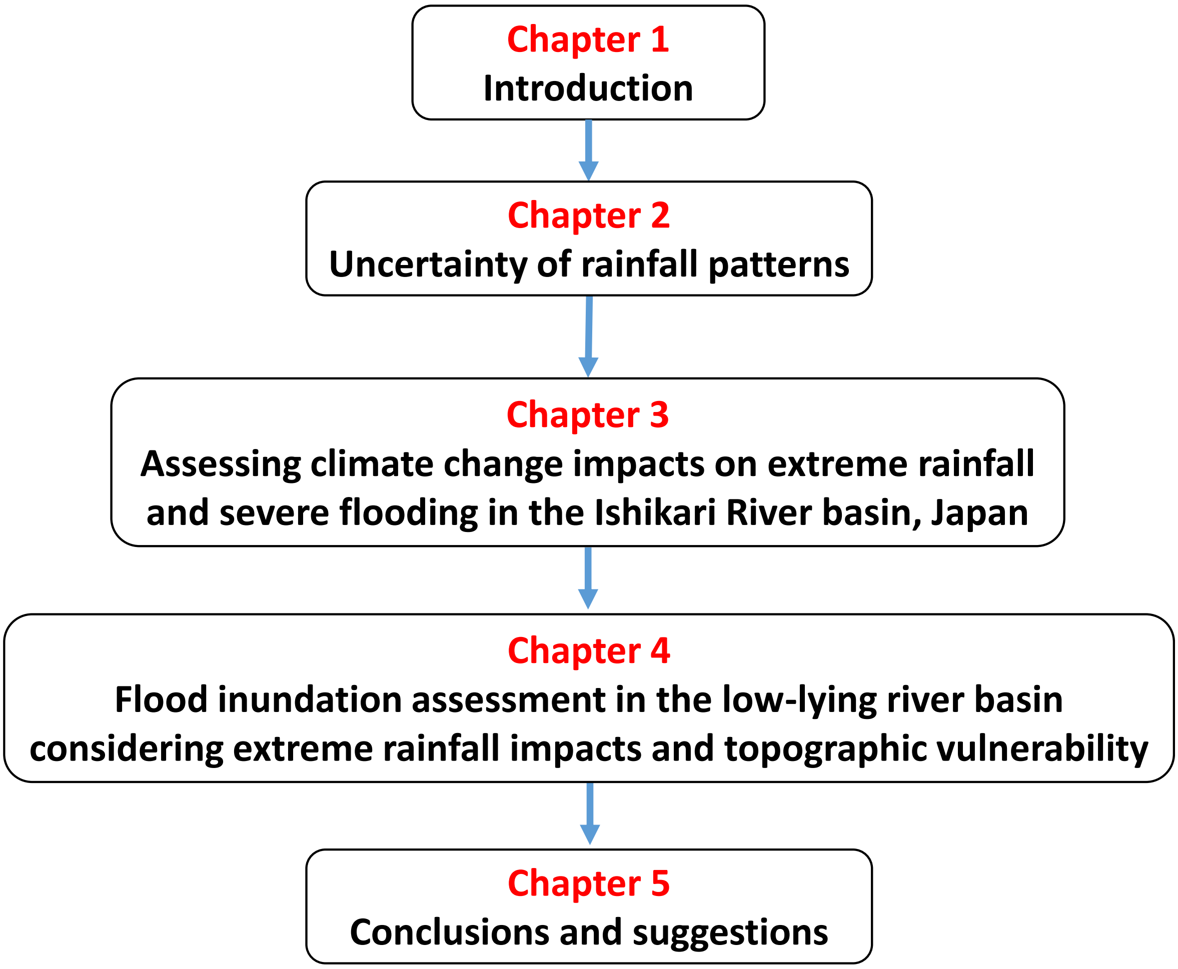

Figure 1.11. Research outline

1.4. References

1. IPCC, 2014: Climate Change 2014: Synthesis Report. Contribution of Working Groups I, II and III to the Fifth Assessment Report of the Intergovernmental Panel on Climate Change [Core Writing Team, R.K. Pachauri and L.A. Meyer (eds.)]. IPCC, Geneva, Switzerland, 151 pp.
2. Intergovermental Panel on Climate Change (IPCC). *Climate Change 2013: The Physical Science Basis. Contribution of Working Group I to the Fifth Assessment Report of the Intergovernmental Panel on Climate Change*; Stocker, T.F., Qin, D., Plattner, G.-K., Tignor, M.M.B., Allen, S.K., Boschung, J., Nauels, A., Xia, Y., Bex, V., Midgley, P.M., Eds.; Cambridge University Press: Cambridge, UK; New York, NY, USA, 2013; Volume 3, pp. 154–196.

3. Japan Meteorological Agency. Climate Change Monitoring Report 2017. Available online: https://www.jma.go.jp/jma/en/NMHS/ccmr/ccmr2017_high.pdf (accessed on 20 December 2020).
4. Wu, F.; Wang, X.; Cat, Y.; Li, C. Spatiotemporal analysis of precipitation trends under climate change in the upper reach of Mekong River basin. *Quat. Int.* **2013**, *392*, 137–146. DOI:10.1016/j.quaint.2013.05.049.
5. Willems, P.; Vrac, M. Statistical precipitation downscaling for small-scale hydrological impact investigations of climate change. *J. Hydrol.* **2011**, *402*, 193–205. DOI:10.1016/j.jhydrol.2011.02.030.
6. Hirabayashi, Y.; Kanae, S.; Emori, S.; Oki, T.; Kimoto, M. Global projections of changing risks of floods and droughts in a changing climate. *Hydrol. Sci. J.* **2008**, *53*, 754–772. DOI:10.1623/hysj.53.4.754.
7. Zenkoji, S.; Oda, S.; Tebakari, T.; Archevarahuprok, B. Spatial characteristics of flooded areas in the Mun and Chi River basins in Northeastern Thailand. *J. Disaster Res.* **2019**, *14*, 1337–1345. DOI:10.20965/jdr.2019.p1337.
8. World Health Organization. 2021. Available online: https://apps.who.int/iris/bitstream/handle/10665/76224/9789241564526_section_2_eng.pdf. (accessed on 04 May 2021).
9. Tanoue, M.; Hirabayashi, Y.; Ikeuchi, H. Global-scale river flood vulnerability in the last 50 years. *Scientific Reports*. **2016**, *6*, 1-9. DOI: 10.1038/srep36021
10. Hirabayashi, Y.; Mahendran, R.; Korala, S.; Konoshima, L.; Yamazaki, D.; Watanabe, S.; Kim, H.; Kanae, S. Global flood risk under climate change. *Nature Climate Change*. **2013**, ***3*,** 816–821. DOI: 10.1038/nclimate1911
11. Arnell, NW.; Lloyd-Hughes, B. The global-scale impacts of climate change on water resources and flooding under new climate and socio-economic scenarios. *Climatic Change*. **2014**, ***122*,** 127–140. DOI: 10.1007/s10584-013-0948-4
12. Winsemius, HC.; Aerts, JCJH.; Beek, LPHv.; Bierkens, MFP.; Bouwman, A.; Jongman, B.; Kwadijk, JCJ.; Ligtvoet, W.; Lucas, PL.; Vuuren, DPv.; Ward, PJ. Global drivers of future river flood risk. *Nature Climate Change*. **2016**, ***6*,** 381–285. DOI: 10.1038/nclimate2893
13. Petit-Boix, A.; Arahuetes, A.; Josa, A.; Rieradevall, J.; Gabarrell, X. Are we

preventing flood damage eco-efficiently? An integrated method applied to post-disaster emergency actions. *Sci. Total Environ*. **2017**, *580*, 873-881. DOI: 10.1016/j.scitotenv.2016.12.034

14. Zhang, D.; Shi, X.; Xu, H.; Jing, Q.; Pan, X.; Liu, T.; Wang, H.; Hou, H. A GIS-based spatial multi-index model for flood risk assessment in the Yangtze River Basin, China. *Environmental Impact Assessment Review*. **2020**, *83*, 106397. DOI: 10.1016/j.eiar.2020.106397
15. Yamada, T.J. Adaptation Measures for Extreme Floods Using Huge Ensemble of High-Resolution Climate Model Simulation in Japan, Summary Report on the Eleventh Meeting of the Research Dialogue. United Nations Framework Convention on Climate Change (UNFCCC), Bonn, Germany. **2019**, pp. 28–29. Available online: https://unfccc.int/sites/default/files/resource/RD11SummaryReport.pdf (accessed on 8 April 2020).
16. Shakti, P.; Nakatani, T.; Misumi, R. Hydrological simulation of small river basins in Northern Kyushu, Japan, during the extreme rainfall event of July 5–6, 2017. *J. Disaster Res*. **2018**, *13*, 396–409, DOI:10.20965/jdr.2018.p0396.
17. River Council for Social Infrastructure Development. Flood Risk Management for Wide-Area and Long-Lasting Rainfall–Multi-Layered Countermeasures for Complex Disasters **2018**. Available online: https://www.mlit.go.jp/river/mizubousaivision/toushin_e/1812_flood_risk_management_e.pdf (accessed on 20 December 2020).
18. Japan Society of Civil Engineers (JSCE). Onsite Field Investigation Team, Site–Investigation Report for the Hokkaido Heavy Rainfall Disasters in August 2016; Title was translated by N. Kimura; JSCE Report; JSCE: Tokyo, Japan, **2017**. (In Japanese).
19. Shrestha, S.; Lohpaisankrit, W. Flood hazard assessment under climate change scenarios in the Yang River basin, Thailand. *International Journal of Sustainable Built Environment*. **2017**, *6*: 285-298. DOI: 10.1016/j.ijsbe.2016.09.006.
20. Try S, Tanaka S, Tanaka K, Sayama T, Hu M, Sok T, Oeurng C. Projection of extreme flood inundation in the Mekong River basin under 4K increasing scenario using large ensemble climate data. *Hydrological Processes*. **2020**, *34*, 4350-4364. DOI: 10.1002/hyp.13859.

21. Try, S.; Tanaka, S.; Tanaka, K.; Sayama, T.; Lee, G.; Oeurng, C. Assessing the effects of climate change on flood inundation in the lower Mekong Basin using high-resolution AGCM outputs. *Prog. Earth Planet. Sci*. **2020**, *7*, 34. DOI: 10.1186/s40645-020-00353-z
22. Yamamoto, K.; Sayama, T. Impact of climate change on flood inundation in a tropical river basin in Indonesia. *Prog. Earth Planet. Sci*. **2021**, *8*, 5. DOI: 10.1186/s40645-020-00386-4
23. Akter, T.; Quevauviller, P.; Eisenreich, SJ.; Vaes, G. Impacts of climate and land use changes on flood risk management for the Schijn River, Belgium. *Environmental Science and Policy*. **2018**, *89*, 163-175. DOI: 10.1016/j.envsci.2018.07.002

Chapter 2

Uncertainty of rainfall patterns

Chapter 2

2.1. Introduction

The Earth's climate past and future always change in response to both natural and anthropogenic drivers. Human emissions of greenhouse gases such as carbon dioxide (CO_2), methane (CH_4), and other greenhouse gases overwhelm the impacts of natural drivers on the external forcing of Earth's climate. Even if the present concentration could be stabilized, the temperature would continue to increase by 0.6 ºC over this period, compared to the period of 1980 – 1999. Over the next few decades, the greenhouse gas concentration is expected to increase, leading to an increase in temperature from 0.3ºC to 0.7ºC [1].

When the temperature increases, the amount of snow and ice has diminished, the sea level has risen, and the occurrence of climate extreme events. The climate extreme events would cause enormous damage to nature and humans in the future. In this context, the climate change scenarios, in which the relationships between human choices, emissions, concentrations, and temperature change were developed. The standard sets of scenarios were used by the climate modelling community as input to global climate model simulations [1]. In recent decades, the Representative Concentration Pathways in 2010 (RCPs) was used commonly in the scientific community to predict the change of climate variables in the future.

The commonly recent set of scenarios, RCPs, builds on these two decades of scenario development. RCPs are not emissions scenarios; they are radiative forcing scenarios. Each scenario is tied to one value: the change in radiative forcing at the tropopause by 2100 relative to preindustrial levels. The four RCPs are numbered according to the change in radiative forcing by 2100: +2.6, +4.5, +6.0, and +8.5 watts per square meter [1]. Table 2.1 shows the RCP scenarios description in more detail. Figure 2.1 shows the global mean temperature anomalies (ºF) relative to 1976-2005 for four RCP scenarios, 2.6 (green), 4.5 (yellow), 6.0 (orange), and 8.5 (red). It can be seen that the future highest temperature corresponds to the highest future greenhouse gas emissions as indicated by red lines color in Figure 2.1.

Table 2.1. RCP scenarios description (Source: IPCC Fifth Assessment Report Summary for Policymakers)

Representative concentration pathway (RCP)	Forcing compared to 1750 (Wm^{-2})	Climate policy asscociated with scenario	CO_2 equivalent (ppm)	Projected global average temperature increase from 1986 – 2005 (°C)
2.6	2.6	Mitigation	475	1.0
4.5	4.5	Stabilization	630	1.8
6.0	6.0	Stabilization	800	2.2
8.5	8.5	None	1313	3.7

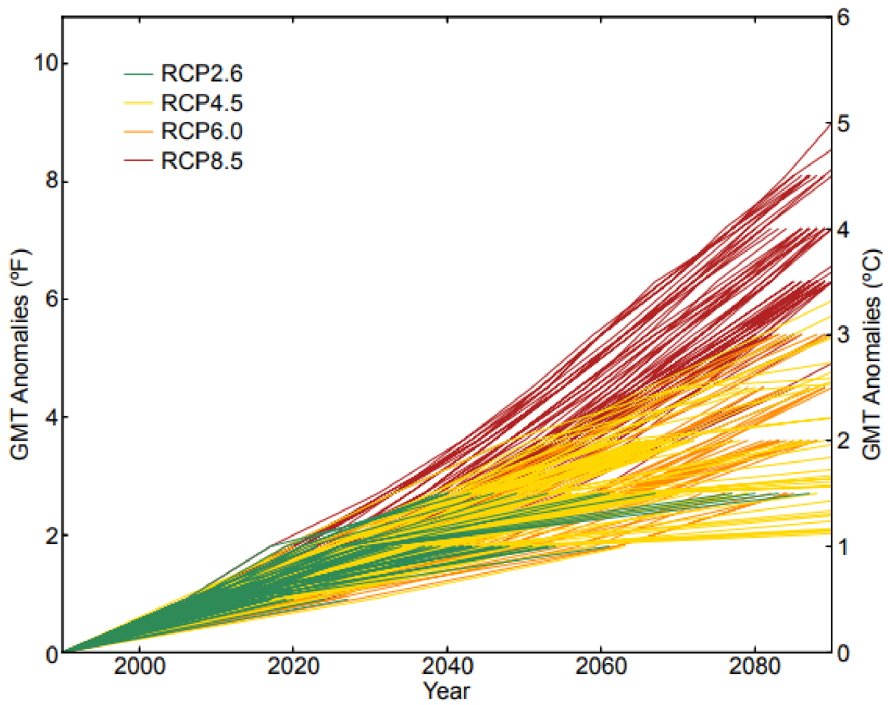

Figure 2.1. Global mean temperature anomalies (°F) relative to 1976-2005 for four RCP scenarios, 2.6 (green), 4.5 (yellow), 6.0 (orange), and 8.5 (red). Each line represents an individual sidạmulation from the CMIP5 archive. Every RCP-based simulation with annual or monthly temperature outputs available was used here. The values shown here were calculated in 0.5°C increments; since not every simulation reaches the next 0.5°C increment before the end of the century, many lines terminate before 2100 [2]

In recent years, Global Climate Models or General Circulation Models (GCMs) are the best way to project the possible future changes in climate variables at the Earth system's level [3,4]. The total number of GCMs and the average horizontal spatial resolution of the models have improved year by year, as computers become more powerful [1]. There are many global climate models that are commonly used today to evaluate the climate variables for many regions in the world. For example, table 2.2 shows the 18 GCMs provided by The Coupled Model Intercomparison Project Phase 5 (CMIP5) [5]. Li et al. (2015) used these 18 GCMs with two experiments: the historical simulation (1950-1999) and the future simulation RCP 4.5 scenario (2050-2099) to evaluate the thermodynamic and dynamic contributions to future changes in regional precipitation in the Southeastern United States [5].

Table 2.2. 18 Global climate models (GCMs) [5]

No	Model	Ensemble members		Years	
		Historical	Future	Historical	Future
1	BCC-CSM1-1	3	1	50	50
2	CCSM4	6	6	50	50
3	CESM1-BGC	1	1	50	50
4	CESM1-WACCM	4	3	50	50
5	CNRM-CM5	10	1	50	50
6	CSIRO-Mk3.6.0	10	10	50	50
7	FGOALS-s2	3	2	50	50
8	GFDL-CM3	3	1	50	50
9	GFDL-ESM2G	3	1	50	50
10	GFDL-ESM2M	3	1	50	50
11	HadGEM2-CC	3	1	50	50
12	INM-CM4	1	1	50	50
13	IPSL-CM5A-LR	5	4	50	50
14	MIROC5	4	3	50	50
15	MIROC-ESM	3	1	50	50
16	MPI-ESM-LR	3	3	50	50
17	MRI-CGCM3	5	1	50	50
18	NorESM1-M	2	1	50	50

Although, there are many global climate models are used in the world today, such as 18 GCMs shown in table 2.2; however, most have few ensemble members. A GCM reproduces a single climate scenario or a few scenarios based on some ensemble members [6]. Therefore, with few ensemble numbers, it would not be sufficient to predict the climate variables for extreme events of return periods 100 years or more [6,7]. Simulations with large ensemble members are necessary to reduce the uncertainty in the estimation of extreme events [6]. In addition, increasing ensemble size could improve the estimation of regional precipitation events [6,8]. Therefore, developing the climate models with large ensemble numbers could address this issue.

In addition, using GCMs in evaluating and predicting future climate variables still has limitations. Generally, GCMs has a coarse horizontal resolution; therefore, it is not suitable for predicting the future climate variables at a regional scale or basin scale. In addition, it is an inaccuracy of describing rainfall extremes, the direct use of their outputs in impact studies on basin scales is also limited. There is often a clear deviation in the statistics of variables generated by GCMs such as rainfall and temperature [4,9,10]. For example, Rotmans et al. (1994) [11] indicated that the precipitation characteristics change so much from region to region and locally within regions. Whereas, these precipitation patterns could be obtained when the scale in the climate models is reduced. The spatial resolution of typical GCMs (approximately 100-400 km) is too coarse to predict major hydrological on basin scales [12]. Sun et al. (2006) [13] and Min et al. (2011) [14] also indicated that low resolution of GCMs tends to prevent simulating realistic extreme events, and high-resolution modeling is necessary to predict climate extremes under global warming. Most available GCMs are only suitable for predicting the hydrological impact of climate change on relatively large watershed or global scales [15,16]. The super-high-resolution model can reproduce actual climate conditions more precisely than lower resolution models [12,17,18].

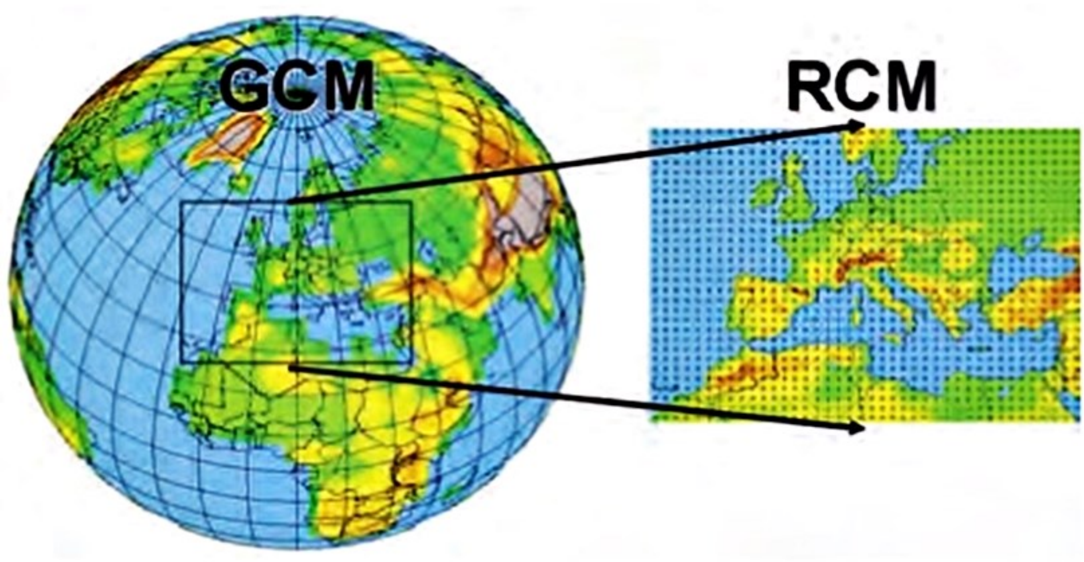

Figure 2.2. Coarse data from Global Climate Models (GCMs) forms the initial and boundary conditions necessary for Regional Climate Models (RCMs) to dynamically downscale to much finer resolution climate data [19]

GCMs generally have a coarse resolution for simulation on a regional scale; such coarse resolution could lead to large uncertainties in the simulation [20,21]. Therefore, to bridge the gaps between the climate model scales and the local scales, high-resolution climate data obtained through downscaling approaches, such as statistical and dynamical downscaling, have been investigated in recent years. For example, from a study by Fowler et al (2007) [22], six Regional Climate Models (RCMs) with a horizontal resolution of 50 km under the SRES A2 emissions scenario were used to evaluate changes in extreme precipitation over Europe by 2070-2110. The results indicated that RCMs could evaluate to underestimate 1 day return values but reasonably simulate longer duration (5-10 day) extreme precipitation. In addition, all RCMs project increases in the magnitude of short and long duration extreme precipitation for most of Europe. This study also showed that both the resolution and number of models in the ensemble will impact projections of change. In a study by Wichakul et al. (2015) [23], the authors showed that the flood risk in the near-future and far-future projection periods becomes higher in the Chao Phraya River, Thailand using MRI-AGCM 3.2S with a high resolution of 20 km.

2.2. Overview of database for Policy Decision making for Future climate change (d4PDF)

Planning for adaptation to climate change impacts needs to based on impact assessments of natural disasters, water resources, ecosystems, and so on in each region. Therefore, the detailed projection of extreme events such as extreme rainfall, drought, and strong wind is required at the regional and watershed scales [24]. Understanding the importance of climate projection models in evaluating and predicting the change in climate variables due to climate change impacts to minimize their damage, a large-ensemble climate simulation database, which is known as the database for policy decision-making for future climate changes (d4PDF) was developed in 2015 [24]. The main purpose of the database is to become a standard for using in policy-making decisions at Japanese ministries and agencies, as well as in climate change impacts assessment studies [25].

The d4PDF consists of large-ensemble climate experiments from the global atmospheric model with a horizontal resolution of 60 km (AGCM), and regional downscaling simulations covering the Japan area, with a horizontal resolution of 20 km (RCM). Four sets of experiments are performed by the AGCM. The duration of each experiment is 60 years. Each set of experiments has 90-100 ensemble members. The settings of experiments shown as below:

- Historical climate simulation: 1951-2010, 100 members
- Non-warming simulation: 1951-2010, 100 members
- 2K future climate simulation: 2031-2090, 54 members
- 4K future climate simulation: 2051-2110, 90 members.

The sea-surface temperature (SST), sea-ice concentration (SIC), and sea-ice thickness (SIT) are prescribed as the lower boundary conditions, and global-mean concentrations of greenhouse gases and three-dimensional distributions of ozone and aerosols as the external forcing [24].

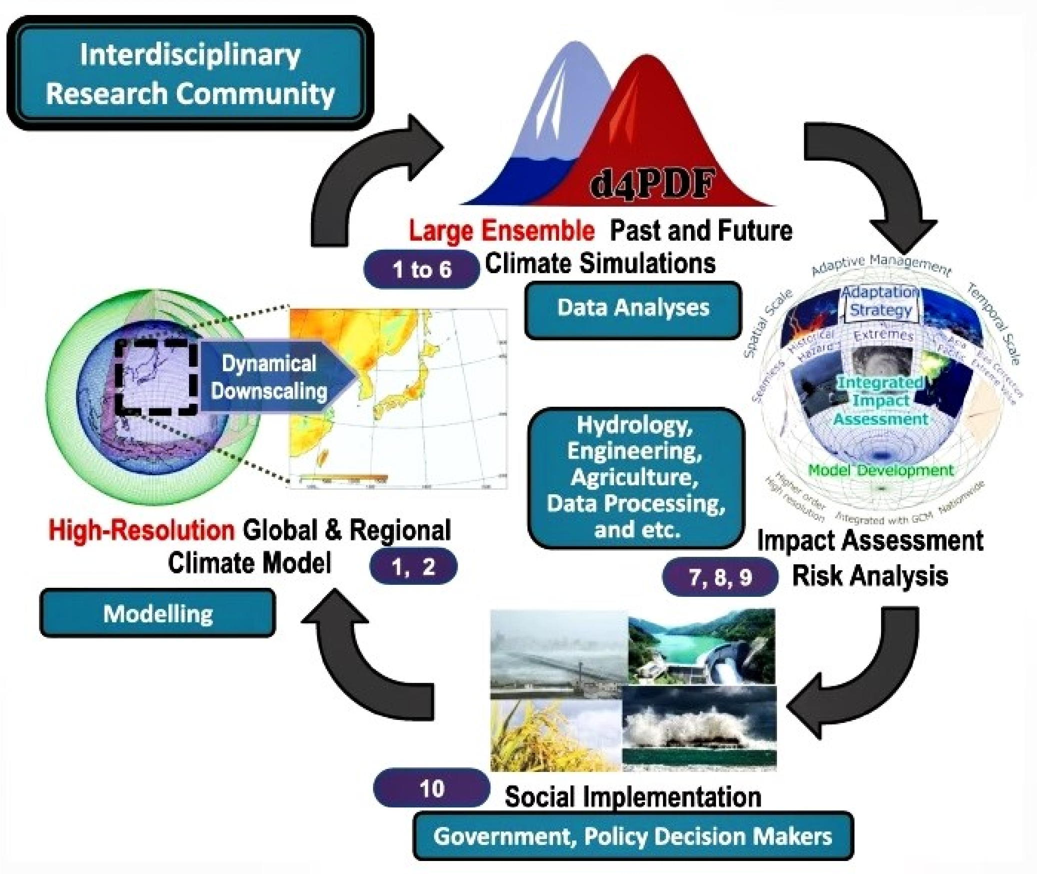

Figure 2.3. A schematic view of these research activities form an interdisciplinary community on global warming research [25]

The +4K future climate simulation was predicted for a global mean air temperature 4°C warmer than the pre-industrial period. The +4K future climate simulation corresponded to the representative concentration pathway 8.5 (RCP 8.5) experiments under phase 5 of Coupled Model Intercomparison Project Phase 5 (CMIP5). For the use of the +4K simulations, climatological SST warming patterns (△SSTs) are added to the observational SST after removing the long-term trend component. Six CMIP5 models were selected, and 15 member ensemble experiments are conducted for each of the six △SSTs, giving a total of 90 members.

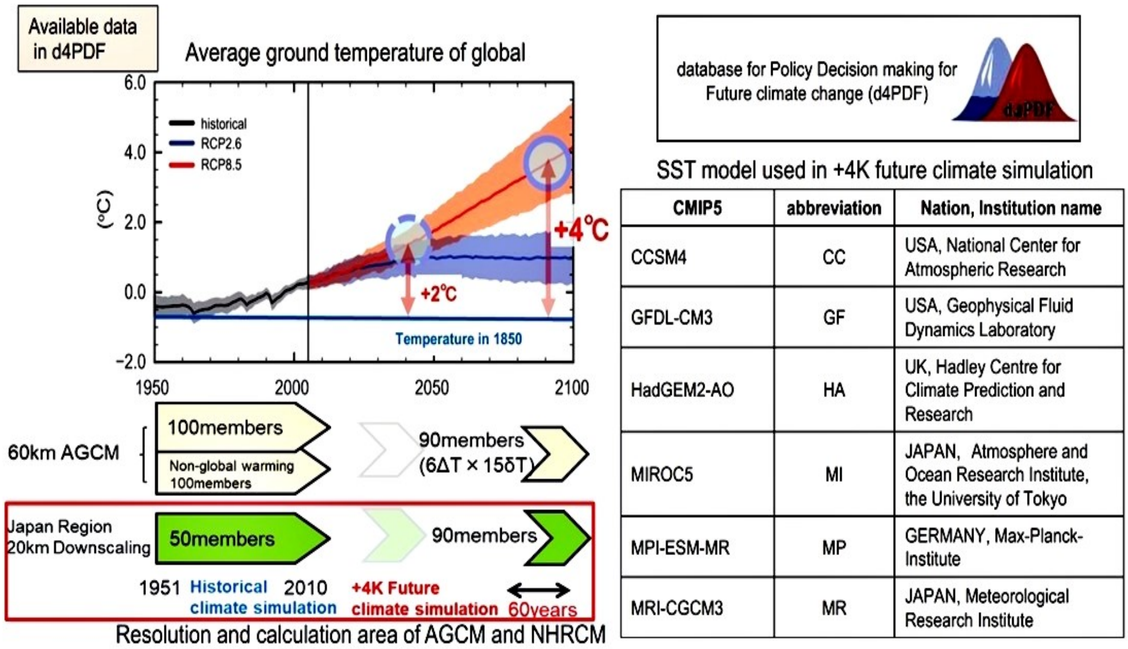

CMIP5	abbreviation	Nation, Institution name
CCSM4	CC	USA, National Center for Atmospheric Research
GFDL-CM3	GF	USA, Geophysical Fluid Dynamics Laboratory
HadGEM2-AO	HA	UK, Hadley Centre for Climate Prediction and Research
MIROC5	MI	JAPAN, Atmosphere and Ocean Research Institute, the University of Tokyo
MPI-ESM-MR	MP	GERMANY, Max-Planck-Institute
MRI-CGCM3	MR	JAPAN, Meteorological Research Institute

Figure 2.4. Description of d4PDF (Source: d4PDF English, database for Policy Decision making for Future climate change) (http://www.miroc-gcm.jp/~pub/d4PDF/design_en.html)

Currently, evaluating the change in climate variables, especially extreme events in regional scale or basin scale, the regions were affected by local topography, the low-resolution models are not suitable for simulation [22,24]. In particular in Asia, where the monsoon and tropical cyclones are major causes of natural hazards and water resources; therefore, changes in these phenomena are the key aspects for regional climate change risk assessments. To address these problems, the RCM downscaling simulations are developed by the Meteorological Research Institute Nonhydrostatic Regional Climate Model (NHRCM). The RCM simulations cover Japan, the Korean Peninsula, and the eastern part of the Asian continent [24].

The dynamical downscaling simulations by the RCM are conducted from AGCM. Using the RCM results is recommended for analyses around the Japan region. Three sets of experiments are performed by the RCM, as shown below:

- Historical climate simulation: 1951-2010, 50 members
- +2K future climate simulation: 2030-2091, 54 members
- +4K future climate simulation: 2051-2110, 90 members

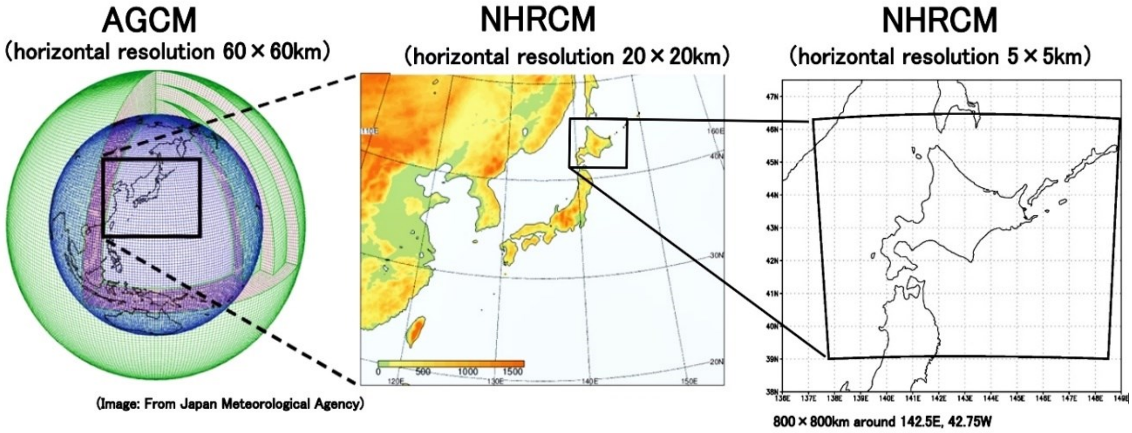

Figure 2.5. Experimental design of d4PDF (Source: Ministry of education, culture, sports, science, and technology et al, the guidance of using d4PDF, 2015.12, http://www.miroc-gcm.jp/~pub/d4PDF/design.htmn (Only Japanese available)

The RCM was used in several studies; for example, Miyasaki et al. (2020) [26] used the Non-Hydrostatic RCM (NHRCM) with a 20 km horizontal resolution [27] to investigate heavy precipitation events exceeding the 100 year return period in the Kanto area and future projections of such events. In another study by Harada et al. (2020) [28], the authors conducted to evaluate climate change impact on flood risk in the Nagara River basin using d4PDF NHRCM with a horizontal resolution of 20 km. The results showed that the frequency distribution of the calculation result of the peak flood discharge was overestimated by about 10% from the frequency distribution of the observed values. Moreover, the distribution of the annual maximum discharge was well reproduced.

In addition, finer-scale projections have been performed over the Japanese region by downscaling from RCM to a super high-resolution of 5 km [24,29,30,31]. The high-resolution large ensemble results could be used to evaluate the statistical change in very rare precipitation events [24]. In a study by Yamada et al. (2018) [31], the super high-resolution 5 km d4PDF dataset was downscaled from the 20 km resolution data via a non-hydrostatic regional climate model [32]. After downscaling, the rainfall amount and spatiotemporal distribution of rainfall were similar to the observed rainfall events. Furthermore, heavy rainfall patterns could be better observed after downscaling, and the 5 km resolution results represented the topography of the study area more precisely.

2.3. Summary

Extreme weather events associated with climate changes have rapidly become one of the global concerns threatening natural environments and human life in recent decades. Therefore, future climate projection models have been developed under various climate change scenarios. A large-ensemble climate simulation database, which is known as the database for policy decision-making for future climate changes (d4PDF), was developed for climate change impacts adaptations and assessments. The database was established in 2015, and it has been growing continuously [25]. It contains the results of large ensemble simulations conducted over a total of thousands of years for historical and future climate simulations using a global atmospheric model with a horizontal resolution of 60 km (AGCM) and a regional climate model with a horizontal resolution of 20 km (RCM). Several sets of future climate simulations are available, in which the global mean surface air temperature becomes +4K, +2K warmer than the preindustrial climate, corresponding to the representative concentration pathway 8.5 (RCP8.5) scenario of CMIP5. The sets of experiments conducted by the AGCM and RCM are presented in the above contents. The advent of the d4PDF database is aimed to become a standard for using in devising policies at Japanese ministries and agencies, as well as applied in the climate change impact assessments studies. More than 70 papers using d4PDF have been published since 2015. The database d4PDF with the high resolution and large ensemble climate simulations are effective for detecting signals of extreme weather events and for practical applications to investigations of future climate changes. The database d4PDF have been performed in various research areas such as natural hazard, hydrology, agriculture, and health. Furthermore, it has helped in establishing an interdisciplinary research community on global climate change across Japan [25].

In addition, Japan often suffered human loss and property damage from short-term extreme rainfall due to Baiu front and typhoons. The short-term extreme rainfall can cause severe flood inundation in Japan. Therefore, the super high-resolution of 5 km was downscaled from the NHRCM with a horizontal resolution of 20 km [24,29,30,31]. The regional climate model with a resolution of 5 km can reproduce local extreme rainfall events realistically [33]. As a result, there are several studies have been used the d4PDF with the super high-resolution of 5 km for climate change impact assessments for watershed scales in Japan. The studies have shown good applicability of d4PDF with high resolution in detecting extreme rainfall events [31,33]. Overall, d4PDF has become an essential tool for climate change adaptation to mitigate the loss of life and property damage caused by extreme weather events, especially in Japan in recent years.

2.4. References

1. Hayhoe, K.; Edmonds, J.; Kopp, RE; LeGrande, AN.; Sanderson, BM.; Wehner, MF.; Wuebbles, J. Climate Models, Scenarios, and Projections. *Climate Science Special Report: Fourth National Climate Assessment*. **2017**. *I*, 133-160.
2. Swain, S and Hayhoe, K. 2015: CMIP5 projected changes in spring and summer drought and wet conditions over North America. *Climate Dynamics*. **2015**, *44*, 2737-2750. Doi: 10.1007/s00382-014- 2255-9
3. Huntingford, C., Hugo Lambert, F., Gash, JHC., Taylor, CM., Challinor, AJ. Aspects of climate change prediction relevant to crop productivity. *Philosophical Transactions of the Royal Society B: Biological Sciences*. **2005**, *360*: 1999-2009.
4. Rana, A. Climate change effects on urban rainfall and management of urban flooding. Doctoral thesis, 2013.
5. Li, L and Li, W. Thermodynamic and dynamic contributions to future changes in regional precipitation variance: focus on the Southeastern United States. *Climate Dynamics*. **2015**, *45*, 67-82. DOI: 10.1007/s00382-014-2216-3
6. Try, S.; Tanaka, S.; Tanaka, K.; Sayama, T.; Hu, M.; Sok, T.; Oeurng, C. Projection of extreme flood inundation in the Mekong River basin under 4 K increasing scenario using large ensemble climate data. *Hydrol. Process*. **2020**, *34*, 4350–4364. DOI: 10.1002/hyp.13859
7. Tanaka, T.; Tachikawa, Y.; Ichikawa, Y.; Yorozu, K. Flood risk curve development with probabilistic rainfall modelling and large ensemble climate simulation data: a case study for the Yodo River basin. *Hydrological Research Letters*, **12**, 28-33. DOI: 10.3178/hrl.12.28
8. Duan, W., Hanasaki, N., Shiogama, H., Chen, Y., Zou, S., Nover, D., Zhou, B., & Wang, Y. Evaluation and Future Projection of Chinese Precipitation Extremes Using Large Ensemble High-Resolution Climate Simulations. *Journal of Climate*. **2019**, *32*, 2169-2183. DOI: 10.1175/JCLI-D-18-0465.1
9. Kay, AL.; Reynard, NS.; Jones, RG. RCM rainfall for UK flood frequency estimation. I. Method and validation. *J. Hydrol*. **2006**, *318*, 151-162.

10. Kotlarski, S. Regional climate model simulations as input for hydrological applications: evaluation of uncertainties. *Advances in geosciences*. **2005**, *5*, 119.
11. Rotmans, J.; Hulme, M.; Downing, TE. Climate change implications for Europe: An application of the ESCAPE model. *Global Environmental Change*. **1994**, *4*, 97-124.
12. Sato, Y.; Kojiri, T.; Michihiro, Y.; Suzuki, Y.; Nakakita, E. Assessment of climate change impacts on river discharge in Japan using the super-high-resolution MRI-AGCM. *Hydrological Processes.* **2013**, *27*, 3264-3279. DOI: 10.1002/hyp.9828
13. Sun, Y.; Solomon, S.; Dai, A.; Portmann, RW. How often does it rain? *Journal of climate*. **2006**, *19,* 916-934. DOI: 10.1175/JCLI3672.1
14. Min, SK., Zhang, X., Zwiers, FW., Hegerl, GC. Human contribution to more- intense precipitation extremes. *Nature*. **2011**, *470*, 378-381. DOI: 10.1038/nature09763
15. Vörösmarty, CJ., Green, P.; Salisbury, J.; and Lammers RB. Global water resources: Vulnerability from climate change and population growth. *Science***. 2000**, *289*, 284-288. DOI: 10.1126/science.289.5477.284
16. Hirabayashi, Y., Kanae, S.; Emori, S.; Oki, T.; and Kimoto, M. Global projections of changing risks of floods and droughts in a changing climate. *Hydrological Sciences Journal*. **2008**, 53, 754-772. DOI: 10.1623/hysj.53.4.754
17. Kitoh, A., Yatagai, A.; Alpert, P. First super-high- resolution model projection that the ancient “Fertile Crescent” will disappear in this century. *Hydrological Research Letters*. **2008**, *2*, 1-4. DOI: 10.3178/hrl.2.1
18. Kusunoki, S., Mizuta, R.; Matsueda, M. Future changes in the East Asian rain band projected by global atmospheric models with 20-km and 60-km grid size. *Climate Dynamics*. **2011**, *37*, 2481-2493. DOI: 10.1007/s00382-011 -1000-x
19. Giorgi, F. Regionalization of climate change information for impact assessment and adaptation. *WMO Bulletin*. **2008**, *57*, 86-92.
20. Try, S.; Tanaka, S.; Tanaka, K.; Sayama, T.; Lee, G.; Oeurng, C. Assessing the effects of climate change on flood inundation in the lower Mekong Basin using high-resolution AGCM outputs. *Progress in Earth and Planetary Science*. **2020**, *7*, 34. DOI: 10.1186/s40645-020-00353-z
21. Li, G.; Zhang, X.; Zwiers, F.; Wen, QH. Quantification of uncertainty in high-resolution temperature scenarios for North America. *Journal of climate.* **2012**, *25*, 3373–3389. DOI: 10.1175/JCLI-D-11-00217.1
22. Fowler, HJ., Ekström, M., Blenkinsop, S., Smith, AP. Estimating change in extreme European precipitation using a multimodel ensemble. *Journal of Geophysical Research*. **2007**, *112*. DOI: 10.1029/2007JD008619

23. Wichakul, S.; Tachikawa, Y.; Shiiba, M.; Yorozu, K. River discharge assessment under a changing climate in the Chao Phraya River Thailand by using MRI-AGCM3.2S. *Hydrological Research Letters*. **2015**, *9*, 84-89. DOI: 10.3178/hrl.9.84
24. Mizuta, R.; Murata, A.; Ishii, M.; Shiogama, H.; Hibino, K.; Mori, N.; Arakawa, O.; Imada, Y.; Yoshida, K.; Aoyagi, T.; et al. Over 5000 years of ensemble future climate simulations by 60-km global and 20-km regional atmospheric models. *Bull. Am. Meteorol. Soc.* **2017**, *98*, 1383–1398. DOI: 10.1175/BAMS-D-16-0099.1
25. Ishii, M.; Mori, N. 4PDF: large-ensemble and high-resolution climate simulations for global warming risk assessment. *Progress in Earth and Planetary Science*. **2020**, *7*, 28. DOI: 10.1186/s40645-020-00367-7
26. Miyasaka, T.; Kawase, H.; Nakaegawa, T.; Imada, Y.; Takayabu, I. Future projections of heavy precipitation in Kanto and associated weather patterns using large ensemble high-resolution simulations. *SOLA*. **2020**, *16*, 125-131. DOI: 10.2151/sola.2020-022
27. Sasaki, H., K. Kurihara, I. Takayabu, and T. Uchiyama, 2008: Preliminary experiments of reproducing the present climate using the non-hydrostatic regional climate model. *SOLA*. **2008**, *4*, 25−28, DOI:102151/sola.2008-007
28. Harada, M.; Maruya, Y.; Kojima, T.; Matsuoka, D.; Nakagawa, Y.; Kawahara, S.; Araki, F. Flood frequency analysis and impact assessment for climate change in the Nagara river basin. *Journal of Japan Society of Civil Engineers, ser B1*. **2020**, *74*, 79-86.
29. Kanada, S., Nakano, M.; Kato, T. Projections of future changes in precipitation and the vertical structure of the frontal zone during the Baiu season in the vicinity of Japan using a 5-km-mesh regional climate model. *J. Meteor. Soc. Japan*. **2012**, ***90A***, 65–86. Doi:10.2151/jmsj.2012-A03
30. Nakano, M., Matsueda, M.; Sugi, M. Future projections of heat waves around Japan simulated by CMIP3 and high-resolution Meteorological Research Institute atmospheric climate models. *J. Geophys. Res. Oceans*. **2013**, ***118***, 3097-3109. Doi:10.1002/jgrc.20375
31. Yamada, T.J.; Hoshino, T.; Masuya, S.; Uemura, F.; Yoshida, T.; Omura, N.; Yamamoto, T.; Chiba, M.; Tomura, S.; Tokioka, S.; et al. The influence of climate change on flood risk in Hokkaido. *Adv. River Eng.* **2018**, *24*, 391–396. (In Japanese).
32. Sasaki, H.; Murada, A.; Hanafusa, M.; Oh'izumi, M.; Kurihara, K. Reproducibility of present climate in a non-hydrostatic regional climate model nested within an atmosphere general circulation model. *SOLA*. **2011**, *7*, 173–176. DOI: 10.2151/sola.2011-044

33. Kanada, S.; Nakano, M.; Hayashi, S.; Kato, T.; Nakamura, M.; Kurihara, K.; Kitoh A. Reproducibility of maximum daily precipitation amount over Japan by a high-resolution non-hydrostatic model. *Scientific Online Letters on the Atmosphere*. **2008**. *4*, 105–108. DOI:10.2151/SOLA.2008- 027

Chapter 3

Assessing climate change impacts on extreme rainfall and severe flooding in the Ishikari River basin, Japan

Chapter 3

3.1.Introduction

The issues of climate change and its impacts on human life and natural environments are the most important challenges for scientists in this century [1]. According to the Fourth Assessment Report (AR4) of the United Nations Intergovernmental Panel on Climate Change (IPCC), severe natural disasters due to extreme climate have become more frequent since 2000 [2]. Approximately 80-90% of all recorded disasters from natural hazards during the past 10 years have caused by floods, droughts, tropical cyclones, heatwaves, and severe storms [3]. Among them, floods are the most frequent type of natural disaster on earth, causing enormous damage all over the world. Floods are considered as extreme weather events that occur frequently and cause severe damage [4,5]. Although several factors contribute to flooding, heavy or prolonged rainfall is considered the most critical factor that causes floods. Based on global climate model (GCM) simulations of the Coupled Model Intercomparison Project Phase 3 (CMIP3), it is evaluated that the frequency of heavy rainfall or the total rainfall amount from heavy rainfall is projected to increase in the 21st century over many regions in the world [2]. Moreover, the same assessment in The IPCC 5th Assessment Report [6], indicated that rainfall is expected to increase in Asia during future summer monsoon seasons, and extreme rainfall is likely to become more frequent. In the context of future global warming, the change rate of heavy rainfall amounts will increase more than that of annual mean rainfall [7,8,9]. Increasing rainfall, especially extreme rainfall, has enhanced the risk of floods in the future [10,11]. According to the World Health Organization (WHO) [3], floods can cause widespread devastation, and it affected more than 2 billion people worldwide from 1998 to 2017. People who live in floodplain areas, or non-resistant buildings, or lack warning early flood systems are the most affected by flooding. Flood disasters are becoming more frequent and higher intensity in the future [3].

In this context, future projections of extreme rainfall, and its impact on severe flood risk should be investigated for different regions in the world for the purpose of flood damage mitigation. In recent years, many researchers have attempted to predict extreme rainfall as well as severe floods for many river basins in the world to minimize flood damage [12,13, 14,15,16]. For example, in a study by Try et al. (2020) [12], the authors assessed the impacts of climate change on river flow in the Mekong River basin and flood inundation in the Lower Mekong basin using the Rainfall-Runoff-Inundation (RRI) model. The results indicated that flood magnitude in the Lower Mekong Basin will be severer by the end of the twenty-first century. The impact of climate change on flood inundation in a tropical river basin in Indonesia was also evaluated in a study by Yamamoto et al. (2021) [16]. The results showed that flooding will increase in this region. In particular, the flood inundation volume corresponding to a 20 year return period will increase by 3.3 times.

In Japan, extreme flood events from extreme rainfall have been recorded regularly in recent years. Japan often suffered enormous damage from short-term heavy rainfall [17]. For example, large-scale flooding due to heavy rainfall occurred during July 5-8, 2018 in western Japan, causing extensive damage over numerous prefectures and resulting in 224 deaths, 21,460 collapsed houses and 30,439 inundated houses. In the Oda River and its three tributaries, levees were breached at eight points due to the “backwater phenomenon” in which the tributary river floods synchronized with the main river flood [18]. Considering various climate change scenarios, several studies have predicted increased rainfall in the future [17,19]. Kim et al. (2010) [19] indicated that rainfall in Hokkaido is expected to increase by 6.1% and 10.6% in the near and extended future, respectively. Additionally, Yamada (2019) [20] reported that extreme rainfall will be more extensive under future climate conditions.

Attempts have been made to develop flood adaptation strategies to address the critical effects of climate change on the risk of river floods. Several studies have been conducted for the Japanese river basins [21,22,23]. For example, a study by Tachikawa et al. (2009) [22] indicated that severe rainfall would increase in the Yoshido River basin, and the peak flood discharge would increase to a greater extent in the future. Additionally, the trend of extreme rainfall events increasing in a short period of time should be considered. Sato et al. (2012) [21] indicated that climate change is projected to change river discharges significantly, especially in northern Japan.

Therefore, understanding the change in the amount of rainfall, especially considering future extreme rainfall events, and assessing its effect on the risk of river floods in vulnerable basins is necessary to create effective flood control plans. This study investigates the changes in the risk of river flooding associated with climate change in the

Ishikari River basin, a socioeconomically important basin in Hokkaido, Japan. This study is the first to assess the changes in extreme short-term rainfall and extreme river flooding events during the summer monsoon season in the Ishikari River basin as well as in its main sub-basins using an Integrated Flood Analysis System (IFAS) coupled with a large-ensemble rainfall dataset (d4PDF) with a high resolution of 5 km [24]. Additionally, the time differences between the time of peak discharge at the reference stations in each tributary and the time of peak water level at the confluence points in the main river are evaluated. The shorter the time difference, the greater the flood risk. These results will provide additional information about the effect of climate change on the risk of river floods, and thus guide climate change adaptation and flood damage mitigation strategies in vulnerable areas.

3.2. Methodology

3.2.1. Overview of the Ishikari River basin

The study area is the Ishikari River basin, which is located in Hokkaido, Japan. (Figure 3.1). The Ishikari River originates from Mt. Ishikari-dake (1,967 m above sea level) of the Taisetsuzan mountain range, flows through the west of Hokkaido, and then empties into the Ishikari Bay. The river flows through 48 municipalities (including Sapporo, the prefectural capital, which is located in the lower reaches of the river, and Asahikawa, the second-largest city, is located in the upstream region), accounting for roughly 52% of Hokkaido's population. At 268 km in length and with a drainage area of 14,330 km^2, the river is the longest river in Hokkaido and the second largest in terms of the basin area in Japan. This river basin plays an important role in socioeconomic in Hokkaido. The Ishikari plain located around the central and lower regions of the Ishikari River basin is the most productive agricultural area in Hokkaido. In addition, the Ishikari River is an important breeding ground for salmon, and salmon has been artificially hatched along the river for many years [25].

Playing an important role in economics and society in Hokkaido; however, the Ishikari River basin is frequently affected by severe floods, causing massive damage across this basin. For example, the largest flood event in this basin occurred in August 1981 and caused damages approximately JPY 115.2 billion, two fatalities, and 22,500 inundated houses entire Ishikari River basin. Recently, the flood in August 2016 caused damage of approximately 260 million USD and agricultural losses on 40,258 ha of land [26]. Therefore, the projection of flood risk is significant to reduce future flood damage in this basin. The Ishikari River basin includes seven main sub-basin: the Toyohira, Chitose, Yubari, Ikushunbetsu, Sorachi, Uryu, and Chubetsu River basins. Figure 3.1 shows the locations of the Ishikari River basin and its main sub-basins. Table 3.1 shows the characteristics of the Ishikari River basin and its main sub-basins and reference hydrological stations in each sub-basin.

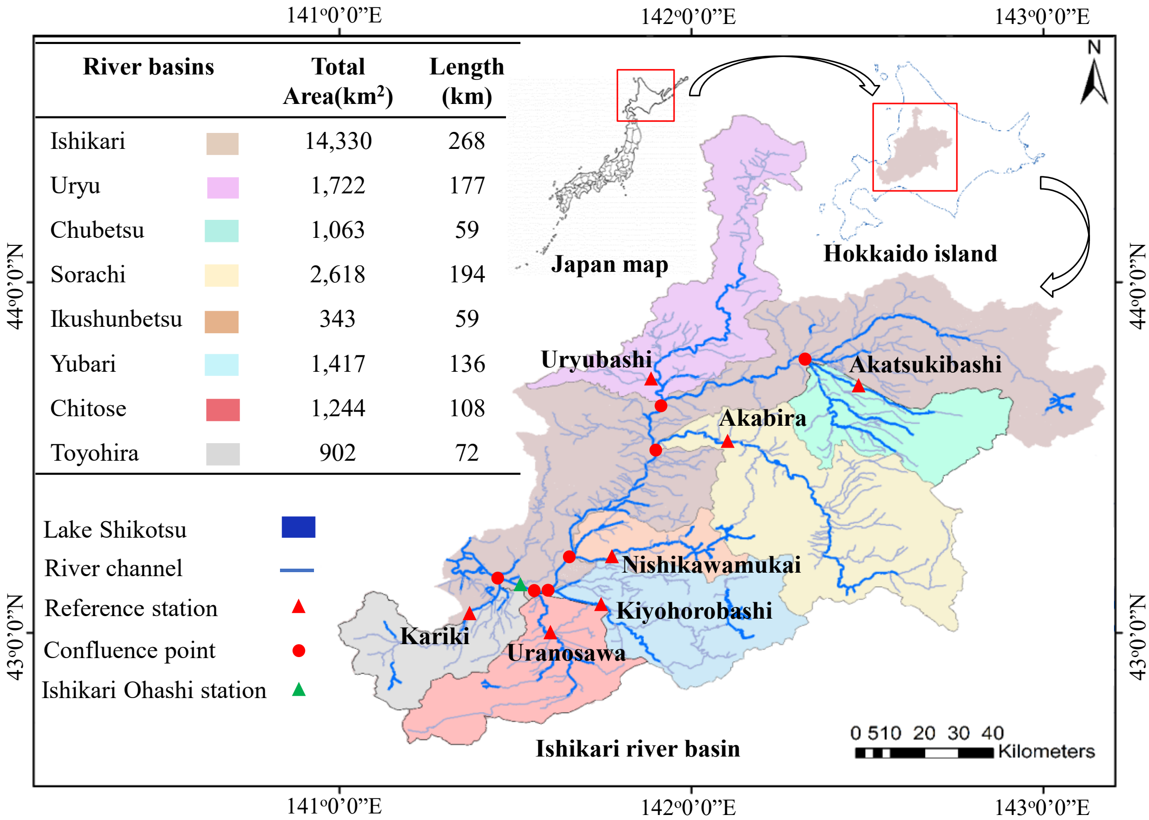

Figure 3.1. Ishikari River basin, Hokkaido, Japan and its main sub-basins

Table 3.1. Characteristics of the Ishikari River basin and its main sub-basins and reference hydrological stations in each sub-basin

River basin	Total Area (km^2)	Length (km)	Hydrological station
Ishikari	14,330	268	Ishikari Ohashi station
Toyohira	902	72	Kariki
Chitose	1,244	108	Uranosawa
Yubari	1,417	136	Kiyohorobashi
Ikushunbetsu	343	59	Nishikawamukai
Sorachi	2,618	194	Akabira
Chubetsu	1,063	59	Akatsukibashi
Uryu	1,722	177	Uryubashi

3.2.2. d4PDF dataset

In this study, the climate model used for the experiment was the large-ensemble climate simulations, which is known as the database for policy decision-making for future climate changes (d4PDF). The d4PDF was developed in 2015 for the main purpose is to become a standard in climate change risk assessments, thereby helping policymakers and managers in devising policies to minimize the damage caused by weather extreme events in Japan. In general, a large-ensemble database d4PDF was developed to assess future changes in extreme climate events occurring rarely, such as extreme rainfall and tropical cyclones [27]. The d4PDF consists data from numerous ensemble climate experiments with 60-km resolution on the global scale [28]. However, the low resolution is not suitable to evaluate the climate variables, especially extreme events in regional scale or basin scale, the regions were affected by local topography [28,29]. To address these problems, the Regional Climate Model (RCM) downscaling simulations are designed by the Meteorological Research Institute Non-hydrostatic Regional Climate Model (NHRCM). The RCM simulation covers Japan, the Korean Peninsula, and the eastern part of the Asian continent [28]. The RCM has a 20-km horizontal resolution. Three sets of experiments are performed by the RCM, as shown below:

- Historical climate simulation: 1951-2010, 50 members
- +2K future climate simulation: 2030-2091, 54 members
- +4K future climate simulation: 2051-2110, 90 members

The dataset spans 60 years (1951-2010) and 50 members (total: 3,000 events) for the historical climate simulation, and 60 years (2051-2110) and comprises 90 members (total: 5,400 events) for the +4K future climate simulation. The +4K future climate in which the global mean surface air temperature becomes 4°C warmer than the preindustrial climate, corresponding to that around the end of the twenty-first century under the representative concentration pathway 8.5 scenarios of CMIP5 [28].

This study used the d4PDF downscaled rainfall data with 5-km super high-resolution from a previous study [24]. The 5-km resolution rainfall data were downscaled from 20-km resolution data via the non-hydrostatic regional climate model [30]. The target period for downscaling was set to 15 days of maximum rainfall for each event in Hokkaido for 3,000 historical simulation events and 5,400 future simulation events [24,31]. After downscaling, the rainfall amount, hourly rainfall intensity, and spatiotemporal distributions of rainfall were similar to those of the recorded rainfall events (Figure3.2). Additionally, the downscaled results can represent the topography of the study area more precisely [24]. These results suggest that the dataset after downscaling can be used to assess the impacts of climate change on a regional scale and basin scale.

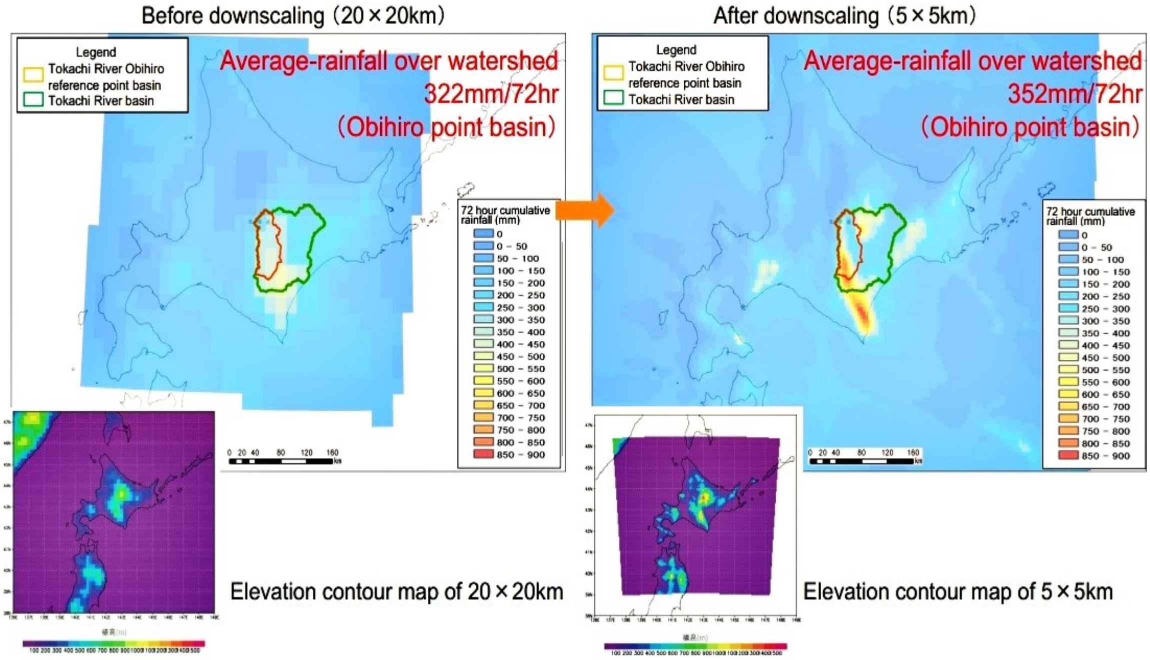

Figure 3.2. +4K future climate simulation for the Tokachi River basin at Obihiro point station with the rainfall data of 20-km resolution (left) and 5-km resolution (right) [24]

In this study, we selected the rainfall data for locations within the Ishikari River basin. Then, we chose the annual maximum rainfall (mm/72 h) for evaluating the change in short-term extreme rainfall and its impact on river flooding between the historical and future simulations in the Ishikari River basin. According to the report of Japan River Association, (2003) [25], the degree of safety for the Ishikari River in Hokkaido was set as 1/150, giving a return period of 150 years. Therefore, this study focused on assessing the severe river flooding events for the top 20 and the top 36 rainfall events out of 3,000 and 5,400 rainfall events corresponding to return period equal to or more than 150 years for the historical and future simulations, respectively.

3.2.3. Overview of the Integrated Flood Analysis System (IFAS) model

Integrated Flood Analysis System (IFAS) model is developed by the International Centre for Water Hazard and Risk Management (ICHARM). IFAS is a concise tool kit with a Graphic User Interface for building Distributed Rainfall-Runoff analysis model. The IFAS uses a Public Works Research Institute (PWRI) – distributed hydrological model developed in the 1990s [32] as the runoff simulation engine [33].

There are great expectations for flood forecasting and early flood warning systems to mitigate flood damage, especially in insufficiently gauged river basins. However, there are several challenges when developing a rainfall-runoff system for these purposes as follows:

- It requires high-level knowledge of civil engineering and computer skills to model a Hydrological model
- It requires a significant budget
- Because of the lack of long-term historical hydrological data, it is difficult to project the river discharge.

As a result, the IFAS model was designed with user-friendly graphic interfaces for data input, data output, model building modules, parameters setting functions, evaluating flood risk can be possible, even in poorly gauged river basins [33]

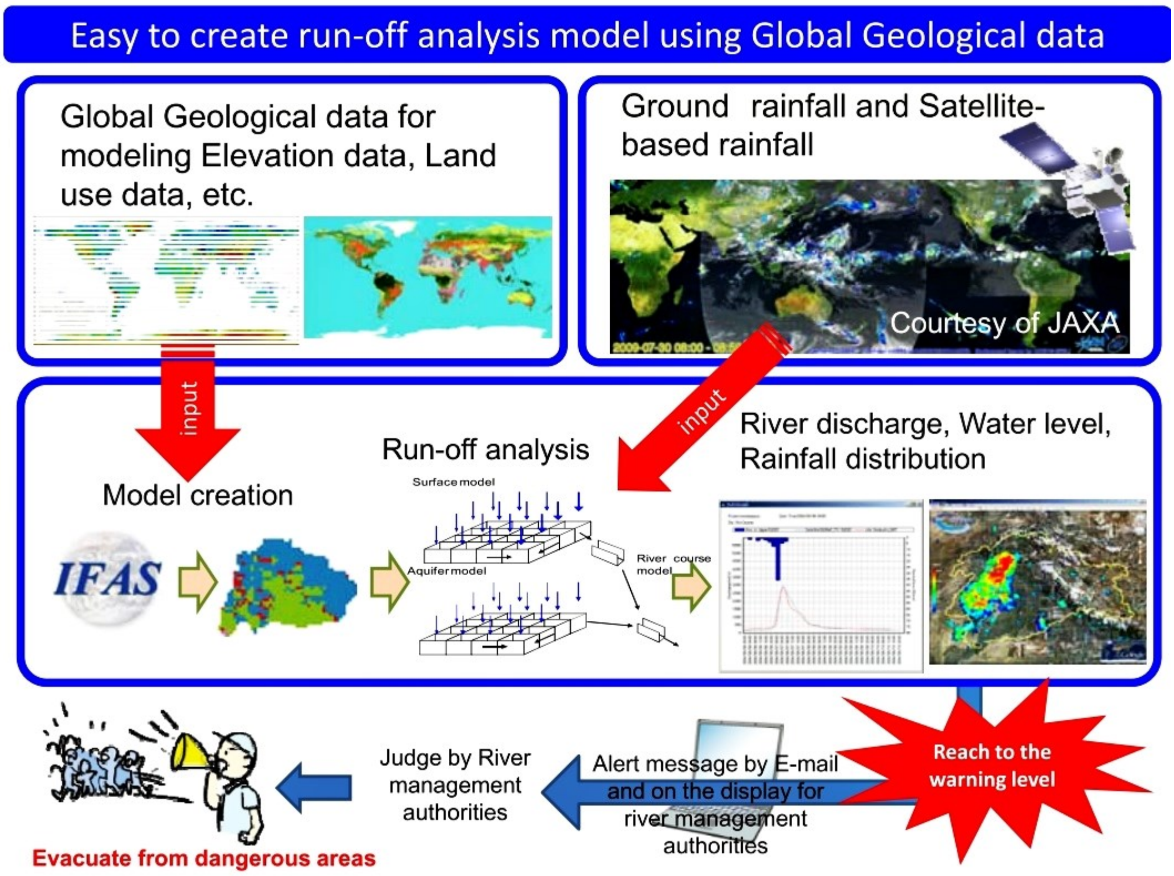

Figure 3.3. Functions of IFAS model [33]

IFAS model has features as below [33]:

- The outflow from each cell is calculated by non-linear relationships based on the tank model philosophy.
- Parameters can be estimated by using grid-based global data sets on topography, soil, geology, land use.
- The storage function runoff model enhances flood reproducibility by modifying saturation rainfall for each flood event. However, it is difficult to forecast saturation rainfall before the flood. PWRI-DHM adopts a nonlinear 2 or 3 layer tank structure. This can solve the problem to modify the parameters for each flood event. As a result, this model does not need to estimate saturation rainfall of future flood events, and this is best used as a flood forecasting model.
- If an actual flood event is reproduced by the storage function method, its reproducibility of floods is not enough in medium/ small size floods in general. This is because the storage function method is a non-linearly 1 layer tank model and it is difficult to reproduce both heavy and medium/small size floods by the same parameters since the characteristics of the runoff phenomenon are different from each other. In PWRI Distributed hydrological model enhances its reproducibility to medium/small size floods by adopting a nonlinear 2 or 3 layer tanks structure.
- For numerical calculation, PWRI-DHM does not use convergence calculation to solve the differential equation. It uses approximation functions to solve the time integral equation. For this reason, the system can conduct numerical calculations smoothly and realize for real-time operation.
- To calculate discharge in the river course tank, PWRI-DHM solves the Kinematic Wave equation. Moreover, PWRI-DHM Ver 2 adopts 2 layer tanks vertically.

The concept of the IFAS model shown in the table below:

Table 3.2. Model configuration [33]

Model	Functions
Surface tank model	Infiltration to unsaturated layer, surface runoff, surface storage, evapotranspiration, rapid
Unsaturated tank model	Infiltration to aquifer, subsurface runoff, subsurface storage, low intermediate outflow
Aquifer tank model	Outflow from aquifer, aquifer loss
River tank model	River course discharge

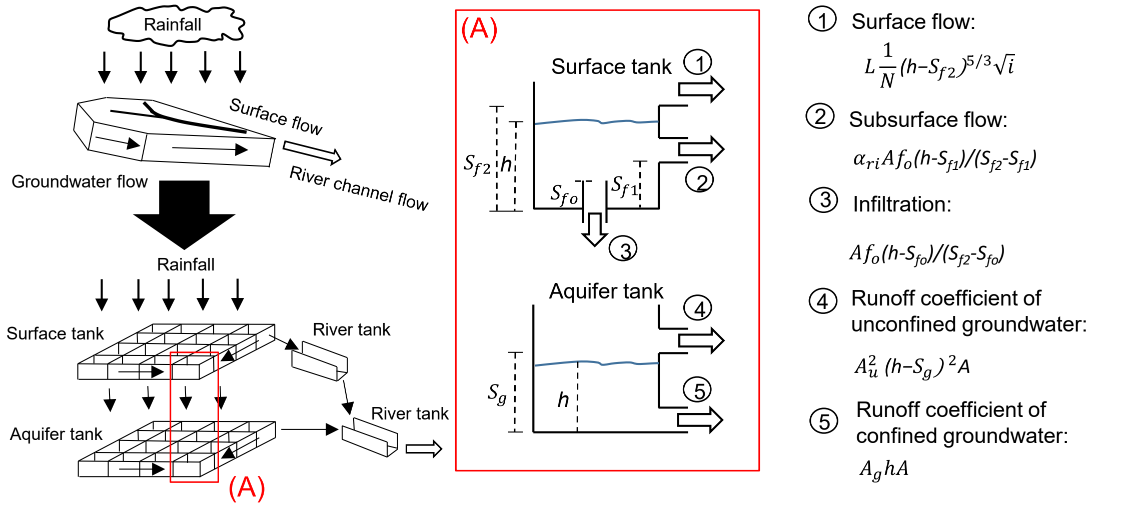

L: length of the cell (m), *N*: roughness coefficient of surface ($m^{-1/3}s$), *h*: height of stored water (m), S_{f2}: maximum storage height (m), *i:* gradient of slope, α_{ri}: regulation coefficient for rapid intermediate flow, *A*: area of the cell (m^2), f_o: final infiltration capacity (cm/s), S_{f1}: rapid intermediate flow (m), S_{fo}: height where ground infiltration occurs (m), A_u: runoff coefficient of slow intermediate outflow $(1/mm/day)^{1/2}$, *Sg*: height where slow intermediate outflow occurs (m), A_g: coefficient of base outflow (1/day) (ICHARM, 2014)

Figure 3.4. Schematic of the IFAS model [33]

IFAS is a GUI for building a distributed rainfall-runoff analysis model for any river basin. IFAS was designed as a concise tool kit for building a Rainfall-Runoff analysis model able to perform the following functions:

(1) Import of geospatial data according to cell size and coordinate set function
(2) Edition of rainfall data set function
(3) Parameter setting function
(4) Execution of Rainfall-Runoff analysis function
(5) Output result function

The IFAS model can reproduce rainfall distribution and water gathering process on the surface and underground into river course. The hydrological model does not have an analysis function to reproduce overtopping from river course and inundation. Therefore, the distributed tank functioned hydrological model is applicable for Rainfall-Runoff analysis until overtopping of river flows.

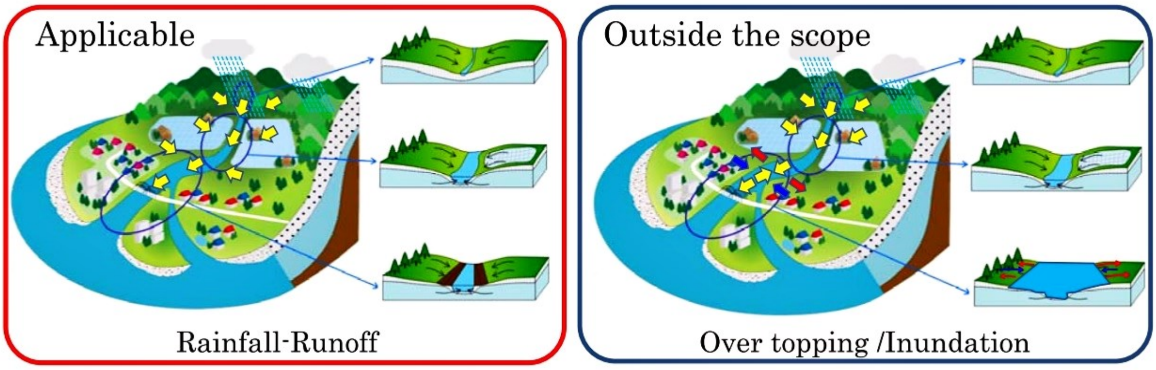

Figure 3.5. Applicable/Outside the scope Phenomenon for IFAS [33]

The IFAS model has been used to estimate the flood risk for many river basins globally and has demonstrated good simulation performance [34,35,36,37]. For example, in the study by Kimura et al. (2018) [35], the impact of the typhoons on floods and changes in future floods in the Tokachi River basin, located in eastern Hokkaido using the IFAS model. The results of the simulation with a simple assumed future climate (with higher precipitation) indicated that future river floods are expected to increase with an increase in precipitation in the Tokachi River basin. In another study, an attempt has been made to develop the nonstructural countermeasures for the downstream reach of the Indus River, Pakistan to mitigate the flood damage. The authors concluded that the IFAS model is practically helpful for the flood early warning and to save the lives and properties damages [34]

The flowchart of the procedure for flood simulation by the IFAS model is shown in Figure 3.6 below:

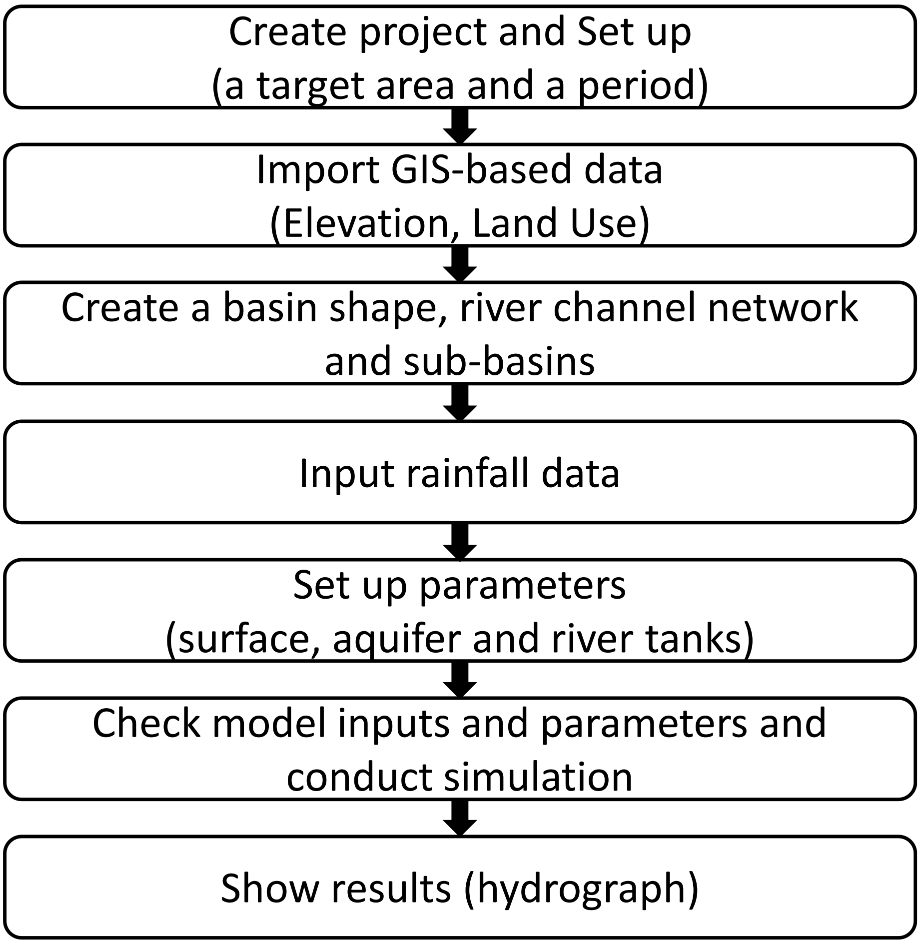

Figure 3.6. Flowchart of the procedure for flood simulation by the IFAS model

3.2.4. Data inputs

For hydrological simulation, the required IFAS input data are elevation, land-use, and rainfall data. The elevation data were obtained from a global digital elevation model (GTOPO30). GTOPO30 is a global data set covering the full extent of latitude from 90 degrees South to 90 degrees North, and the full extent of longitude from 180 degrees West to 180 degrees East. The horizontal grid is 30 arc-second (approximately 1 km). In addition, the land-use data with 30 arc-second (approximately 1 km) resolution is Global Land Cover Characterization (GLCC). GLCC was provided by the U.S. Geological Survey (USGS). The elevation data and the land-use data were shown in Figure 3.7.

In this study, the flood event in August 1981 was used to calibrate the hydrological model. The historical flood events in September 2001, September 2011, and August 2016 were chosen to validate the model. These four extreme flood events were large-scale historical flood events that caused severe damage in the Ishikari River basin. In particular, the flood event in August 1981 was the largest flood event observed in the target basin. The rainfall data for the August 1981 flood were obtained from rain gauge stations provided by the Hokkaido Regional Development Bureau. The rainfall data for the September 2001, September 2011, and August 2016 flood events, and the observed river discharges for the calibration and validation processes were obtained from the Ministry of Land, Infrastructure and Transport, Japan (MLIT) [38]. Additionally, the observed annual maximum rainfall (mm/ 72h) (1926-2018) for the Ishikari River basin was provided by the Sapporo Development and Construction Department, MLIT.

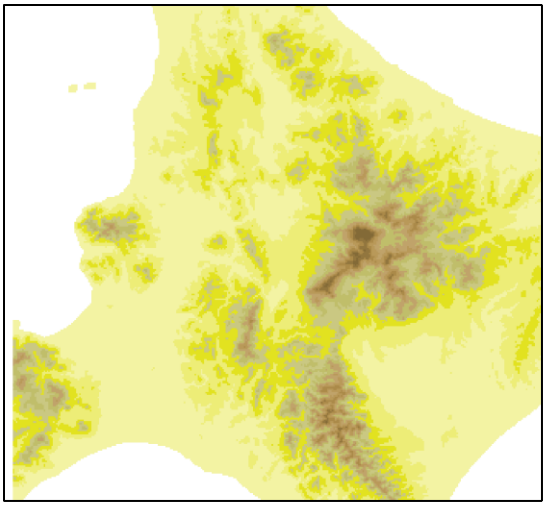

Elevation data

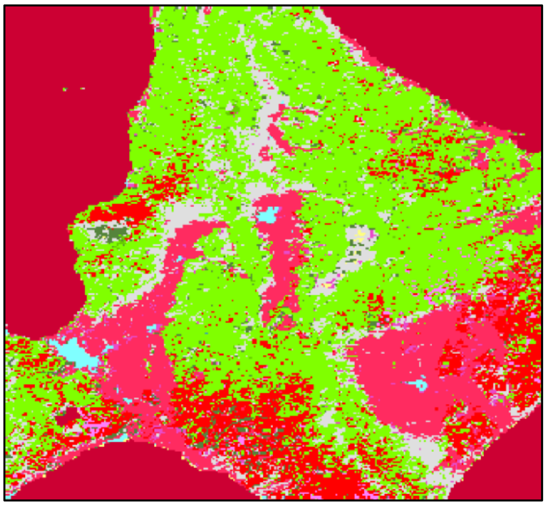

Land-use data

Figure 3.7. Elevation data and Land-use data

3.2.5. Analytical procedure

In this chapter, we assessed the effect of climate change on extreme rainfall and severe river flooding in the Ishikari River basin using the following steps. First, the IFAS model was calibrated and validated against historical flood events. Next, future changes in extreme rainfall were estimated based on a large ensemble rainfall dataset d4PDF with a super high-resolution of 5 km. The Student's t-test was used to find a significant difference between the two sets of samples (observed rainfall data and rainfall data obtained from the historical simulation). The hypothesis of the test is stated as follows.

H_o: $\mu_1 = \mu_2$

H_1: $\mu_1 \neq \mu_2$

Here, μ_1 and μ_2 are the means of the observed rainfall data and rainfall data obtained from the historical simulation, respectively. The null hypothesis is rejected if the *p*-value is less than the significance level α of 0.05. Additionally, the Student's t-test was used to find the significant difference between the two sets of samples (historical and future simulations); the hypothesis of this test is stated as follows.

H_o: $\mu_2 \leq \mu_1$

H_1: $\mu_2 > \mu_1$

Here, μ_1 and μ_2 are the means of annual maximum rainfall (mm/ 72h) in the historical and future simulations, respectively. The null hypothesis is rejected if the *p*-value is less than the significance level α of 0.05.

Then, future changes in extreme rainfall between the top 20 and top 36 rainfall events were evaluated for the Ishikari River basin and in its main sub-basins. After that, the IFAS model was calibrated using the flood event in August 1981. The flood events in September 2001, September 2011, and August 2016 were chosen to validate the model. The simulations were conducted for an additional period of two weeks prior to the main period of flooding events for model warmup and to allow time for the water to reach the downstream area. We calculated the river discharge at the Ishikari Ohashi station, which is approximately 26.6 km upstream from the river mouth (Figure 3.1).

To quantitatively evaluate the performance of the IFAS for the historical flood events, we used the Nash-Sutcliffe coefficient (*NSE*) [39] and the three indices of wave shape error (E_w), volume error (E_v), and peak discharge error (E_p) [34,40], defined as follows.

$$NSE = 1 - \frac{\sum_{i=1}^{n}\left[Q_{M(i)} - Q_{C(i)}\right]^2}{\sum_{i=1}^{n}\left[Q_{M(i)} - Q_{AVG(i)}\right]^2} \tag{1}$$

$$E_w = \frac{1}{n}\sum_{i=1}^{n}\left[\frac{Q_{M(i)} - Q_{C(i)}}{Q_{M(i)}}\right]^2 \tag{2}$$

$$E_v = \frac{\sum_{i=1}^{n} Q_{M(i)} - \sum_{i=1}^{n} Q_{C(i)}}{\sum_{i=1}^{n} Q_{M(i)}} \tag{3}$$

$$E_p = \frac{Q_{MP} - Q_{CP}}{Q_{MP}} \tag{4}$$

Here, Q_M: observed discharge (m^3/s); Q_c: simulated discharge (m^3/s); n: number of data points; Q_{AVG}: average observed discharge (m^3/s); Q_{MP}: peak value of the observed discharge (m^3/s); and Q_{CP}: peak value of the simulated discharge (m^3/s). The simulation model is acceptable if $NS > 0.7$; and the smaller the E_w, E_v, and E_p errors are, the better the model is.

After validation, the IFAS model was used to estimate the river discharge at 8 reference stations located in the Ishikari River basin, in its main sub-basins, and 7 confluence points (Figure 3.1) for the top 20 and top 36 rainfall events. Changes in extreme river flooding between the top 20 and top 36 rainfall events in the Ishikari River basin and in its main sub-basins were investigated. Finally, the differences between the time of peak discharge at the reference station in each tributary and the time of peak water level at the confluence point in the main river were evaluated. The average values of the time differences over all the flood events in each of the sub-basins were estimated and compared between the top 20 and top 36 rainfall events.

3.3. Results and discussion

3.3.1. Hydrological model calibration and validation

Table 3.3 shows the parameter value settings in the IFAS model after calibration and validation.

Table 3.3. Parameter value settings in the IFAS model

Surface tank parameters							
Parameter	Final infiltration capacity (f_o, cm/s)	Maximum storage height (S_{f2}, m)	Rapid intermediate flow (S_{f1}, m)	Height where ground infiltration occurs (S_{f0}, m)	Surface roughness coefficient (N, m$^{-1/3}$s)	Rapid intermediate flow regulation coefficient (α_{ri})	Initial storage height (m)
1	0.0001	0.1	0.01	0.005	0.7	0.8	0
2	0.00001	0.05	0.01	0.005	2	0.6	0
3	0.00001	0.05	0.01	0.005	2	0.5	0
4	0.00001	0.001	0.0005	0.0001	0.1	0.9	0
5	0.000001	0.05	0.01	0.005	2	0.5	0

Aquifer tank parameters				
Parameter	Regulation coefficient of slow intermediate outflow (A_u, (1/mm/day)$^{1/2}$)	Coefficient of base outflow (A_g, 1/day)	Height where slow intermediate outflow occurs (S_g, m)	Initial storage height of groundwater tank (m)
1	0.1	0.003	2	2
2	0.11	0.003	2	2
3	0.12	0.003	2	2
4	0.13	0.003	2	2

River tank parameters										
Parameter	Constant of the Resume Law (c)	Constant of the Resume Law (s)	Manning roughness coefficient of channel (n, m$^{-1/3}$s)	Initial water table of river channel (m)	Infiltration of aquifer tank (1/day)	Coefficient of cross shape (*RHW*)	Coefficient of cross shape (*RHS*)	Coefficient of cross shape (*RBH*)	Coefficient of cross shape (*RBET*)	Coefficient of cross shape (*RLCOF*)
1	7	0.5	0.035	0.2	0	9999	1	0.5	0.05	1.4
2	7	0.5	0.035	0.2	0	9999	1	0.5	0.05	1.4
3	7	0.5	0.035	0.2	0	9999	1	0.5	0.05	1.4

* Note: Surface tank: 1,2,3,4,5 - Classification of Land-use
Aquifer tank: 1,2,3,4 - Classification of Geology
River tank : 1,2,3 – The number of upper cells (n)
1: ($n \leq 4$), 2: ($5 < n < 64$), 3: ($n \geq 65$)

Figure 3.8(a) compares the simulated discharges and observed discharges for the flood event of August 1981 after calibration. Figure 3.8 (b), (c), and (d) compare the simulated discharges and observed discharges in the validation process for flooding events in September 2001, September 2011, and August 2016, respectively. The model calibration was performed using a "trial and error" process. As shown in Figure 3.8, the IFAS closely reproduced the flood duration and peak discharge in most cases. For the August 1981 flood, the simulated discharges showed close agreement with the observed discharges, as indicated by a high *NSE* value of 0.95, an E_w of 0.08, E_v of 0.04, and E_p of -0.01.

In the validation process, the simulated discharges matched well with the observed discharges for September 2001, September 2011, and August 2016 floods, with high *NSE* values of 0.96, 0.92, and 0.90, respectively. The simulated peak discharges were evaluated to be slightly lower than the observed peak discharges for the September 2011 and August 2016 flood events. However, the statistical performance indices suggested good performance for all cases. The detailed indicators are shown in Table 3.4. These results suggest that the IFAS model can perform reasonably well for the Ishikari River basin.

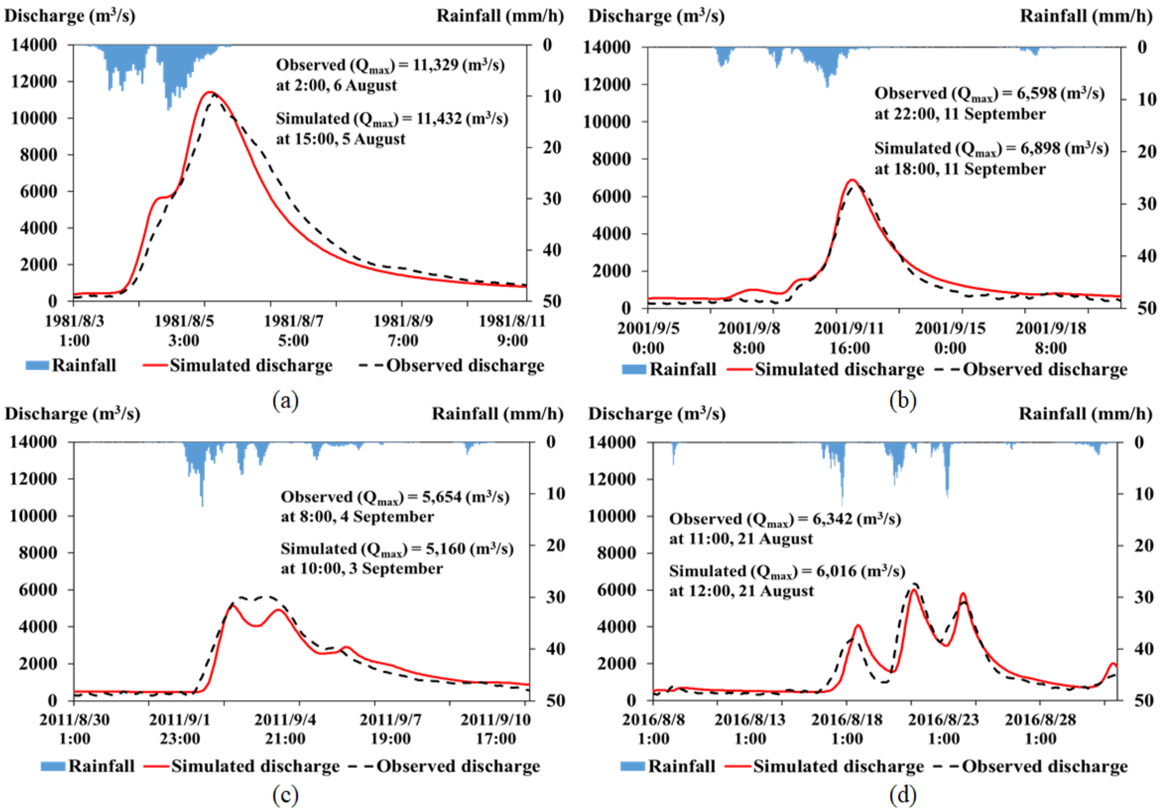

Figure 3.8. Comparison of observed and simulated discharges at Ishikari Ohashi station for the (a) 1981 flood event, (b) 2001 flood event, (c) 2011 flood event, (d) 2016 flood event

Table 3.4. Performance of the IFAS model in the Ishikari River basin

	Flood events	Nash coefficient (*NSE*)	Wave shape error (E_w)	Volume Error (E_v)	Peak Discharge Error (E_p)
Calibration	August 1981	0.95	0.08	0.04	-0.01
	September 2001	0.96	0.38	-0.16	-0.05
Validation	September 2011	0.92	0.08	0.03	0.09
	August 2016	0.90	0.11	-0.01	0.05

3.3.2. Future changes in extreme rainfall

Figure 3.9 shows the relative frequency of annual maximum rainfall (mm/ 72h) in the Ishikari River basin for the observed rainfall data, the historical and future simulations. The results indicate that the annual maximum rainfall (mm/ 72h) in the historical simulation and the rainfall amount (mm/ 72 h) from the observation data have simular frequencies. The result from Student's t-test demonstrates a p-value of 0.214, which exceeds α. This result implies that the mean of the observed rainfall data is similar to the mean of rainfall data obtained from the historical simulation.

Addition, the rainfall amount is projected to increase significantly in the future. The mean value of the rainfall amount in the future simulation is 86.3 (mm/ 72h), which is 1.13 times that in the historical simulation (76.6 mm/ 72h). The Student's t-test result shows that the p-value is less than 2.2 x 10^{-6}, i.e. much smaller than 0.05. This adequately proves that validity of H_1. Therefore, the frequency and magnitude of extreme rainfall are expected to increase in the future.

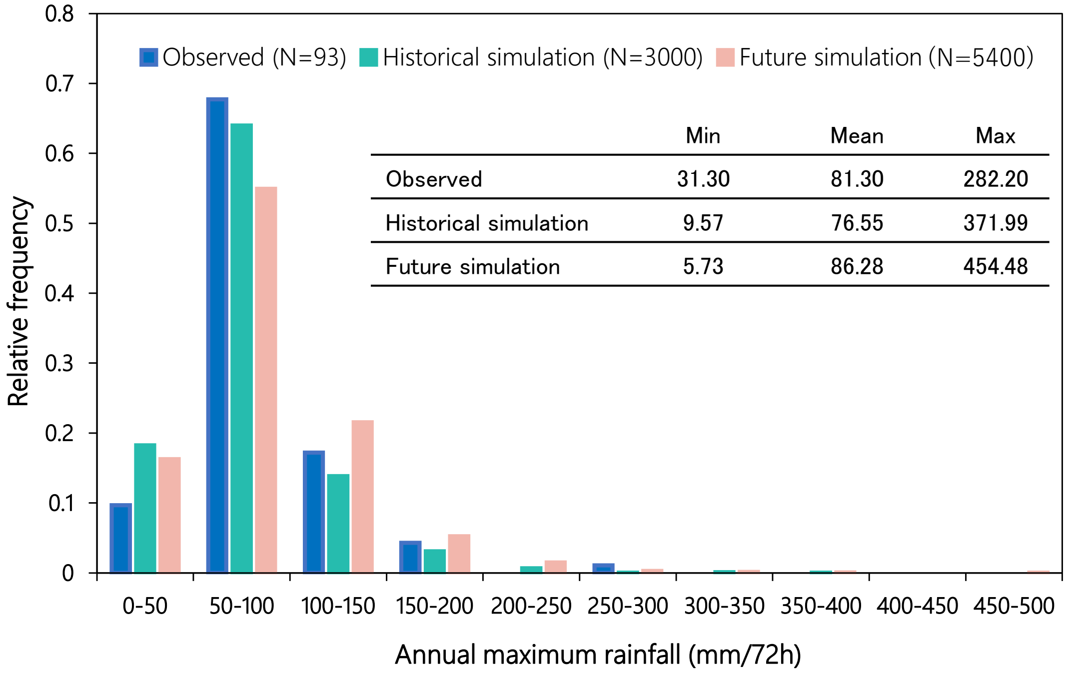

Figure 3.9. Relative frequency of annual maximum rainfall (mm/ 72h) in the Ishikari River basin for the observed rainfall data, and the historical and future simulations

3.3.3. Future changes in extreme rainfall between the top 20 and top 36 rainfall events

Table 3.5 and Table 3.6 show the annual maximum rainfall (mm/ 72h) for the top 20 and top 36 rainfall events in the Ishikari River basin and in its main sub-basins.

Table 3.5. Top 20 rainfall events in the Ishikari River basin and in its main sub-basins

No.	Name of the event	Annual maximum rainfall (mm/72h)							
		Ishikari River basin	Toyohira River basin	Chitose River basin	Yubari River basin	Ikushunbetsu River basin	Sorachi River basin	Uryu River basin	Chubetsu River basin
1	HPB_m043_2006	**372***	**545***	**621***	423	394	258	**406***	228
2	HPB_m004_1957	346	346	525	**514***	**413***	**418***	148	349
3	HPB_m063_1968	314	343	382	415	397	335	293	242
4	HPB_m010_1976	303	236	124	218	337	276	229	**480***
5	HPB_m089_2002	254	127	336	362	364	276	124	301
6	HPB_m065_2007	244	211	259	299	268	249	176	267
7	HPB_m086_1988	238	296	156	354	402	251	60	366
8	HPB_m045_1957	237	226	290	347	290	282	142	217
9	HPB_m004_2000	234	268	330	234	187	242	222	174
10	HPB_m007_1970	233	330	397	274	263	209	167	191
11	HPB_m005_2005	221	242	228	255	277	252	113	254
12	HPB_m084_1955	220	344	243	213	196	166	253	145
13	HPB_m088_1955	218	246	280	237	256	166	235	184
14	HPB_m006_1994	216	246	209	222	241	220	188	185
15	HPB_m061_1964	214	194	256	246	230	206	182	238
16	HPB_m064_1987	211	175	209	238	204	283	144	267
17	HPB_m024_1996	208	148	173	248	198	231	208	225
18	HPB_m025_1962	207	105	167	209	200	194	190	256
19	HPB_m046_1980	206	287	282	236	172	190	143	229
20	HPB_m043_1995	204	227	209	261	232	219	196	203

Note: (*) The maximum rainfall event (mm/72h)

Table 3.6. Top 36 rainfall events in the Ishikari River basin and in its main sub-basins

No.	Name of the event	Annual maximum rainfall (mm/72h)							
		Ishikari River basin	Toyohira River basin	Chitose River basin	Yubari River basin	Ikushunbetsu River basin	Sorachi River basin	Uryu River basin	Chubetsu River basin
1	HFB_MP_m112_2062	**454***	184	418	**719***	656	567	343	487
2	HFB_MI_m108_2094	**454***	454	400	644	**751***	**707***	112	**502***
3	HFB_GF_m110_2052	386	242	454	706	505	525	130	432
4	HFB_GF_m104_2072	373	208	375	401	479	368	353	358
5	HFB_MR_m102_2062	356	276	279	273	455	350	332	419
6	HFB_HA_m102_2065	345	248	394	462	495	333	328	298
7	HFB_CC_m114_2085	331	357	380	517	406	400	169	329
8	HFB_MI_m103_2103	325	560	426	152	230	144	**600***	135
9	HFB_MI_m106_2059	315	392	449	308	304	282	333	254
10	HFB_MP_m101_2067	311	483	420	325	336	318	234	251
11	HFB_MI_m106_2083	305	262	321	367	387	317	229	278
12	HFB_CC_m107_2084	304	188	243	338	340	290	330	311
13	HFB_HA_m102_2067	301	131	163	251	340	349	229	368
14	HFB_MR_m105_2091	300	**894***	**723***	222	241	187	220	131
15	HFB_GF_m112_2053	296	351	341	308	338	254	272	269
16	HFB_HA_m102_2105	288	430	462	349	317	180	368	156
17	HFB_MR_m111_2066	287	358	295	356	330	338	136	290
18	HFB_MI_m107_2060	279	122	326	502	351	387	91	360
19	HFB_MP_m103_2078	271	665	537	241	213	312	218	178
20	HFB_MI_m114_2085	270	248	319	296	352	332	201	186
21	HFB_MP_m114_2070	270	378	382	322	336	270	145	264
22	HFB_MI_m113_2099	269	275	311	131	306	238	264	287
23	HFB_GF_m110_2066	266	418	334	260	235	229	253	224
24	HFB_MI_m115_2063	259	315	567	394	456	206	69	187
25	HFB_MI_m102_2060	258	106	219	360	274	285	218	286
26	HFB_GF_m108_2052	256	117	353	418	421	301	86	306
27	HFB_HA_m115_2103	255	323	377	349	223	253	193	227
28	HFB_GF_m111_2109	254	37	44	102	146	212	338	376
29	HFB_MI_m113_2110	248	142	118	222	338	276	187	452
30	HFB_GF_m112_2102	244	101	324	358	392	235	232	195
31	HFB_MR_m102_2074	242	279	280	260	322	238	200	208
32	HFB_MI_m101_2083	241	300	326	299	451	348	80	217
33	HFB_HA_m104_2082	239	394	368	265	269	158	230	139
34	HFB_HA_m101_2066	238	304	368	330	253	262	160	161
35	HFB_HA_m105_2083	236	305	291	247	236	188	278	190
36	HFB_CC_m110_2051	234	201	226	305	295	248	174	239

Note: (*) The maximum rainfall event (mm/72h)

Figure 3.10 shows the boxplots of annual maximum rainfall (mm/ 72h) for the top 20 and top 36 rainfall events in the Ishikari River basin and in its main sub-basins. In addition, the percentage difference in the median value of annual maximum rainfall (mm/ 72h) between the top 20 and top 36 rainfall events for the Ishikari River basin and in its main sub-basins is shown in Figure 3.11. It is shown that the median 72-h value in the Ishikari River basin is projected to be 21% higher in the future. It can be seen that extreme rainfall is expected to increase significantly not only in the Ishikari River basin but also in its main sub-basins. The extreme rainfall is projected to increase the most in the Chitose, Ikushunbetsu, and Yubari River basins located in the southern part of the Ishikari River basin, with an estimated increase of 35%, 30%, and 39%, respectively. Moreover, the spatial distributions of annual maximum rainfall (mm/ 72h) averaged for the top 20 and top 36 rainfall events, and the percentage difference between the selected historical and future events are shown in Figure 3.12. These results also indicate that the increase in extreme rainfall is expected to be particularly significant in the Ikushunbetsu and Chitose River basins.

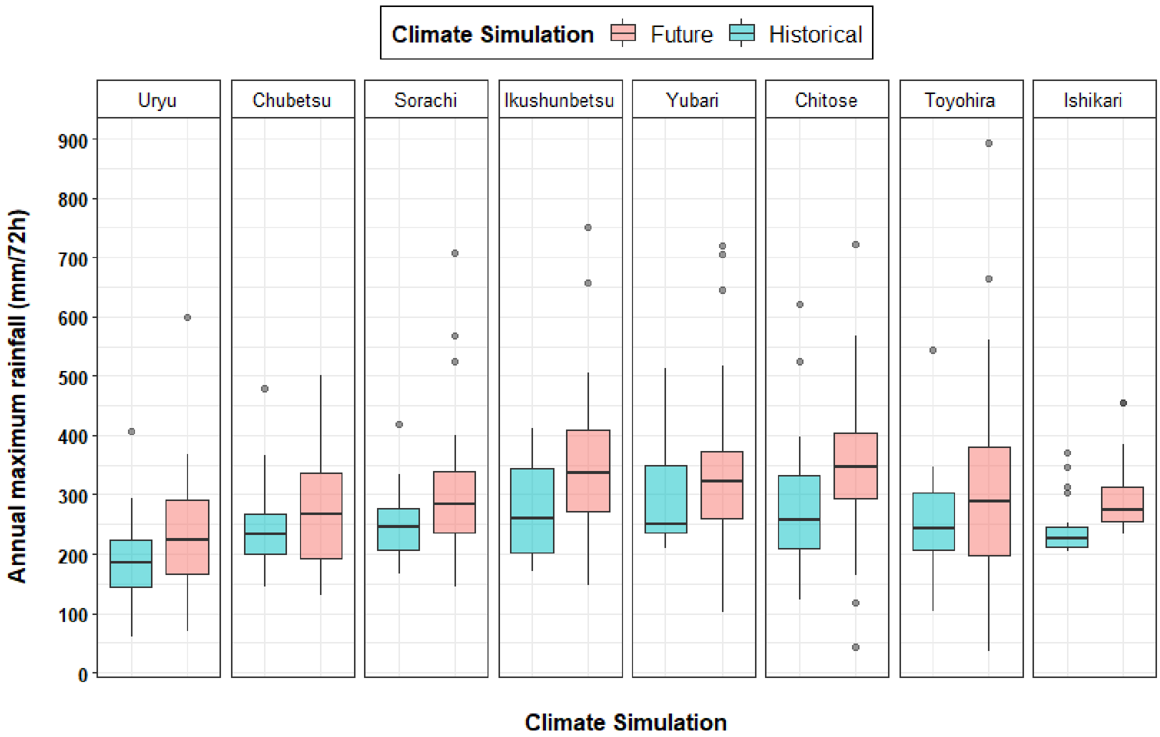

Figure 3.10. Boxplots of annual maximum rainfall (mm/ 72h) for the top 20 and top 36 rainfall events in the Ishikari River basin and in its main sub-basins

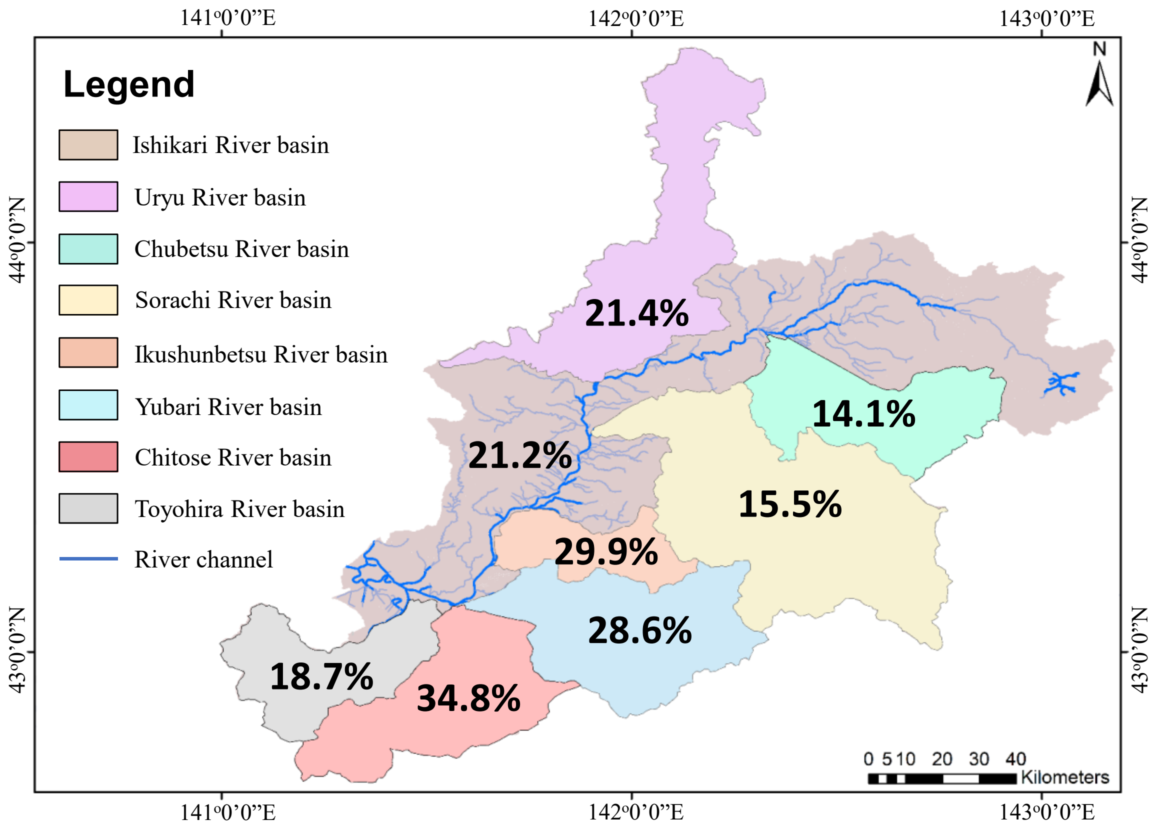

Figure 3.11. Percentage difference in the median of annual maximum rainfall (mm/ 72h) between the top 20 and top 36 rainfall events

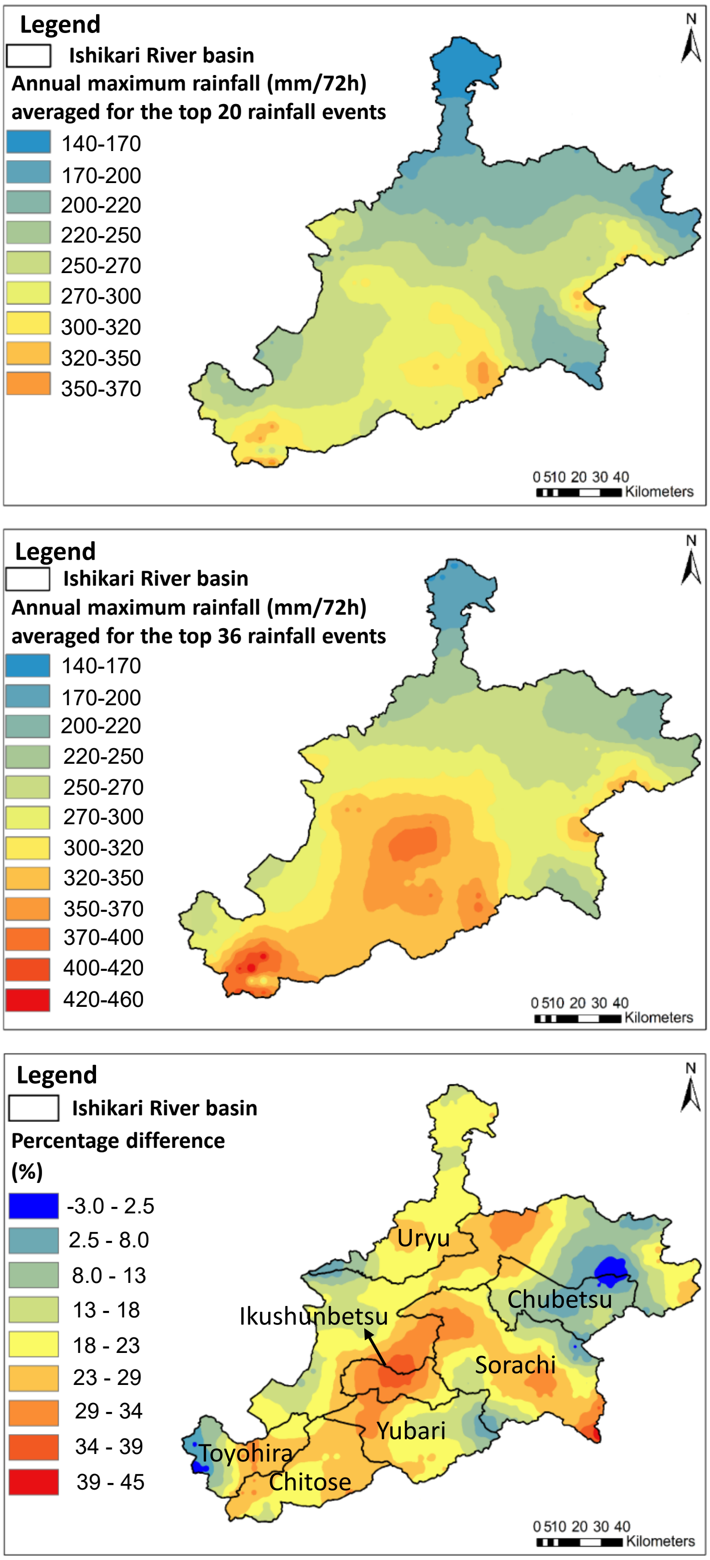

Figure 3.12. Spatial distribution of annual maximum rainfall (mm/ 72h) averaged for the (a) top 20 rainfall events and (b) top 36 rainfall events; (c) percentage difference between the selected historical and future events

3.3.4. Future changes in river floods between the top 20 and top 36 rainfall events

Table 3.7 and Table 3.8 show the results of peak discharge for the top 20 and top 36 rainfall events at 8 reference stations in the Ishikari River basin and in its main sub-basins.

Table 3.7. Peak discharge results for the top 20 rainfall events in the Ishikari River basin and in its main sub-basins

No.	Name of the event	Peak discharge Q_{max} (m^3/s)							
		Ishikari River basin	Toyohira River basin	Chitose River basin	Yubari River basin	Ikushunbetsu River basin	Sorachi River basin	Uryu River basin	Chubetsu River basin
1	HPB_m043_2006	13,905	2,629	**3,575***	2,038	643	1,936	**2,614***	552
2	HPB_m004_1957	**19,386***	1,076	3,447	**3,664***	965	**5,726***	800	959
3	HPB_m063_1968	13,463	1,244	1,580	2,859	940	3,667	1,600	630
4	HPB_m010_1976	18,926	822	237	539	564	3,652	1,678	**2,607***
5	HPB_m089_2002	11,566	190	1,453	1,543	1,007	2,692	354	1,093
6	HPB_m065_2007	12,143	560	972	2,184	446	3,306	1,073	1,179
7	HPB_m086_1988	10,157	1,690	426	1,331	**1,142***	2,984	208	1,457
8	HPB_m045_1957	8,381	510	1,214	1,826	489	2,835	708	637
9	HPB_m004_2000	10,791	1,106	2,774	1,095	204	2,385	1,413	391
10	HPB_m007_1970	12,007	2,162	2,814	1,799	760	2,898	776	781
11	HPB_m005_2005	6,900	738	845	806	482	2,039	393	607
12	HPB_m084_1955	8,982	**2,982***	1,365	731	231	1,146	2,344	309
13	HPB_m088_1955	10,615	1,526	2,057	1,468	612	1,745	1,937	700
14	HPB_m006_1994	9,894	585	670	869	415	2,727	1,181	483
15	HPB_m061_1964	7,641	521	1,687	873	292	1,679	958	680
16	HPB_m064_1987	6,547	271	457	735	192	2,647	595	788
17	HPB_m024_1996	9,309	265	503	1,426	224	3,375	1192	883
18	HPB_m025_1962	9,947	205	685	1,125	303	2,172	1,940	797
19	HPB_m046_1980	8,023	1,453	1,676	951	173	1,540	649	800
20	HPB_m043_1995	6,707	543	956	1,012	320	1,728	901	418

Note: (*) The greatest peak discharge event (m^3/s)

Table 3.8. Peak discharge results for the top 36 rainfall events in the Ishikari River basin and in its main sub-basins

No.	Name of the event	Peak discharge Q_{max} (m^3/s)							
		Ishikari River basin	Toyohira River basin	Chitose River basin	Yubari River basin	Ikushunbetsu River basin	Sorachi River basin	Uryu River basin	Chubetsu River basin
1	HFB_MP_m112_2062	**32,677***	392	2,559	6,633	2,943	8,067	3,026	1,874
2	HFB_MI_m108_2094	23,029	1,960	1,601	3,915	2,810	9,925	439	2,224
3	HFB_GF_m110_2052	28,213	501	2,820	**10,544***	2,321	**11,503***	484	2,280
4	HFB_GF_m104_2072	25,018	368	1,493	2,268	1,384	5,259	3,454	1,749
5	HFB_MR_m102_2062	15,462	659	1,208	1,536	906	5,197	2,535	1,452
6	HFB_HA_m102_2065	19,876	1,077	1,820	3,091	1,799	5,003	2,981	863
7	HFB_CC_m114_2085	12,105	2,450	2,943	4,076	723	4,796	924	1,212
8	HFB_MI_m103_2103	20,280	2,185	1,664	369	231	1,161	**11,235***	234
9	HFB_MI_m106_2059	18,480	2,096	3,185	2,105	532	3,763	3,364	791
10	HFB_MP_m101_2067	12,441	2,074	1,827	1,542	584	3,468	1,402	697
11	HFB_MI_m106_2083	15,311	580	1,286	2,090	1,251	4,453	1,735	853
12	HFB_CC_m107_2084	11,153	298	730	1,403	442	2,750	1,536	779
13	HFB_HA_m102_2067	13,480	204	462	1,138	812	4,026	1,205	1,049
14	HFB_MR_m105_2091	9,454	6,281	4,854	661	227	1,791	1,795	384
15	HFB_GF_m112_2053	18,090	3,458	2,895	2,880	1,533	4,017	3,569	1,598
16	HFB_HA_m102_2105	13,299	2,482	2,899	1,707	604	1,321	4,332	310
17	HFB_MR_m111_2066	13,599	1,698	1,705	2,304	535	4,602	725	735
18	HFB_MI_m107_2060	14,931	131	1,608	5,481	1,748	5,290	332	1,476
19	HFB_MP_m103_2078	12,446	**7,770***	**5,724***	1,845	495	1,654	2,134	1,141
20	HFB_MI_m114_2085	9,827	998	1,714	967	745	3,756	1,289	356
21	HFB_MP_m114_2070	11,362	1,553	1,396	1,546	794	2,996	601	890
22	HFB_MI_m113_2099	17,119	1,632	1,589	358	1,532	8,106	2,959	2,305
23	HFB_GF_m110_2066	9,586	2,261	2,084	916	267	1,997	1,611	455
24	HFB_MI_m115_2063	11,564	933	4,054	1,904	1,121	1,698	224	392
25	HFB_MI_m102_2060	12,406	135	670	2,045	647	2,578	1,579	1,014
26	HFB_GF_m108_2052	23,284	199	1,999	4,057	**3,014***	7,421	427	**2,724***
27	HFB_HA_m115_2103	11,477	2,491	2,904	2,092	272	3,677	1,054	930
28	HFB_GF_m111_2109	10,610	59	85	319	226	1,663	2,865	801
29	HFB_MI_m113_2110	8,057	775	412	643	456	2,023	891	1,118
30	HFB_GF_m112_2102	16,536	174	2,670	3,641	1,440	4,426	2,044	763
31	HFB_MR_m102_2074	10,223	563	881	936	315	2,286	1,466	652
32	HFB_MI_m101_2083	12,225	1,645	2,008	2,189	1,618	7,646	289	1,685
33	HFB_HA_m104_2082	13,697	3,760	3,003	2,079	724	1,804	2,571	396
34	HFB_HA_m101_2066	10,250	1,162	1,557	1,539	353	3,085	1,211	524
35	HFB_HA_m105_2083	14,549	2,792	2,491	1,537	505	2,050	3,046	556
36	HFB_CC_m110_2051	9,888	523	901	1,569	669	2,166	918	432

Note: (*) The greatest peak discharge event (m^3/s)

Figure 3.13 shows boxplots of the peak runoff depth (mm/h) for the top 20 and top 36 rainfall events in the Ishikari River basin and in its main sub-basins. Figure 3.14 shows the percentage difference in the median of the peak runoff depth between the top 20 and top 36 rainfall events in the Ishikari River basin and in its main sub-basins.

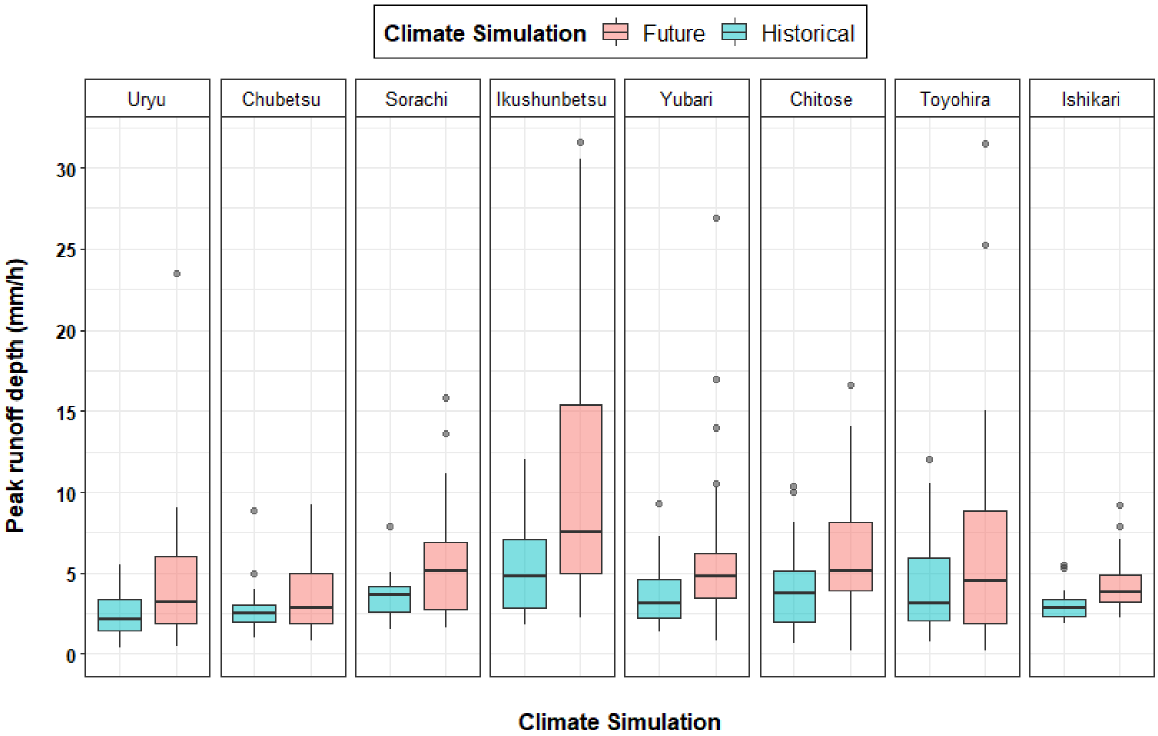

Figure 3.13. Boxplots of the peak runoff depth (mm/h) for the top 20 and top 36 rainfall events in the Ishikari River basin and in its main sub-basins

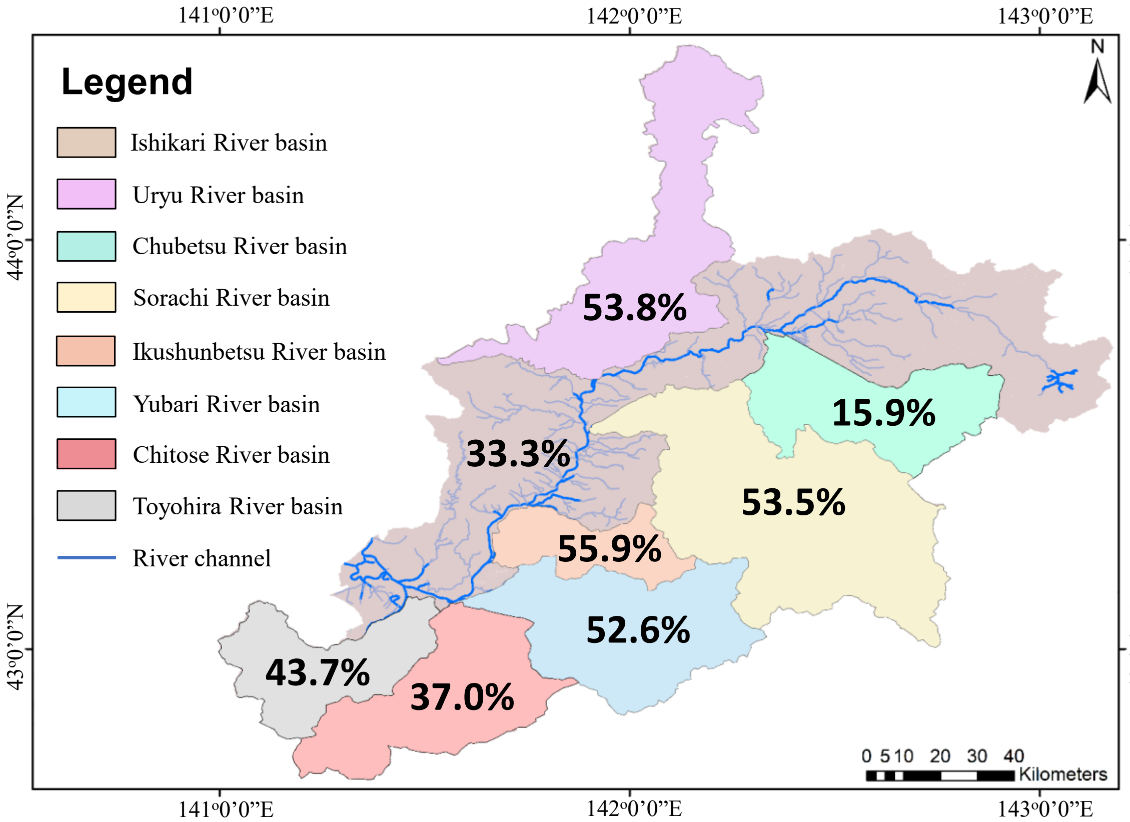

Figure 3.14. Percentage difference in the median of peak runoff depth between the top 20 and top 36 rainfall events in the Ishikari River basin and in its main sub-basins

These results indicate that the river floods were projected to increase significantly in the Ishikari River basin and in its main sub-basins. In particular, the Ikushunbetsu, Yubari, and Toyohira River basins were more likely to experience extremely large river flooding events with peak runoff depths exceeding 25 mm/h.

The percentage difference in the median of the peak runoff depth between the top 20 and top 36 rainfall events indicated that the peak runoff depth is projected to increase by 33% in the Ishikari River basin. The Ikushunbetsu, Uryu, Sorachi, and Yubari river basins are expected to undergo remarkable increases of 56%, 54%, 54%, and 54%, respectively, in peak runoff depths. In particular, the Ikushunbetsu and Yubari river basins located in the southern part of the Ishikari River basin are expected to experience a significant increase in extreme rainfall and river floods. However, the river floods from extreme rainfall will increase to a greater extent.

3.3.5. Time difference prediction

The difference between the time of peak discharge at the reference station in each tributary and the time of peak water level at the confluence point in the main river was estimated for the top 20 and top 36 rainfall events. Figure 3.15 shows the time difference averaged for the top 20 and top 36 rainfall events in each of the sub-basins.

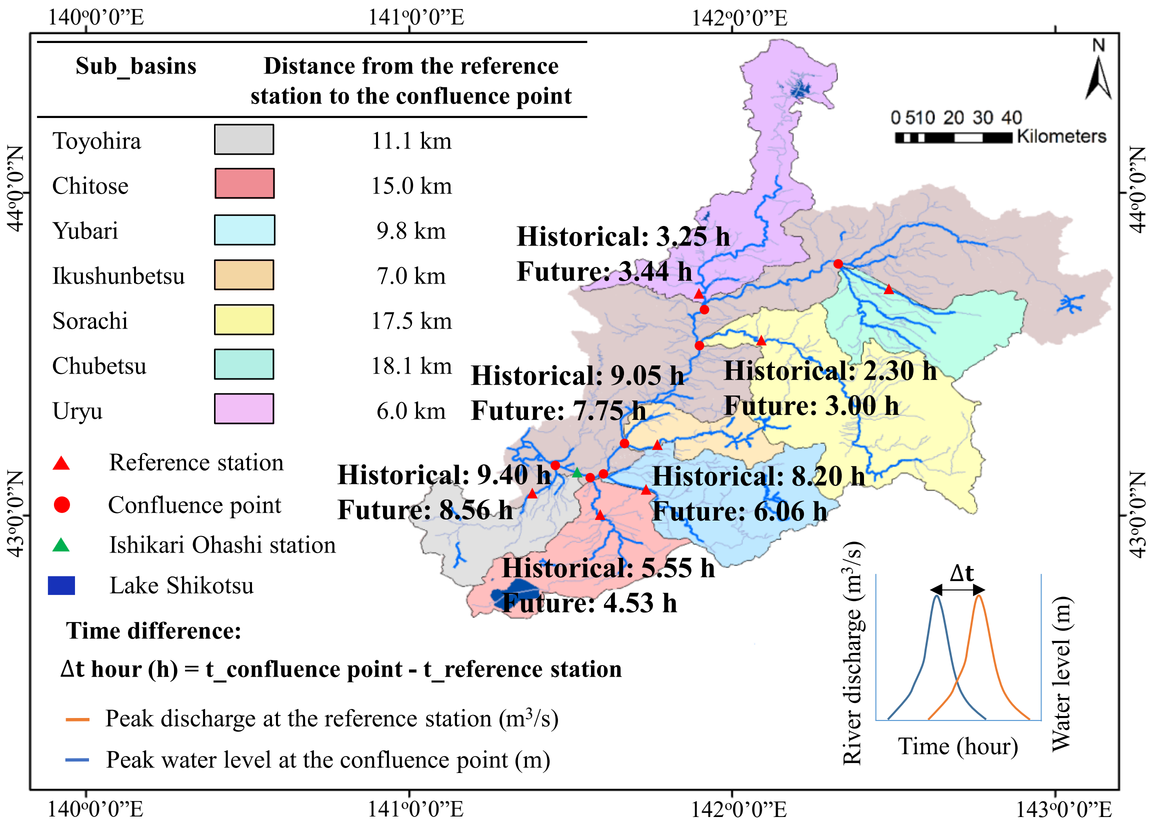

Figure 3.15. Time difference averaged for the top 20 and top 36 rainfall events in each of the sub-basin

The results show a slight increase of 0.19 h and 0.70 h in the future time difference in the Uryu and Sorachi River basins, respectively. Conversely, the time differences in the Ikushunbetsu, Yubari, Chitose, and Toyohira River basins are expected to decrease by 1.30, 2.14, 1.02, and 0.84 h, respectively. The time difference in the Chubetsu river basin was almost unchanged with a slight decrease of 0.05 h. The shorter the time difference, the greater the flood risk. These results can serve as a useful additional reference for flood damage mitigation strategies in vulnerable areas. Particular attention should be paid to the Chitose River basin because it is a lowland area prone to flood damage.

3.4. Conclusions

The following conclusions were drawn from this study:

- Following validation, the IFAS model can provide reasonable simulations of river discharges in the Ishikari River basin.
- Severe rainfall and river flooding events are expected to increase significantly in the Ishikari River basin and in its main sub-basins in the future. Additionally, the river flooding resulting from extreme rainfall would increase to a greater extent than the increase in extreme rainfall in the Ishikari River basin and in its main sub-basins. The effect of climate change is significant in the sub-basins located in the southern part of the Ishikari River basin, where extreme rainfall is expected to increase by 29%-35%, whereas the river discharge is likely to increase drastically by 37%-56%. The difference between the time of peak discharge at the reference station and the time of peak water level at the confluence point in the main river is expected to decrease by 1.02 h to 2.14 h in these regions.
- Special attention should be paid to the Chitose River basin, as it is located in a lowland area of the Ishikari River basin that is prone to flood damage.

These results will provide additional information about the effect of climate change on the risk of river floods for establishing climate change adaptation and flood damage mitigation strategies in vulnerable areas.

We have obtained useful findings; however, we have some limitations that need to addressed in further study. Because our approach focused on natural hazards, we ignored future changes in land-use activities and populations. Additionally, we did not consider the existing flood control facilities in the basin. However, we predict that short-term extreme rainfall events will have much greater effects on river flooding than the aforementioned factors. In addition, in this chapter, we assessed the change in time difference between the time of peak discharge at the reference station and the time of peak water level at the confluence point in the main river using the IFAS model. This effort aims to provide useful information for early flood warning systems to minimize flood damage. However, in this chapter, we used the IFAS model, which uses a kinematic wave for river channel flow simulation. The IFAS model does not have an analysis function to reproduce overtopping from river course and inundation. Therefore, the prediction might not accurately reflect the predicted results. The time difference prediction will be improved in further studies using the hydrodynamic model.

3.5. References

1. Giorgi, F. Regionalization of climate change information for impact assessment and adaptation. *WMO Bulletin*. **2008**, *57*, 86-92.
2. Intergovernmental Panel on Climate Change (IPCC). 2012. Managing the Risks of Extreme Events and Disasters to Advance Climate Change Adaptation; A Special Report of Working Groups I and II of the IPCC; Field CB, Barros V, Stocker TF, Qin D, Dokken DJ, Ebi KL, Mastrandrea MD, Mach KJ, Plattner GK, Allen SK (eds). *Cambridge University Press*, Cambridge, UK, New York, USA.
3. World Health Organization. 2021. Available online: https://apps.who.int/iris/bitstream/handle/10665/76224/9789241564526_section_2_eng.pdf. (accessed on 04 May 2021).
4. Doocy, S.; Daniels A.; Murray, S.; Kirsch, TD. The human impact of floods: A historical review of events 1980-2009 and systematic literature review. *PLoS currents*. **2013**, *5*. DOI: 10.1371/currents.dis.f4deb457904936b07c09daa98ee8171a
5. Hirabayashi, Y.; Kanae, S. First estimate of the future global population at risk of flooding. *Hydrological Research Letters*. **2009**, *3*, 6-9. DOI: 10.3178/hrl.3.6
6. Intergovernmental Panel on Climate Change (IPCC). 2013. The physical science basis in the fifth assessment report of the intergovernmental panel on climate change. IPCC. *Cambridge University Press*, Cambridge, UK; 1535.
7. Kitoh, A.; Endo, H. Changes in precipitation extremes projected by a 20 km mesh global atmospheric model. *Weather and Climate Extremes*. **2016**. *11*, 41-52. DOI: 10.1016/j.wace.2015.09.001
8. Sun, Y., Solomon, S., Dai, A., Portmann, RW. How often will it rain? *Journal of climate*. **2007**. *20*, 4801–4818.
9. Sillmann, J., Kharin, VV., Zwiers, FW., Zhang, X., Bronaugh, D. Climate ex- tremes

indices in the CMIP5 multimodel ensemble: Part 2. Future climate projections. *J. Geophys. Res. Atmos.***2013**.*118*, 2473–2493. Doi: 10.1002/ jgrd.50188

10. Higashino, M.; Stefan, HG. Variability and change of precipitation and flood discharge in a Japanese river basin. *Journal of Hydrology: Regional Studies*. **2019**, *21*, 68-79. DOI: 10.1016/j.ejrh.2018.12.003.
11. Hirabayashi, Y.; Kanae, S.; Emori, S.; Oki, T.; Kimoto, M. Global projections of changing risks of floods and droughts in a changing climate. *Hydrological Sciences Journal*. **2008**, *53*, 754-772. DOI: 10.1623/hysj.53.4.754.
12. Try, S.; Tanaka, S.; Tanaka, K.; Sayama, T.; Lee, G.; Oeurng, C. Assessing the effects of climate change on flood inundation in the lower Mekong Basin using high-resolution AGCM outputs. *Prog. Earth Planet. Sci*. **2020**, *7*, 34. DOI: 10.1186/s40645-020-00353-z.
13. Fujita, M., Mizuta, R., Ishii, M., Endo, H., Sato, T., Okada, Y., Kawazoe, S., Sugimoto, S., Ishihara, K., Watanabe, S. Precipitation changes in a climate with 2 K surface warming from large ensemble simulations using 60 km global and 20 km regional atmospheric models. *Geophysical Research Letters*. **2018**, *46*, 435-442. DOI: 10.1029/2018GL079885
14. Sato, Y.; Kojiri, T.; Michihiro, Y.; Suzuki, Y.; Nakakita, E. Assessment of climate change impacts on river discharge in Japan using the super-high-resolution MRI-AGCM. *Hydrological Processes.* **2013**, *27*, 3264-3279. DOI: 10.1002/hyp.9828
15. Miyasaka, T.; Kawase, H.; Nakaegawa, T.; Imada, Y.; Takayabu, I. Future projections of heavy precipitation in kanto and associated weather patterns using large ensemble high-resolution simulations. *SOLA*. **2020**, *16*, 125-131. DOI: 10.2151/sola.2020-022
16. Yamamoto, K.; Sayama, T.; Apip. Impact of climate change on flood inundation in a tropical river basin in Indonesia. *Prog. Earth Planet. Sci*. **2021**, *8*, 5. DOI: 10.1186/s40645-020-00386-4
17. Kitoh, A.; Ose, T.; Kurihara, K.; Kusunoki S, Sugi, M. Projection of changes in future weather extremes using super-high-resolution global and regional atmospheric models in the KAKUSHIN Program: Results of preliminary experiments. *Hydrological Research Letters*. **2009**. *3*, 49-53. DOI: 10.3178/HRL.3.49
18. River Council for Social Infrastructure Development. 2018. Council Report Flood Risk Management for Wide-area and Long-lasting Rainfall – Multi-layered

countermeasures for complex disasters. https://www.mlit.go.jp/river/mizubousaivision/toushin_e/1812_flood_risk_management_e.pdf. Last access July 1, 2020.
19. Kim, S.; Nakakita, E.; Tachikawa, Y.; Takara, K. Precipitation changes in Japan under the A1B climate change scenario. *Annual Journal of Hydraulic Engineering, JSCE*. **2010**, *54*, 127-132.
20. Yamada TJ. 2019. Adaptation measures for extreme floods using huge ensemble of high-resolution climate model simulation in Japan. Summary report on the eleventh meeting of the research dialogue. United Nations Framework Convention on Climate Change (UNFCCC), Bonn, Germany: 28-29.https://unfccc.int/sites/default/files/resource/RD11SummaryReport.pdf. Last access April 8, 2020.
21. Sato, Y.; Kojiri, T.; Michihiro, Y.; Suzuki, Y.; Nakakita, E. Estimates of climate change impact on river discharge in Japan based on a super-high-resolution climate model. *Terrestrial, Atmospheric and Oceanic Sciences*. **2012**, *23*, 527-540. DOI:10.3319/TAO.2012.05.03.02(WMH).
22. Tachikawa, Y.; Takino, S.; Ichikawa, Y.; Shiiba, M. Study on the impact of climate change on river flow regime in the Mogami and Yoshino River basins. *Annual Journal of Hydraulic Engineering*. **2009**, *53*, 475-480 (in Japanese).
23. Hoshino, T.; Yamada, TJ. Assessment of climate change effect on precipitation amount within river domains of Hokkaido. Proceedings of 2017 Annual Conference, Japan Society of Hydrology and Water Resources. **2017**, *12*. DOI: 10.11520/jshwr.30.0_12.
24. Yamada, TJ.; Hoshino, T.; Masuya, S.; Uemura, F.; Yoshida, T.; Omura, N.; Yamamoto, T.; Chiba, M.; Tomura, S.; Tokioka, S.; Sasaki, H.; Hamada, Y.; Nakatsugawa, M. The influence of climate change on flood risk in Hokkaido. *Advances in River Engineering*. **2018**, 24, 391–396 (in Japanese)
25. Japan River Association. 2003. The Ishikari River. http://www.japanriver.or.jp/EnglishDocument/DB/file/002%20Hokkaido%2003.pdf. Last access May 20, 2019.
26. Japan Society of Civil Engineers (JSCE). Onsite Field Investigation Team, Site–Investigation Report for the Hokkaido Heavy Rainfall Disasters in August 2016; Title was translated by N. Kimura; JSCE Report; JSCE: Tokyo, Japan, **2017**. (In Japanese).

27. Ishii, M.; Mori, N. 4PDF: large-ensemble and high-resolution climate simulations for global warming risk assessment. *Progress in Earth and Planetary Science*. **2020**, *7*, 28. DOI: 10.1186/s40645-020-00367-7
28. Mizuta, R.; Murata, A.; Ishii, M.; Shiogama, H.; Hibino, K.; Mori, N.; Arakawa, O.; Imada, Y.; Yoshida, K.; Aoyagi, T.; et al. Over 5000 years of ensemble future climate simulations by 60-km global and 20-km regional atmospheric models. *Bull. Am. Meteorol. Soc.* **2017**, *98*, 1383–1398. DOI: 10.1175/BAMS-D-16-0099.1
29. Fowler, HJ., Ekström, M., Blenkinsop, S., Smith, AP. Estimating change in extreme European precipitation using a multimodel ensemble. *Journal of Geophysical Research*. **2007**, *112*. DOI: 10.1029/2007JD008619
30. Sasaki, H.; Murada, A.; Hanafusa, M.; Oh'izumi, M.; Kurihara, K. Reproducibility of Present Climate in a NonHydrostatic Regional Climate Model Nested within an Atmosphere General Circulation Model. *SOLA*, **2011**, *7*, 173–176. DOI: 10.2151/sola.2011-044
31. Hoshino, T.; Yamada, TJ.; Kawase, H. Evaluation for characteristics of tropical cyclone induced heavy rainfall over the sub-basins in the central Hokkaido, northern Japan by 5-km large ensemble experiments. *Atmosphere*. **2020**, *11*, 435. DOI: 10.3390/atmos11050435.
32. Yoshino, F.; Yoshitani, J.; Sugiura, M. A conceptual distributed model for large-scale mountainous basins. In Lang H, Musy A (eds). *Hydrology in Mountainous Regions. I − Hydrological Measurements; the Water Cycle; IAHS*, Lausanne, Switzerland. **1990**, *193*, 685–692.
33. International Centre for Water Hazard and Risk Management (ICHARM). 2014. IFAS ver 2.0 Technical manual. http:// www.icharm.pwri.go.jp/research/ifas/ifas_2.0_top.html. Last access October 20, 2018.
34. Aziz, A.; Tanaka, S. Regional parameterization and applica- bility of Integrated Flood Analysis System (IFAS) for flood forecasting of upper-middle Indus River. *Pakistan Journal of Meteorology*. **2010**, *8*, 21–38.
35. Kimura, N.; Kiri, H.; Kitagawa, I. The Impact of Multiple Typhoons on Severe Floods in the Mid-Latitude Region (Hokkaido). *Water*. **2018**, *10*, 843. DOI: 10.3390/w10070843
36. Shrestha, BB.; Okazumi, T.; Miyamoto, M.; Nabesaka, S.; Tanaka, S.; Sugiura, A. Fundamental Analysis for Flood Risk Management in the Selected River Basins of

Southeast Asia. *Journal of Disaster Research*. **2014**, *9*, 858-869. DOI: 10.20965/jdr.2014.p0858

37. Kimura, N.; Kiri, H.; Kanada, S.; Kitagawa, I.; Yoshinaga, I.; Aiki, H. Flood simulations in mid-latitude agricultural land using regional current and future extreme weathers. *Water*. **2019**, *11*, 2421. DOI: 10.3390/w11112421
38. Ministry of Land, Infrastructure, Transport and Tourism (MLIT). 2020. Water Information System. http://www1.river.go.jp/. Last access September 20, 2020
39. Nash, J.; Sutcliffe, J. River flow forecasting through conceptual models part I-A discussion of principles. *Journal of Hydrology*. **1970**, *10*, 282-290. DOI: 10.1016/0022-1694(70)90255-6.
40. Japan Institute of Construction Engineering (JICE). 2011. Outflow analysis system, analytical technique manual Ver 2.3. http://www.jice.or.jp/. Last access April 15, 2019.

Chapter 4

Flood inundation assessment in the low-lying river basin considering extreme rainfall impacts and topographic vulnerability

Chapter 4

4.1. Introduction

In recent decades, extreme weather events associated with climate changes have rapidly become one of the global concerns threatening natural environments and human life. According to the IPCC Fifth Assessment Report [1], on the longer time scale, the global average surface temperature increased by about 0.73ºC per century, and this trend is likely to continue into the new millennium. In addition, precipitation is one of the most critical and useful indicators reflecting changes in climate conditions [2]. The IPCC Fifth Assessment Report (2013) [1] also indicated that rainfall is expected to increase in the future, especially in extreme rainfall patterns.

Among many physical factors influencing river flooding, precipitation is the main factor affecting runoff formation and flow regimes [2,3]. Additionally, other factors caused by human interactions such as land-use changes and rapid development of socio-economic activities also promote floods [4]. Due to the complex nature of these factors on river flooding, all of them are considered a challenging task for hydrologists. However, assessing flood risk by considering the main factors affecting river floods is possible for each river basin's characteristics.

The risk of severe natural events, such as flood inundation, landslides, and sediment-related disasters caused by extreme rainfall, is likely to increase in the future [5,6]. During summer, severe flood risk from extreme rainfall events is a common phenomenon, particularly throughout Asia [7]. Moreover, large-scale damage caused by flood inundation has been reported around the world in recent years [8,9]. Therefore, many attempts have been made to evaluate and predict flood inundation risk along many important river basins in the world to minimize damage due to loss of life and property [4,10,11,12,13,14,15,16]. For example, evaluating the river flood risk in small and ungauged river basins is currently one of the most common challenges for hydrologists. Hence, several studies have been conducted to investigate and map the flood hazards for these river basins to minimize flood damage [13,14,15].

In Japan, a new record has been reached for temperature and precipitation almost every year in recent times [17]. According to the Japan Meteorological Agency (2017) [18], on a longer time scale, the annual mean surface temperature over Japan has increased by 1.19 per century, which is higher than the global average surface temperature increase (0.73ºC). Additionally, the annual number of days when precipitation is equal to or greater than 200 mm has increased (statistically significant at a confidence level of 99%) during the period from 1901 to 2017 in Japan [18]. Flood inundation disasters due to extreme rainfall have occurred frequently in Japan and caused considerable damage in recent years. For example, an extreme rainfall event on 5-6 July 2017 caused severe floods in many parts of Kyushu, Japan, and resulted in extensive damage [19]. One year later, during 5-8 July 2018, a widespread flood disaster caused by torrential rainfall occurred in western Japan. The Oda River and its three tributaries exhibited the "backwater phenomenon", where the tributary river floods intersected with the main river floods causing levees to break at eight points [20]. This backwater phenomenon is projected to occur anywhere across Japan because of the presence of several river systems with similar conditions. In the northernmost Japanese island, Hokkaido, extreme rainfall caused severe flood inundation in August 2016; this disaster reportedly caused approximately USD 260 million in damage, in addition to agricultural losses of over 40,258 ha of land throughout Hokkaido [21]. Most recently, on 1-13 October 2019, severe flooding and landslides occurred in many river basins in the central northern parts of Japan, causing great losses to life and properties [22]. In this context, to mitigate water-related disasters due to climate changes, especially flood inundation disasters, many researchers have attempted to predict extreme rainfall and severe river flooding events along many important river basins in Japan [23,24,25,26]. These attempts could provide useful information to policymakers for climate change adaptations as well as flood mitigation strategies.

Prediction of changes in the flow regime is a challenge [10,27] as it demands future climate datasets under various climate change scenarios. Popular methods of future projection are the general circulation models (GCMs), whose rainfall and evapotranspiration data could be used as inputs to hydrological models to assess changes in river floods. However, GCMs generally have a coarse resolution for simulation on a regional scale; such coarse resolution could lead to large uncertainties in the simulations [10,28]. Therefore, high-resolution climate data obtained through downscaling approaches, such as statistical and dynamical downscaling, have been investigated in recent years. For example, in a study by Sato (2012) [29], the impact of climate change on river discharge was investigated for several major river basins in Japan using the latest version of an atmospheric GCM (AGCM) with a 20 km horizontal resolution. In a study by Yamada et al. (2018) [30], the super-high-resolution 5 km d4PDF dataset was downscaled from the 20 km resolution data via a non-hydrostatic regional climate model [31]. After downscaling, the rainfall amount and spatiotemporal distribution of rainfall were similar to the observed rainfall events. Furthermore, heavy rainfall patterns could be better observed after downscaling, and the 5 km resolution results represented the topography of the study area more accurately [23,30]. This suggests that the 5 km downscaled results may be appropriate for estimating changes in heavy rainfall as well as flood inundation on the basin scales.

The hydrological model is a fundamental approach to further understand the process of river flow. In recent years, numerous hydrological models have been developed and applied to simulate and predict potential river floods along many river basins worldwide, such as the HEC-HMS [32], IFAS [33], TOPMODEL [34], and SWAT models [35]. However, these models cannot simulate flood inundation along the river basin and must be combined with hydraulic models, such as HEC-RAS [36], FLO-2D [37], and MIKE 21 [38], which are popular. The 1D models cannot simulate the inundation risk in floodplains, while 2D flood models require a long simulation time. Therefore, both these types of models were integrated for comprehensive flood inundation simulations and reduced computation time. Some popular integrated 1D–2D models are SOBEK [39] and the Rainfall–Runoff–Inundation (RRI) model [40–42]. In a study by San et al. (2020) [43], the performances of RRI and SOBEK models were compared in terms of user-friendliness, cost, type of output, and correlation between simulated and observed data in the Bago River basin. The results indicated that although the SOBEK model could provide more accurate results, the RRI model is preferable considering the calculation time, cost, and user interface friendliness. In addition, the RRI model is more applicable to the near-real-time inundation mapping and the flood early warning system. Therefore, due to these advantages, flood inundation risk was assessed using the RRI model in this study. It can simulate rainfall–runoff and inundation processes simultaneously in both the floodplain and mountainous zones [40–42]. Several studies have used this model to estimate flood inundation for many river basins globally and have demonstrated its good performance

[10,11,44–48].

From the results of chapter 3, as well as in a study by Nguyen [23], changes in extreme rainfall and changes in river discharges were evaluated in the Ishikari River basin, Japan, as well as its sub-basins using the IFAS model coupled with a large-ensemble rainfall dataset (d4PDF) with 5 km resolution. The results indicated that extreme rainfall was projected to increase by 21.2% in the Ishikari River basin and 34.8% in the Chitose River basin, whereas the river discharge could increase drastically by 33.3% in the Ishikari River basin and 37% in the Chitose River basin. The effect of climate change is significant in the Chitose River basin, the downstream lowland area of the Ishikari River basin. This river basin is considered to be the most flood-prone in the Ishikari River basin. In addition, the time difference between the peak discharge at the reference station in each tributary and the peak water level at the confluence point for the seven Ishikari River main sub-basins using the IFAS model was also predicted. However, since the IFAS model uses a kinematic wave for river channel flow simulation [33], the prediction might not accurately reflect the predicted results.

Considering the aforementioned information, this study aims to assess the change in flood inundation risk comprehensively (including inundation area, inundation volume, peak inundation depth, inundation frequency, and inundation duration) considering the extreme rainfall impacts and topographic vulnerability in the Chitose River basin using the RRI model and rainfall data extracted from d4PDF with a high-resolution of 5 km. Owing to the topographical characteristics of its low-lying area, the Chitose River basin is frequently affected by backwater from the Ishikari River and experiences severe flood inundation. Moreover, this study is conducted to improve the time difference prediction result considering the dangerous impacts of backwater phenomenon on flood inundation risk in the Chitose River basin using the RRI model, which uses a 2D distributed hydrodynamic model with diffusive wave models. The time difference is evaluated between the peak discharge at the reference station in the Chitose River basin and the peak water level at the confluence point intersecting the main river. With this effort, we believe that the result might provide more reliability compared to previous studies of the Chitose River basin. Flood inundation is more severe when the time difference is shorter. The study results are expected to provide useful information for developing climate change adaptation measurements and mitigating future flood inundation damage in the floodplain areas.

4.2. Materials and Methods

4.2.1. Description of the study area

The study area considered herein is the Ishikari River basin, which is located in Hokkaido, Japan (Figure 4.1). At a length of 268 km, this is the longest river in Hokkaido and the third-longest river in Japan. In addition, this river has the second largest basin area in Japan, with a drainage area of 14,330 km^2. The river originates from Mt. Ishikari-dake (1967 m above sea level), passes through the west of Hokkaido, and empties into the Sea of Japan. It flows through 48 municipalities (including Sapporo, the prefectural capital, and Asahikawa, the second-largest city), accounting for 52% of the population of Hokkaido. The Ishikari Plain occupies most of the basin's area and is located around the central and downstream basin area, which is the most productive agricultural area in Hokkaido. The Ishikari River basin plays a vital role in the socioeconomic development of Hokkaido. The mean annual precipitation in this basin is 1300 mm; the hydrologic peaks generally occur from March to May during the snow-melt period and from August to September during the rainy season [49]. The Chitose River basin is one of the main tributaries of Ishikari River (Figure 4.1). Owing to the topographical characteristics of its low-lying area, the Chitose River basin is frequently affected by backwater from the main river, causing severe flood inundation. Therefore, the Chitose River basin is considered a vulnerable region in the Ishikari River basin. The Chitose River has a length of 108 km and a total basin area of 1244 km^2. The main parts of the New Chitose Airport belong to this basin area [50].

In the past, the Ishikari River basin has experienced large-scale historical flood events and severe damage. For example, the largest flood event in this basin occurred in August 1981, and severe damage was recorded in the target basin. Figure 4.2 shows the flood inundation from August 1981 in the Chitose River basin. The backwater phenomenon was observed when the water levels at the confluence point surged higher and water from the main river flowed back into the tributary, which combined with inland water and caused severe flood inundation. This flood event caused damages amounting to approximately

JPY 115.2 billion, two fatalities, and 22,500 inundated houses throughout the Ishikari River basin. For the Chitose River basin, 192 km^2 of land was inundated and 2,700 inundated houses were recorded for this serious flood event [49,50].

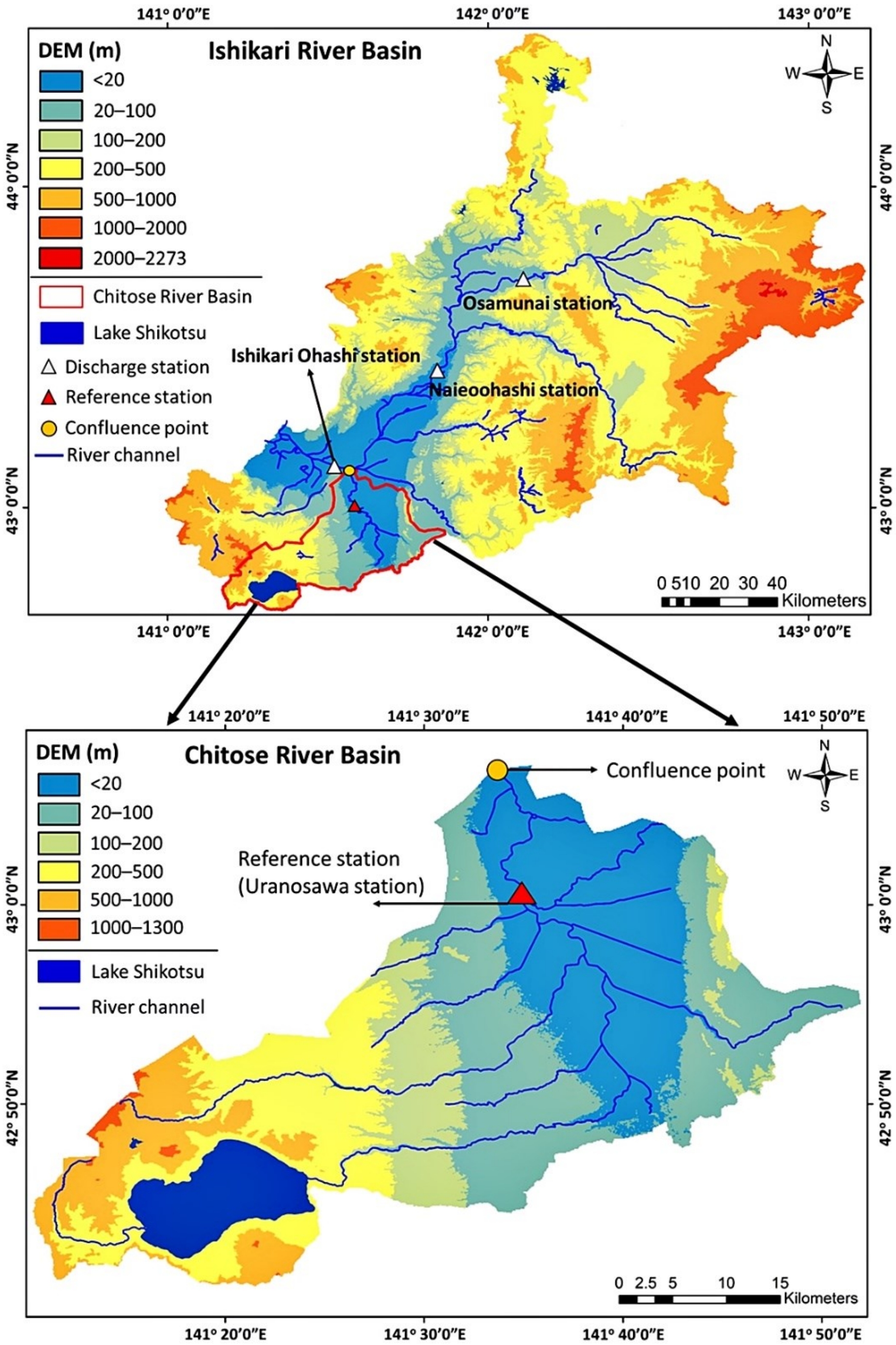

Figure 4.1. Locations of the Ishikari River basin and Chitose River basin

Figure 4.2. Severe flood inundation event in August 1981 in the Chitose River basin. Data source: Hokkaido Regional Development Bureau

4.2.2. d4PDF Dataset

This chapter used the large-ensemble rainfall dataset from the database of Policy Decision making for Future climate change (d4PDF) [55], which consists of large-ensemble climate experiments from the global atmospheric model, with a horizontal resolution of 60 km, and regional downscaling simulations covering the Japan area, with a horizontal resolution of 20 km. The d4PDF consists of historical climate simulations (1951–2010) with 50 ensembles (historical simulation: 50 ensembles × 60 years = 3000 events), and the +4 K future climate simulations (2051–2110) with 90 ensembles, including six sea surface temperature (SST) patterns and 15 ensembles for each SST (+4K future simulation: 6 SST × 15 ensembles × 60 years = 5400 events). The +4 K future climate was predicted for a global mean air temperature of 4 °C warmer than the preindustrial period. The +4 K future climate simulation corresponded to the representative concentration pathway 8.5 (RCP8.5) experiments under phase 5 of the CMIP5 [56]. This study used the d4PDF rainfall data with a 5 km resolution, which were downscaled from the 20 km resolution data [23]. The target rainfall data were defined from 1 June to 1 December, where the annual maximum rainfall (mm/72 h) was obtained over the target basin for each of the 3000 historical and 5400 future simulation events. The rainfall data with a high resolution of 5 km reflect the topography of the study area more accurately [23,30]. In this chapter, we used the top 20 and top 36 rainfall events from the results of chapter three to evaluate changes in flood inundation risk comprehensively in the Chitose River basin using the RRI model.

4.2.3. Overview of the Rainfall-Runoff-Inundation (RRI) model

The RRI model was employed to simulate flood inundation and identify flood-prone areas. The RRI model was developed by the International Center for Water Hazard and Risk Management (ICHARM). The RRI model is a two-dimensional model that is capable of simulating rainfall–runoff and flood inundation simultaneously [40–42]. At a grid cell in which a river channel is located, the model assumes that both slope and river are positioned within the same grid cell. The channel is discretized as a single line along its centerline of the overlying slope grid cell. The flow on the slope grid cells was calculated with the 2D diffusive wave model, whereas the channel flow was calculated with the 1D diffusive wave model. The RRI model simulates the lateral subsurface, vertical infiltration, and surface flows to better represent flood characteristics. The lateral subsurface flow, which is more important in mountainous regions, was treated in terms of the discharge–hydraulic gradient relationship, including both saturated subsurface and surface flows, whereas the vertical infiltration flow was evaluated using the Green–Ampt model. The details of the model are shown below [41].

A storage cell-based inundation model [51] was used to calculate lateral flows on slope grid cells. The governing equations for the 2-dimensional unsteady flow model include the mass balance equation (Equation (1)) and momentum equations (Equations (2) and (3)):

$$\frac{\partial h}{\partial t} + \frac{\partial q_x}{\partial x} + \frac{\partial q_y}{\partial y} = r - f \tag{1}$$

$$\frac{\partial q_x}{\partial t} + \frac{\partial u q_x}{\partial x} + \frac{\partial v q_x}{\partial y} = -gh\frac{\partial H}{\partial x} - \frac{\tau_x}{\rho_\omega} \tag{2}$$

$$\frac{\partial q_y}{\partial t} + \frac{\partial u q_y}{\partial x} + \frac{\partial v q_y}{\partial y} = -gh\,\frac{\partial H}{\partial y} - \frac{\tau_y}{\rho_\omega} \tag{3}$$

where h is the water level from the local surface; q_x and q_y are the unit width discharges in the x and y directions, respectively; u and v are the flow velocities in the x and y directions, respectively; r is the rainfall intensity; f is the infiltration rate; H is the water level from the datum; p_ω is the density of water; g is the gravitational acceleration; and τ_x and τ_y are the shears stresses in the x and y directions, respectively.

The second terms of the right side of Equations (2) and (3) were calculated with Manning's equation.

$$\frac{\tau_x}{\rho_\omega} = \frac{gn^2 u\sqrt{u^2+v^2}}{h^{1/3}} \tag{4}$$

$$\frac{\tau_y}{\rho_\omega} = \frac{gn^2 v\sqrt{u^2+v^2}}{h^{1/3}} \tag{5}$$

where n is the Manning's roughness parameter.

The RRI model spatially discretized the mass balance (Equation (1)) as follows:

$$\frac{dh^{i,j}}{dt} + \frac{q_x^{i,j-1} - q_x^{i,j}}{\Delta x} + \frac{q_y^{i-1,j} - q_y^{i,j}}{\Delta y} = r^{i,j} - f^{i,j} \tag{6}$$

where $q_x^{i,j}$, $q_y^{i,j}$ are the x and y direction discharges from a grid cell at (i, j), respectively.

Equations (7) and (9) describe the saturated subsurface flow based on the Darcy law, while Equations (8) and (10) describe the combination of the saturated subsurface flow and the surface flow. For the kinematic wave model, the hydraulic gradient was assumed to be equal to the topographic slope, whereas the RRI model assumed the water surface slope as the hydraulic gradient.

$$q_x = -k_a h \frac{\partial H}{\partial x}, \quad (h \le d_a) \tag{7}$$

$$q_x = -\frac{1}{n}(h - d_a)^{\frac{5}{3}} \sqrt{\left|\frac{\partial H}{\partial x}\right|} sgn\left(\frac{\partial H}{\partial x}\right) - k_a h \frac{\partial H}{\partial x}, \quad (d_a < h) \tag{8}$$

$$q_y = -k_a h \frac{\partial H}{\partial y}, \quad (h \le d_a) \tag{9}$$

$$q_y = -\frac{1}{n}(h - d_a)^{\frac{5}{3}} \sqrt{\left|\frac{\partial H}{\partial y}\right|} sgn\left(\frac{\partial H}{\partial y}\right) - k_a h \frac{\partial H}{\partial y}, \quad (d_a < h) \tag{10}$$

where k_a is the lateral saturated hydraulic conductivity and d_a is the effective porosity of the soil depth times.

Equations (11) and (12) were used to simulate the effect of unsaturated subsurface flows, saturated subsurface flows, and the surface flows with the single variable of h.

$$q_x = \begin{cases} -k_m d_m \left(\frac{h}{d_m}\right)^{\beta} \frac{\partial H}{\partial x}, & (h \le d_m) \\ -k_a(h - d_m)\frac{\partial H}{\partial x} - k_m d_m \frac{\partial H}{\partial x}, & (d_m < h \le d_a) \\ -\frac{1}{n}(h - d_a)^{\frac{5}{3}} \sqrt{\left|\frac{\partial H}{\partial x}\right|} sgn\left(\frac{\partial H}{\partial x}\right) - k_a(h - d_m)\frac{\partial H}{\partial x} - k_m d_m \frac{\partial H}{\partial x}, & (d_a < h) \end{cases} \tag{11}$$

$$q_y = \begin{cases} -k_m d_m \left(\frac{h}{d_m}\right)^{\beta} \frac{\partial H}{\partial y}, & (h \le d_m) \\ -k_a(h - d_m)\frac{\partial H}{\partial y} - k_m d_m \frac{\partial H}{\partial y}, & (d_m < h \le d_a) \\ -\frac{1}{n}(h - d_a)^{\frac{5}{3}} \sqrt{\left|\frac{\partial H}{\partial y}\right|} sgn\left(\frac{\partial H}{\partial y}\right) - k_a(h - d_m)\frac{\partial H}{\partial y} - k_m d_m \frac{\partial H}{\partial y}, & (d_a < h) \end{cases} \tag{12}$$

Infiltration is an important hydrological process. For relatively flat areas, the vertical infiltration process during the first period of rainfall has more impact on large-scale flooding. Therefore, the vertical infiltration can be treated as loss for event-based simulation. In RRI, infiltration loss f is calculated with the Green–Ampt infiltration model. The Green–Ampt infiltration model is a simplified physical model and based on the Richard equation. It relates the rate of infiltration to measurable soil properties such as the porosity, hydraulic conductivity, and soil water content of a particular soil column [41,52].

$$f = k_v \left[1 + \frac{(\emptyset - \theta_i)S_f}{F}\right] \tag{13}$$

where k_v is the vertical saturated hydraulic conductivity; $\emptyset$ is the soil porosity; θ_i is the initial water volume content; S_f is the suction at the vertical wetting front and F is the cumulative infiltration depth.

The flow interactions between the river channel and slope were estimated using different overflow formulas [41].

(1) Flow from slope to river under the normal condition: when the river water level is lower than the ground level, the discharge from the slope into the river is defined by Equation (14):

$$q_{sr} = \mu_1 h_s \sqrt{g h_s} \tag{14}$$

where q_{sr} is discharge from slope to river; μ_1 is the constant coefficient (=0.544), and h_s is the water depth on a slope cell.

(2) No water exchange between slope and river: when the river water level is higher than the ground level and both the river and slope water levels are lower than the levee height.

(3) Overtopping flow from the river to slope: when the river water level is higher than the levee height and the slope water level:

$$q_{rs} = \mu_2 h_1 \sqrt{2 g h_1} \tag{15}$$

where q_{rs} is discharge from the river to slope; μ_2 is the constant coefficient (=0.35), and h_1 is the difference between the river water level and the levee height.

(4) Overtopping flow from slope to the river: when the slope water level is higher than the levee height and river water level, and the river water level is higher than the levee height. The flow exchange was calculated by Equation (15), with h_1 presenting the difference between the two water levels and q_{rs} being replaced with q_{sr}.

To solve the diffusive equations, the RRI model uses the fifth-order Runge–Kutta method with adaptive time-step control. A detailed explanation is given by Sayama et al. (2012) [41]. The RRI model provides the output of river discharge, river water level, inundation area, and inundation depth simultaneously. A schematic of this model is shown in Figure 4.3. This model has been applied to several important river basins to evaluate river floods as well as flood inundation, and good simulation results have been obtained [10,11,44–48].

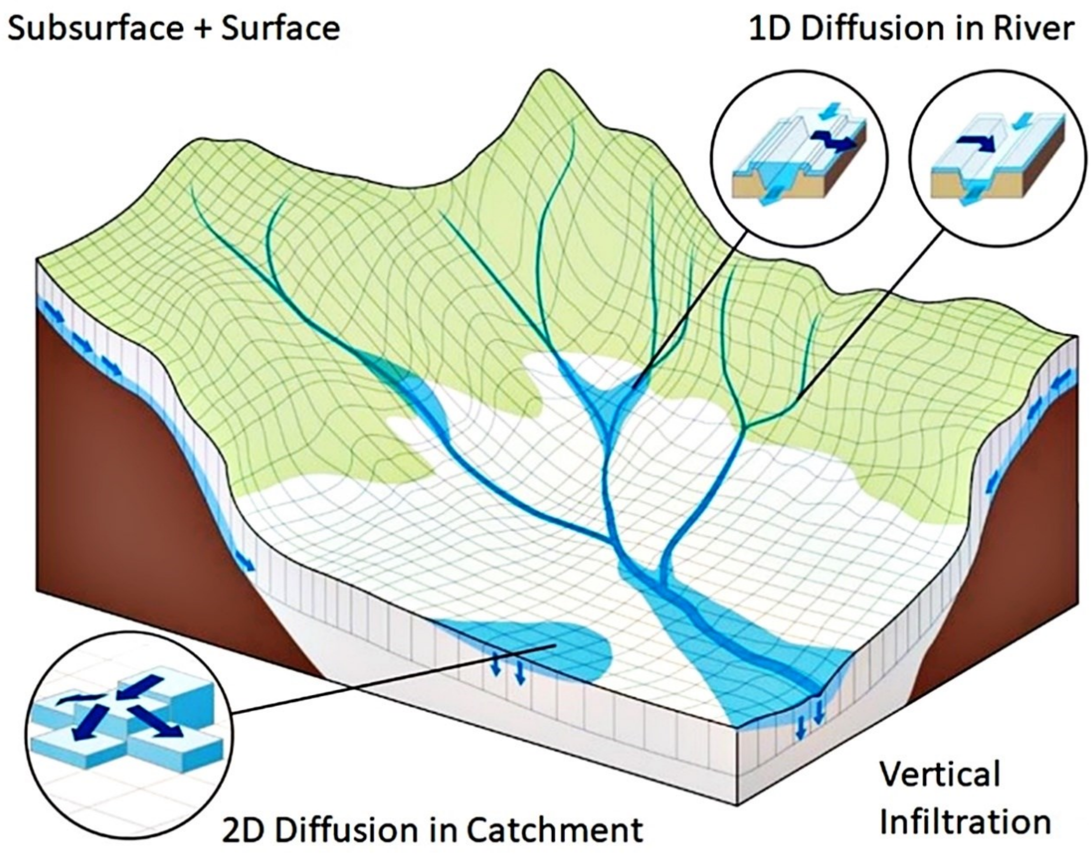

Figure 4.3. Schematic of the rainfall-runoff-inundation (RRI) model

4.2.4. Data inputs

- ***Topographic data:***

The topography data, including digital elevation model (DEM), flow direction (DIR), and flow accumulation (ACC), were obtained from the HydroSHEDS project provided by the U.S. Geological Survey (USGS) [53]. HydroSHEDS is derived primarily from elevation data of the Shuttle Radar Topography Mission (SRTM) data. HydroSHEDS offers a suite of geo-referenced datasets in raster and vector format, including stream networks, watershed boundaries, drainage directions. The HydroSHEDS supports regional and global watershed analyses, hydrological modelling, and freshwater conservation planning. Available resolutions of HydroSHEDS are 5 min, 30 arc-seconds, 15 arc-seconds, and 3 arc-seconds (approximately 10 km, 1 km, 500 m, and 90 m at the equator, respectively). The topography of the HydroSHED data is available at https://www.hydrosheds.org/ (accessed on 1 February 2021). The higher DEM resolution could provide a finer resolution of inundation mapping. However, this requires greater computational power compared to the lower DEM resolution. The HydroSHEDS data at 3 arc-seconds (approximately 90 m) were used in this study. However, to reduce computational time due to the large study area, a topography data scale-up algorithm was used in the RRI model to convert the original topography data to 24 arc-seconds (approximately 720 m) for the entire IRB, and to 9 arc-seconds (approximately 270 m) for the Chitose River basin. The DEM, DIR, and ACC data were converted to ASCII format, which is the required format for the RRI model. Topographic data as inputs for the RRI model was shown in Figure 4.4.

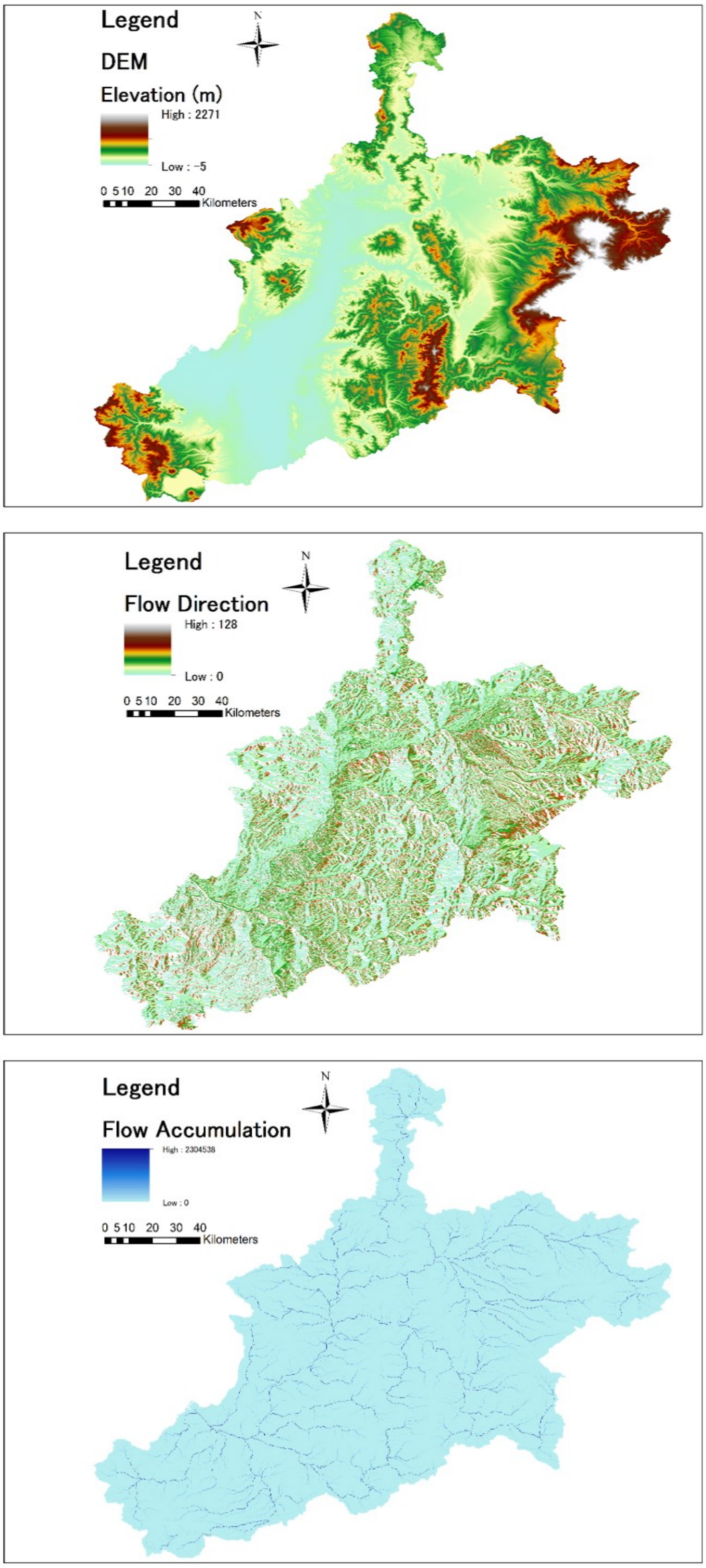

Figure 4.4. Topographic data as inputs for the RRI model

- ***Land Cover data***

Global Land Cover Characterization (GLCC-V2) data with 1 km resolution provided by the USGS were used in this study. Land cover has a crucial impact on the hydrological process, and the original land cover data for the target basin has 14 distinct land cover types. However, these 14 types are too detailed to assign different parameters in the RRI model; therefore, similar land cover types were merged and three land cover types, namely forest, sparse vegetation, and cropland/floodplain, were finalized using the ArcGIS function. The reclassified land cover data were resampled to the same resolution as the topography data to input the RRI model. Land cover classification in the Ishikari River basin of original GLCC-V2 with 14 land cover types, and reclassified land cover types were shown in Figure 4.5 (a) and (b), respectively.

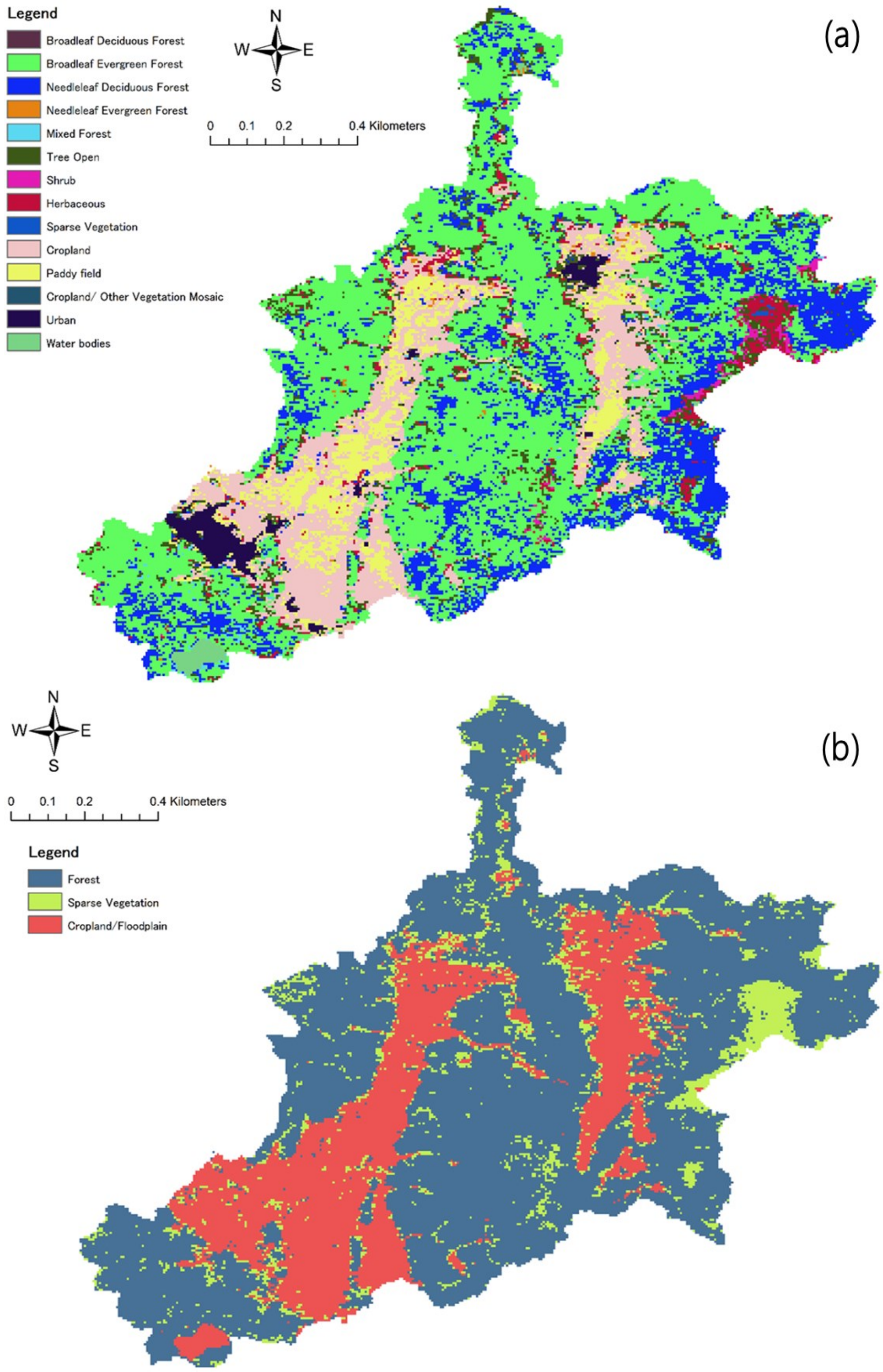

Figure 4.5. Land cover classification in the Ishikari River basin for (a) original Global Land Cover Characterization, and (b) reclassified land cover types

➢ ***River cross-section data:***

The river cross-section (river width and depth) is an important parameter to input the RRI model to minimize uncertainties in the output of the hydrologic simulation. In the RRI model, a rectangular cross-section is applied to the cross-section of the river channel. The river width (*W*) and river depth (*D*) was approximated by the following equations:

$$W = C_W A^{S_W} \tag{16}$$

$$D = C_D A^{S_D} \tag{17}$$

where A is the upstream contributing area (km^2), W is the channel width (m), and D is the channel depth (m). C_w, S_w, C_D, and S_D are geometrical parameters. The parameters of the equations were estimated by regression analysis with the cross-section data at 42 locations spanning the Ishikari River basin. In addition, the parameters of the equations were estimated at 33 locations across the CRB. The obtained parameters for the Ishikari River cross-section are $C_w = 1.73$, $S_w = 0.60$, $C_D = 0.18$, $S_D = 0.45$ and the obtained parameters for the Chitose River cross-section are $C_w = 14.45$, $S_w = 0.34$, $C_D = 0.022$, and $S_D = 0.80$. Plot of river width and river depth with contributing area for the Ishikari River basin was shown in Figure 4.6. Plot of river width and river depth with contributing area for the Chitose River basin was shown in Figure 4.7.

In addition, to increase the reliability of future flood inundation hazard assessments under the various climate change scenarios in the vulnerable areas, the Ishikari River and Chitose River cross-sections of future plans were provided by the River Management Division of the Sapporo Development and Construction Department, Hokkaido Regional Development Bureau and future flood inundation simulations were applied in this study. The obtained parameters for the Ishikari River cross-section plan are: $C_w = 1.68$, $S_w = 0.60$, $C_D = 0.17$, and $S_D = 0.46$. The Chitose River cross-section future plan remained unchanged compared to the present river cross-section; therefore, the Chitose River cross-section future plan parameters are $C_w = 14.45$, $S_w = 0.34$, $C_D = 0.022$, and $S_D = 0.80$. Plot of river width and river depth with contributing area for the Ishikari River basin future plan was shown in Figure 4.8.

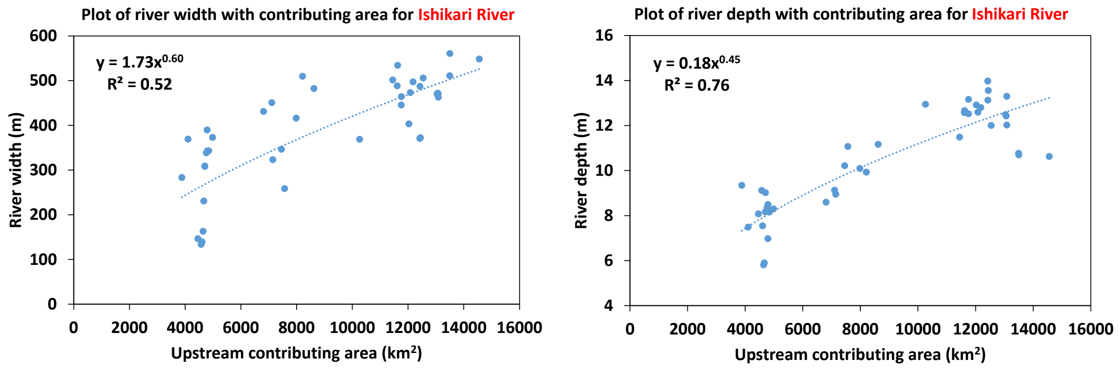

Figure 4.6. Plot of river width and river depth with contributing area for the Ishikari River basin

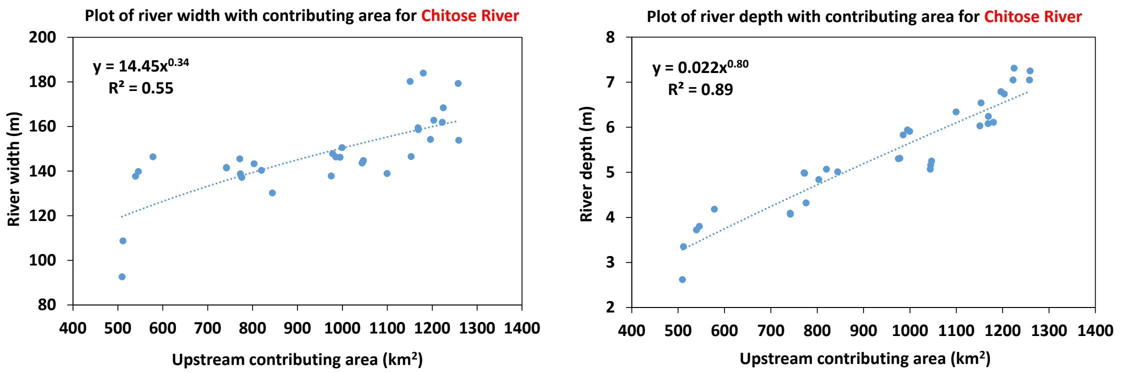

Figure 4.7. Plot of river width and river depth with contributing area for the Chitose River basin

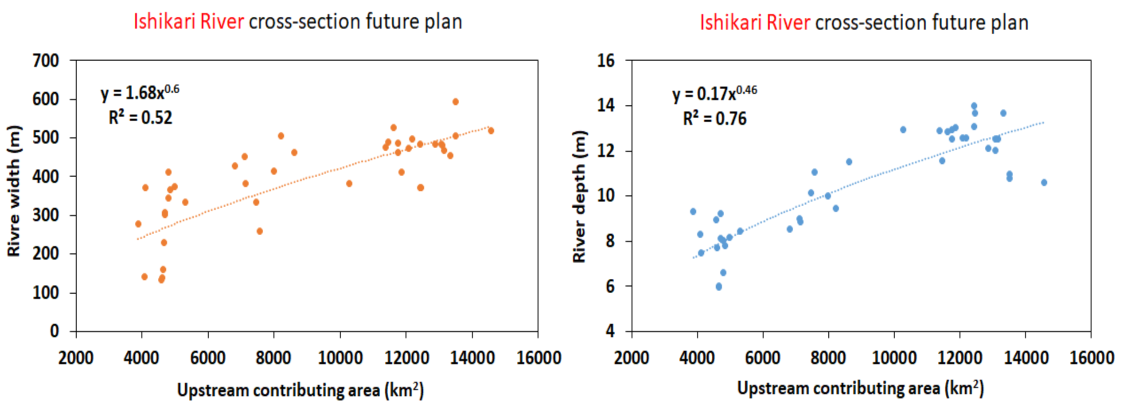

Figure 4.8. Plot of river width and river depth future plan with contributing area for the Ishikari River basin

➢ ***Gauged Rainfall and Runoff data:***

In the past, the Ishikari River basin experienced severe large-scale historical flood events. In particular, the flood event of August 1981 was the largest in the target basin. Notably, during this flood event, the Chitose River basin was severely affected—backwater phenomenon integrated inland flooding was observed and caused tremendous damage. Therefore, in this study, we used this large-scale flood event to calibrate the RRI model. Additionally, three severe historical flood events in September 2001, September 2011, and August 2016 were chosen to validate the model.

To evaluate the performance of the RRI model, a comparison between the observed and simulated river discharges was employed at the Ishikari Ohashi station, approximately 26.6 km upstream from the river mouth (Figure 4.1). In addition, the inundated area in the Chitose River basin was evaluated and compared with the observed inundated area for the flood event from August 1981 to calibrate the RRI model.

The gauged rainfall data and observed river discharge for the August 1981 flood event were provided by the Hokkaido Regional Development Bureau (HRDB). The observed inundated area in the Chitose River basin for the August 1981 flood event was also provided by the HRDB. The gauged rainfall for September 2001, September 2011, and August 2016 flood events and the observed river discharges for the validation process were obtained from the Water Information System managed by the Ministry of Land, Infrastructure, and Transport, Japan (MLIT) [54].

4.2.5. Analytical procedure

This study was conducted to assess changes in severe river flooding in the Ishikari River basin as well as changes in flood inundation in the Chitose River basin using the top 20 and top 36 rainfall events from the d4PDF dataset from the results of chapter 3 as well as from the study by Nguyen et al (2020) [23] as the input rainfall data to the RRI model. This chapter was performed according to the following steps. First, the RRI model was calibrated to a large historical flood event in August 1981 using the "trial and error" method. The RRI model calibration and validation process performances were evaluated using four statistical indicators, including the Nash-Sutcliffe (*NSE*), coefficient of determination (R^2), relative volume error (*VE*), and peak discharge error (E_p). Four statistical indicators were defined as follows:

$$NSE = 1 - \frac{\sum_{i=1}^{n}\left[Q_{Si(i)} - Q_{Ob(i)}\right]^2}{\sum_{i=1}^{n}\left[Q_{Si(i)} - \overline{Q_{Ob}}\right]^2} \tag{18}$$

$$R^2 = \frac{\left[\sum_{i=1}^{n}\left(\left(Q_{Ob(i)} - \overline{Q_{Ob}}\right) \times \left(Q_{Si(i)} - \overline{Q_{Si}}\right)\right)\right]^2}{\sum_{i=1}^{n}\left(Q_{Ob(i)} - \overline{Q_{Ob}}\right)^2 \times \sum_{i=1}^{n}\left(Q_{Si(i)} - \overline{Q_{Si}}\right)^2} \tag{19}$$

$$VE = \frac{\sum_{i=1}^{n} Q_{Si(i)} - \sum_{i=1}^{n} Q_{Ob(i)}}{\sum_{i=1}^{n} Q_{Ob(i)}} \tag{20}$$

$$E_p = \frac{Q_{MOb} - Q_{MSi}}{Q_{MOb}} \tag{21}$$

where Q_{Si} is the simulated discharge (m^3/s); Q_{Ob} is the observed discharge (m^3/s); Q_{MOb} is the peak observed discharge (m^3/s); Q_{MSi} is the peak simulated discharge (m^3/s); and n is the total number of measurements.

Then, the optimal parameters were used for the validation process of the flood events in September 2001, September 2011, and August 2016. The optimal parameters after calibration and validation were applied to the RRI model to evaluate future changes in severe river discharges in the Ishikari River basin and flood inundation in the Chitose River basin. To evaluate the flood inundation in the Chitose River basin, the time series of water levels at the confluence point (Figure 4.1) was used as a boundary condition in the RRI model. The simulations were conducted for an extra period of two weeks before the main period for model warmup and also for initial moisture conditions in the target basin. Changes in flood inundation in the Chitose River basin were investigated comprehensively in terms of the inundation area, inundation volume, peak inundation depth, inundation frequency, and inundation duration. The statistical Kolmogorov–Smirnov (K–S) test, which is a nonparametric test of two samples, was used to examine the variations in flood inundation between the top 20 rainfall events (historical simulation) and top 36 rainfall events (future simulation). The value of the test statistic for the two samples is defined by

$$D = sup|F_1(x) - F_2(x)| \quad (22)$$

where F_1 and F_2 are the empirical distribution functions based on the two samples, and sup is the supremum function. The hypothesis of the test is as follows:

H_0: The two samples have no significant differences in their cumulative distribution functions.

H_1: Two samples have different trends in the cumulative distribution functions.

The null hypothesis is rejected if the p-value is less than the significance level α of 0.05.

Finally, the time difference prediction results between peak discharge at the reference station in the Chitose River basin and the peak water level at the confluence point intersecting the Ishikari River were improved compared to the results of chapter 3 using the RRI model.

4.3. Results and discussions

4.3.1. RRI model calibration and validation

The RRI model was calibrated for the largest flood event in the Ishikari River basin in August 1981. The optimal parameters of the RRI model after calibration are listed in Table 4.1. The simulation results are shown in Figure 4.9. As shown in Figure 4.9, the RRI model closely reproduced the wave shape and flood duration in most cases. Figure 4.9(a) compares the observed and simulated discharges at the Ishikari Ohashi station for the flood event of August 1981 after calibration. The simulated discharges show close agreement with the observed discharges. This result is determined by reasonable statistical indicators NSE, R^2, and VE with values of 0.96, 0.98, and −0.006, respectively. The observed peak discharge (11,330 m^3/s) has good synchronization with the simulated one (11,310 m^3/s), as indicated by an E_p value of 0.002. The optimal parameters after the calibration process were used for the validation process of the flood events in September 2001, September 2011, and August 2016, as shown in Figure 4.9 (b), (c), (d), respectively. It can be seen that the simulated discharges matched well with the observed discharge in most cases, as indicated by the reasonable NSE, R^2, and VE values. However, the simulated peak discharges were found to be slightly higher than the observed peak discharges for these flood events. This result is demonstrated by the E_p values of −0.234, −0.1, and −0.17 for the flood events in September 2001, September 2011, and August

2016, respectively. The detailed statistical indicators are listed in Table 4.2. Overall, these results suggest that the RRI model can perform reasonably well for further analysis in the next sections.

Table 4.1. Optimal parameter settings of the RRI model

Parameters	Notation	Unit	Mountains	Plains
Manning's coefficient for river	n_{river}	($m^{-1/3}s$)	0.035	0.035
Manning's coefficient for slope	n	($m^{-1/3}s$)	0.15	0.15
Soil depth	d	(m)	1.0	1.0
Soil porosity	Φ_a	(-)	0.12	0.472
Vertical hydraulic conductivity	k_v	(cm/h)	-	0.06
Wetting front soil suction head	S_f	(-)	-	0.273
Lateral saturated hydraulic conductivity	k_a	(m/s)	0.17	-
Unsaturated porosity	Φ_m	(-)	0.03	-
Parameter of unsaturated hydraulic conductivity	β	(-)	8.0	-

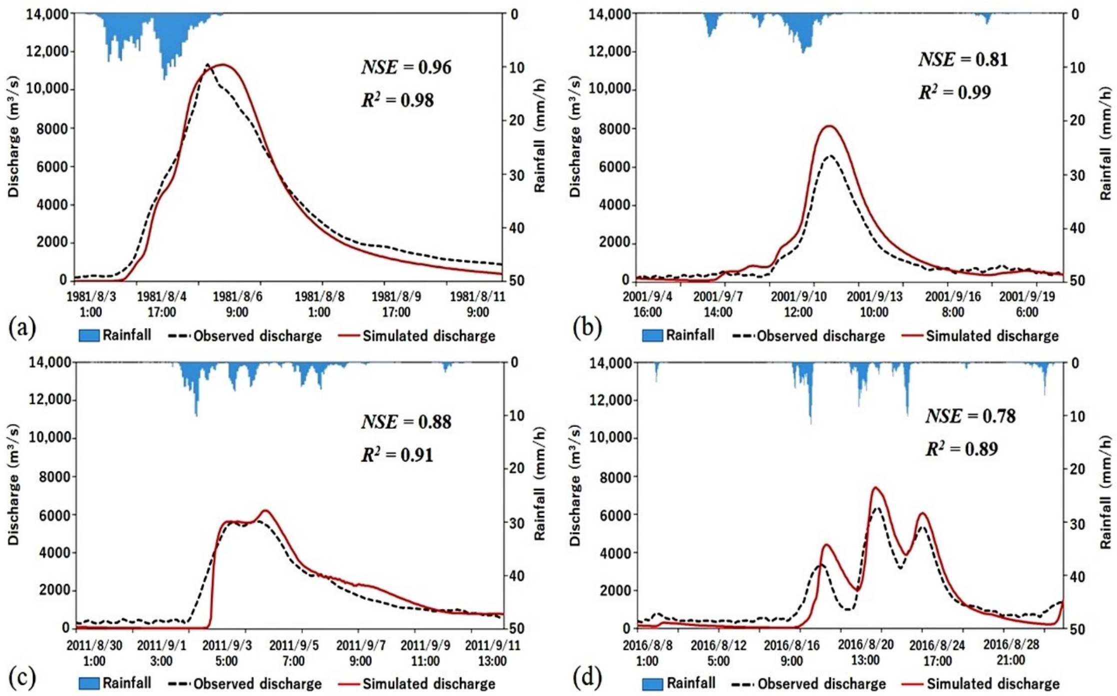

Figure 4.9. Comparison between the simulated and observed discharges at Ishikari Ohashi station for (a) the August 1981 flood event, (b) the September 2001 flood event, (c) the September 2011 flood event, and (d) the August 2016 flood event

Table 4.2. Statistical indicators of the RRI model performance

	Flood events	*NSE*	R^2	*Ep*	*VE*
Calibration	August 1981	0.96	0.98	0.002	-0.006
Validation	September 2001	0.81	0.99	-0.234	0.246
	September 2011	0.88	0.91	-0.10	0.0007
	August 2016	0.78	0.89	-0.17	-0.002

Figure 4.10 shows the simulated maximum flood inundation depth and inundation areas for the August 1981 flood event in the Chitose River basin. As shown in Figure 4.10, the simulated inundation area defined with a water depth threshold of 0.5 m overlaps with the observed inundation area for the flood event in August 1981 in the downstream area of the Chitose River basin. Owing to the limitations of the observed inundation data, inundation depth data were not available. A comparison between the simulated and observed inundation areas was conducted using the basic photo provided by the Hokkaido Regional Development Bureau. The observed flood depth data were not available; therefore, in this study, we selected the threshold of water depth is 0.2 and 0.5 m to classify the inundated and non-inundated areas. According to the simulation results, the simulated inundation areas are 252 and 240 km^2 for the 0.2 and 0.5 m water depth thresholds, respectively. Additionally, the observed inundation area was 192 km^2 [50]. The simulated inundation area for the threshold of 0.5 m water depth was more similar to the observed ones compared with the simulated inundation area for the threshold of 0.2 m water depth. Additionally, the simulated inundation area and peak inundation depth for the August 1981 flood event are quite close to the simulated results estimated by Oki et al. (2017) [50] of 209 km^2 for the inundated area. Furthermore, the peak inundation depth is similar to the value simulated by Oki et al. (2017) [50]. As a result, the threshold of 0.5 m water depth was chosen to classify the inundated and non-inundated areas in the Chitose River basin in the following sections of this study.

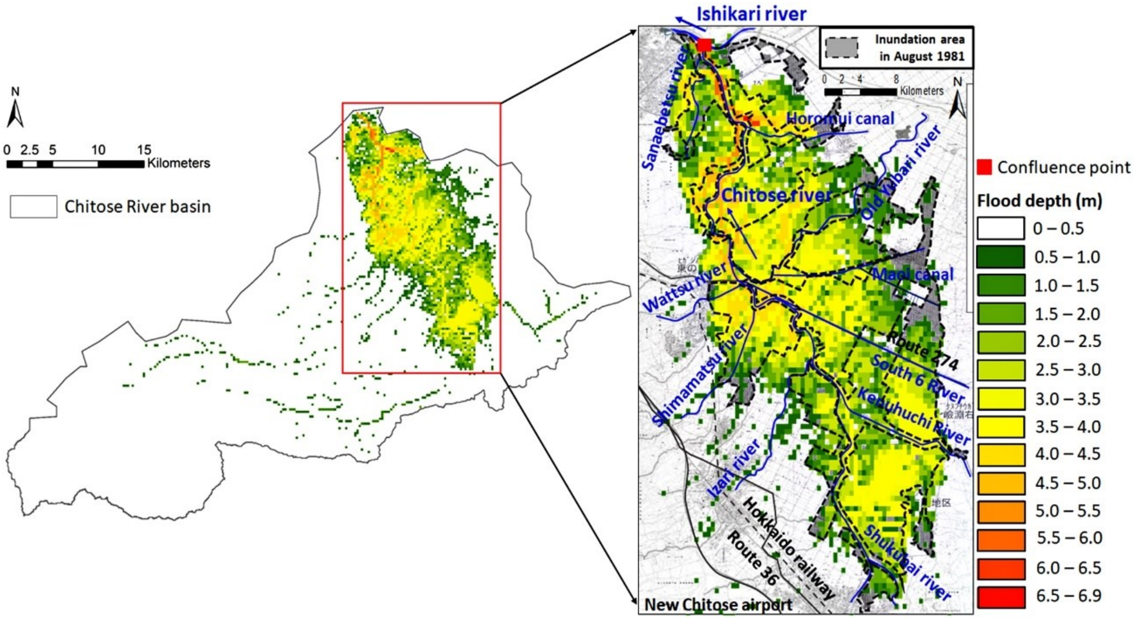

Figure 4.10. Comparison between the simulated and observed inundation areas for the flood event of August 1981 in the Chitose River basin

4.3.2. Evaluation of climate change impacts on river flood in the Ishikari River basin

The optimal parameters of the RRI model after calibration and validation were used to evaluate the changes in severe river floods in the Ishikari River basin, as well as the flood inundation in the Chitose River basin using the top 20 and top 36 rainfall events extracted from the d4PDF rainfall dataset as input data to the RRI model. The simulations were conducted for an additional period of 72 h before the main period as an initial condition for model warmup.

Changes in severe river flooding were examined at three stations along the main river of the Ishikari River basin. The locations of the three stations are shown in Figure 4.1, including the Osamunai station (located in the upstream river), Naieoohashi station (located in the middle river), and Ishikari Ohashi station (located in the downstream river). From the simulation results at three stations along the main river, the percentage differences in the means of the peak discharge between the top 20 and top 36 rainfall events indicated that severe river floods are expected to increase by 21–24% in the target basin. These results indicate that severe river flooding is projected to increase by a similar extent throughout the entire Ishikari River basin. The greatest increase of 24% is observed at the Naieoohashi station, which is located in the middle of the Ishikari River.

4.3.3. Evaluation of climate change impacts on flood inundation in the Chitose River basin

Future changes in severe flood inundation were evaluated for the Chitose River basin. To further understand the changes in the flood inundation risk in the Chitose River basin, the flood inundation area, and flood inundation volume was evaluated for an inundation depth equal to or larger than 0.5 and 3.0 m in this study. Figure 4.11 shows the inundation area averaged for the top 20 rainfall events (historical simulation) and top 36 rainfall events (future simulation) for flood depths equal to or larger than 0.5 (Figure 4.11a) and 3.0 m (Figure 4.11b). Table 4.3 shows the percentage difference of the mean values of the inundation areas and inundation volumes for an inundation depth ≥0.5 m and inundation depth ≥3.0 m between the top 20 rainfall events (historical simulation) and the top 36 rainfall events (future simulation).

The results indicate that flood magnitudes are projected to increase significantly in the future in the Chitose River basin. For flood depths ≥0.5 m, the inundation area, and inundation volume are expected to increase by 24.5 and 46.5%, respectively. As shown in Figure 4.11a, the downstream area of the Chitose River basin is the area with more severe flood inundation in the future. In addition, flood inundation was observed on the main sub-basins of the Chitose River basin. Severe flood inundation events for flood depths ≥3.0 m are expected to increase drastically in the Chitose River basin by 124.6 and 134.2% for the inundation area and inundation volume, respectively. In particular, an inundation depth equal to or larger than 3.0 m was observed only in the downstream area of the target basin. Owing to the low-lying characteristics, this area is the most vulnerable area in the Chitose River basin. The results of the K–S tests of the inundation area with inundation depths equal to or larger than 0.5 and 3.0 m demonstrate significant differences between the top 20 and top 36 rainfall events, with p-values of 0.0003 and 0.0001 (i.e., much smaller than alpha of 0.05), respectively. A similar K–S test result for the inundation volume with the inundation depths equal to or greater than 0.5 and 3.0 m also revealed remarkable differences between the top 20 and top 36 rainfall events, with p-values of 0.0006 and 0.0001, respectively.

Table 4.3. Percentage difference of the mean values of the inundation area and inundation volume for inundation depths of ≥0.5 and ≥3.0 m between the top 20 rainfall events (historical simulation) and top 36 rainfall events (future simulation)

	Inundation Area	Inundation Volume
Inundation depth ≥0.5 m	24.5	46.5
Inundation depth ≥3.0 m	124.6	134.2

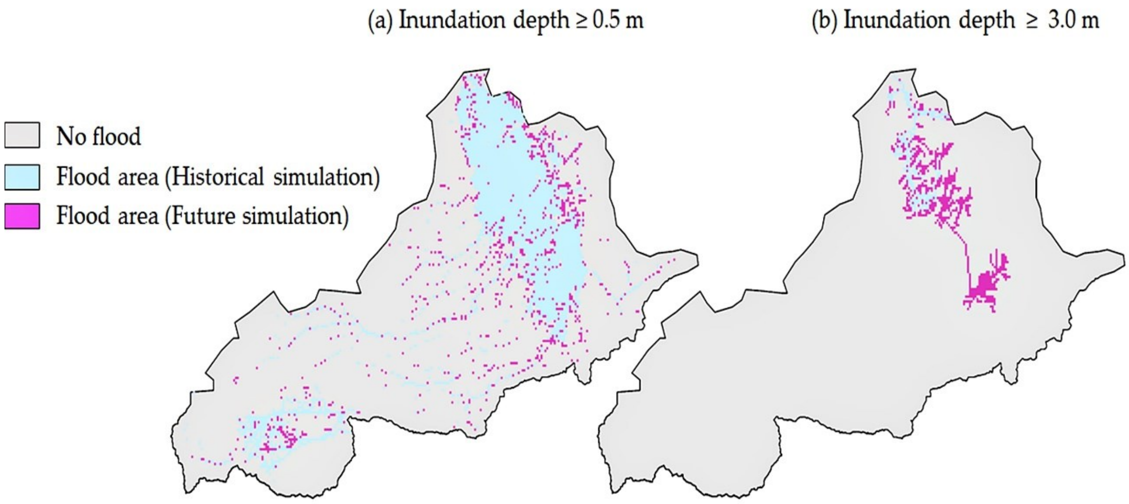

Figure 4.11. Inundation area averaged for the top 20 rainfall events (historical simulation) and top 36 rainfall events (future simulation) with (a) inundation depth ≥0.5 m, and (b) inundation depth ≥3.0 m

Figure 4.12 shows the boxplots of the peak inundation depth (Figure 4.12a), inundation volumes with an inundation depth ≥0.5 m (Figure 4.12b), and inundation volumes with an inundation depth ≥3.0 m (Figure 4.12c) for the top 20 past and top 36 future rainfall events in the Chitose River basin. In addition to the significant increase in inundation area and inundation volume, the peak inundation depth is predicted to significantly increase by a factor of 13.8% in the future. Notably, the peak inundation depth can reach 8.45 m in the future in the Chitose River basin. This inundation depth is a very serious level of classification based on the risk categories for inundation depths in Japan. In addition, there was a huge variation in peak inundation depth in the Chitose

River basin. The first quartile value of the peak inundation depth for the future simulation is 6.02 m, which was greater than the third quartile value for the historical simulation (6.0 m). Similarly, the inundation volume with the flood depth ≥0.5 m for the future simulation is 0.55 km^3, which was equal to the third quartile value from the historical simulation. For the flood depth ≥3.0 m, the first quartile value for the inundation volume is 0.13 km^3, which is greater than the third quartile value from the historical simulation of 0.12 km^3.

In addition, the median inundation volume with a flood depth ≥0.5 m is expected to increase significantly by 52.9% in the Chitose River basin, whereas a drastic increment of 330% was projected in the Chitose River basin for the flood depth ≥3.0 m. The K–S test also shows a significant difference for the peak inundation depth between the top 20 past and top 36 future rainfall events at a significance level of 5% (p-value = 0.0001). A similar K–S test result for the inundation volume with inundation depths equal to or greater than 0.5 and 3.0 m also revealed remarkable differences between the top 20 and top 36 rainfall events.

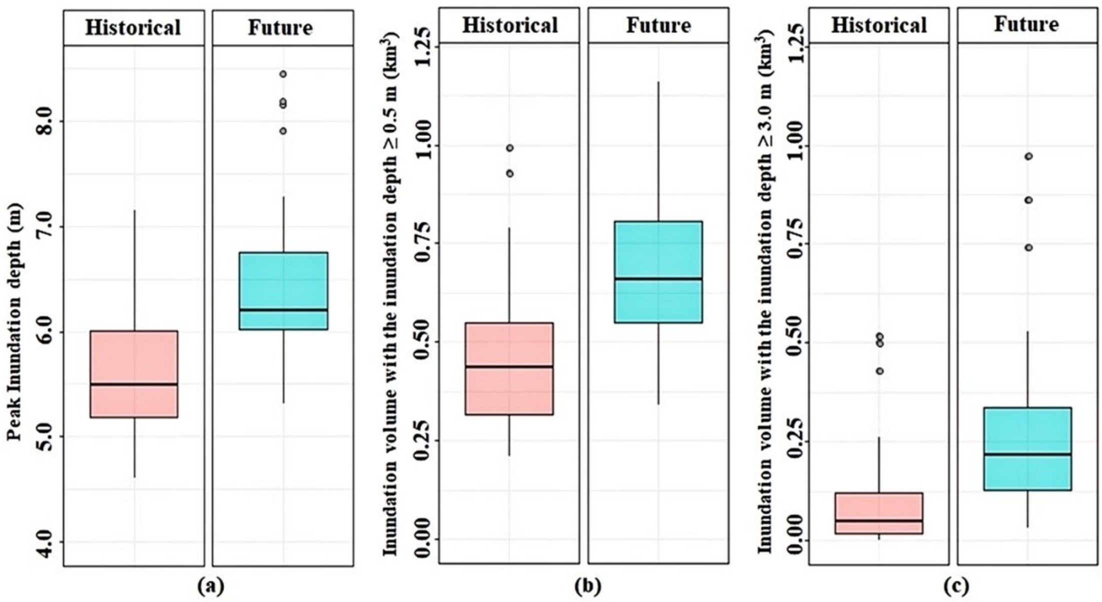

Figure 4.12. Boxplots of (a) peak inundation depths, (b) inundation volumes with inundation depth ≥0.5 m, and (c) inundation volumes with inundation depth ≥3.0 m for the top 20 past and top 36 future rainfall events in the Chitose River basin

Figure 4.13 shows the spatial distribution of the inundation frequency for the top 20 past and top 36 future rainfall events, and the inundation frequency difference (IFD) between these rainfall events. As shown in Figure 4.13a,b, the downstream area of the Chitose River basin is clearly seen to be the most severe flood inundation. This result is suitable for the terrain characteristics of this basin. It can be seen that flood inundation is likely to occur in this area in the future with a frequency of 90–100%. Moreover, the flood inundation was observed in the tributaries of the Chitose River for both historical and future simulations. This would increase the risk of flood inundation in the downstream area of the Chitose River basin, in which the inland flooding integrated to the backwater phenomenon from the main river. In addition, in Figure 4.13c, the IFD indicates a positive value for almost all areas in the Chitose River basin. The proportion for the area with an inundation frequency smaller than 0 is only 4.2%. Therefore, 95.8% of the area had an inundation frequency larger than 0, in which the area proportional to $0 < \mathrm{IFD} \leq 0.3$ is 74.7%, and the area proportional to $0.3 \leq \mathrm{IFD} \leq 0.6$ is 21.1%. On the other hand, this result clearly indicates that the flood-prone areas downstream of the Chitose River basin will be more widely spread in the future. Hence, this area should be specially considered in the future to mitigate severe flood inundation damage.

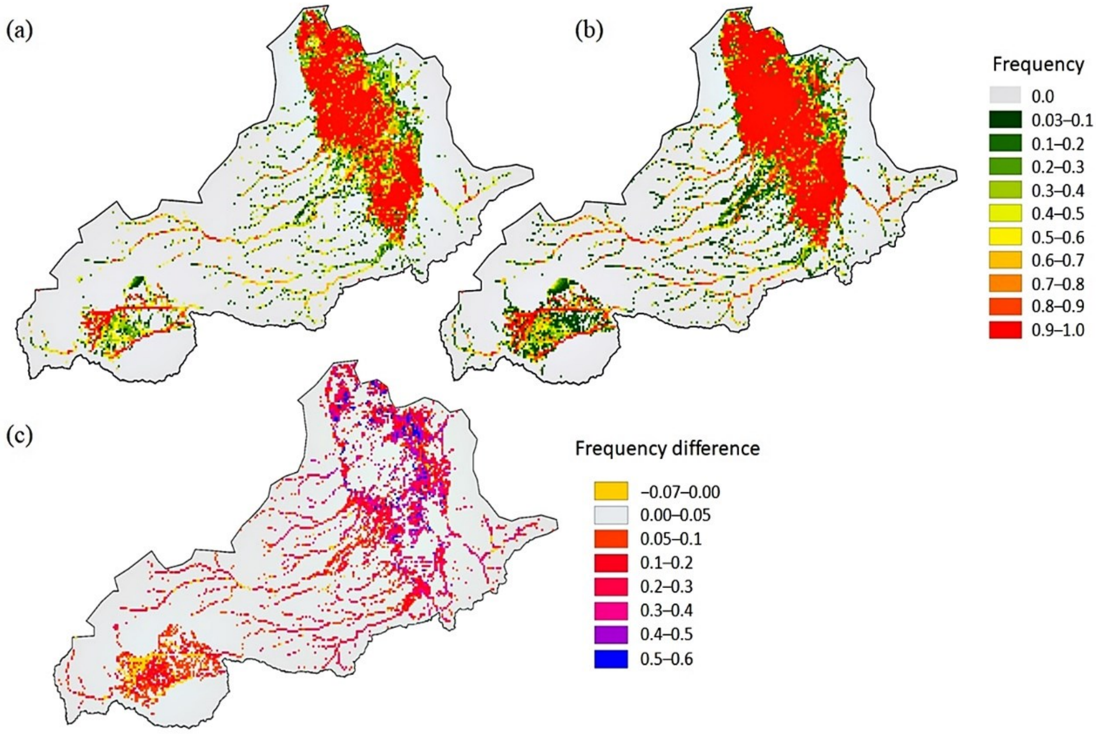

Figure 4.13. Spatial distribution of the inundation frequency averaged for (a) the top 20 rainfall events (historical simulation), (b) the top 36 rainfall events (future simulation), and (c) inundation frequency difference between the top 20 past and top 36 future rainfall events.

In addition to evaluating the inundation area, inundation volume, peak inundation depth, and inundation frequency, the future changes in inundation duration were also investigated for the top 20 past and top 36 future rainfall events in this study. Figure 4.14 shows the spatial distribution of the inundation duration for the top 20 past and top 36 future rainfall events as well as for the difference between them. This study focused on assessing the changes in extreme flood inundation during the short-term period (72 h). Each event from the top 20 past and top 36 future rainfall events is the annual maximum rainfall (mm/72 h) [23].

It can be seen that the longer durations of inundation were observed in the downstream area of the Chitose River basin for both historical and future simulations. The inundation in most tributaries lasts for a short duration of 0.03 to 10 h, whereas the inundation duration in the downstream area of the Chitose River basin lasts from 20 to 40 h (approximately 1–2 days) for these rainfall events. Overall, the increment of flood inundation was observed at the tributaries and floodplain areas in the Chitose River basin. The proportion of the area with an inundation duration difference of more than 0 h is 99.7% in the entire Chitose River basin, and only 0.3% of the areas will remain unchanged in terms of inundation duration in the future. The results indicate that the inundation duration is expected to increase by approximately 5–10 h in vulnerable areas in the Chitose River basin, as shown in Figure 9c. Additionally, the results reveal that the area with high inundation frequency corresponds to the long inundation duration and vice versa in this basin.

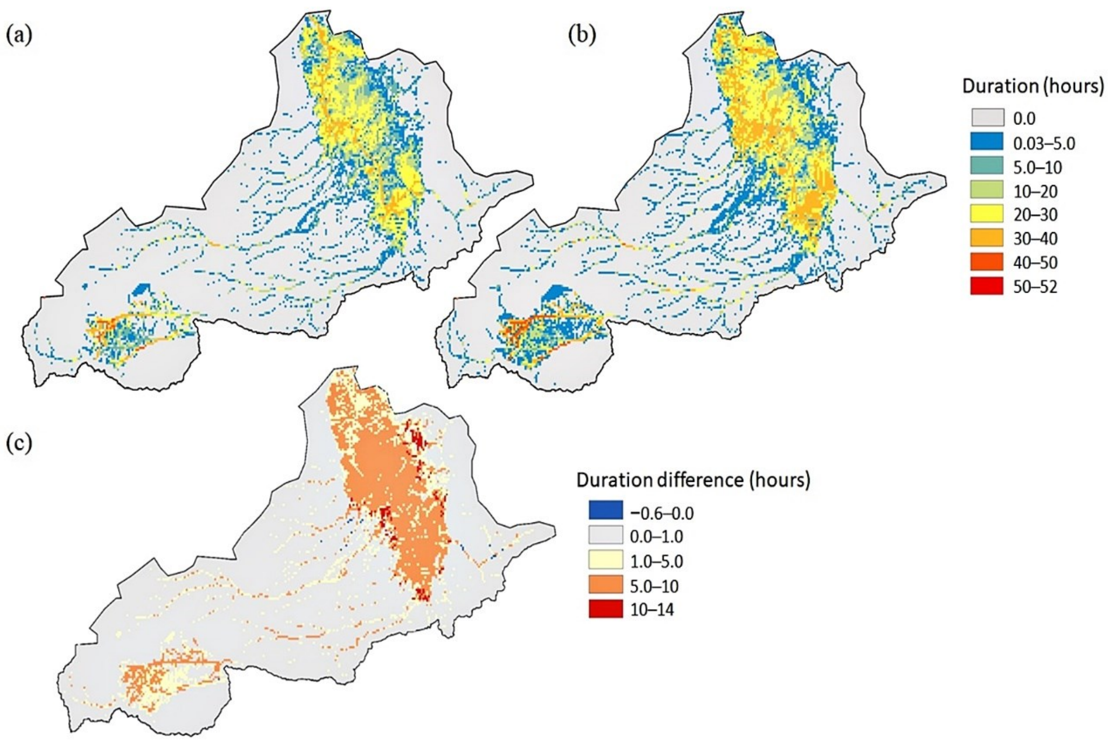

Figure 4.14. Spatial distribution of inundation durations averaged for (a) the top 20 rainfall events (historical simulation), (b) the top 36 rainfall events (future simulation), and (c) inundation duration differences between the top 20 past and top 36 future rainfall events

4.3.4. Evaluation of time difference impacts on flood inundation in the Chitose River basin

Owing to the topographical characteristics of its low-lying area, the Chitose River basin is frequently affected by backwater from the main river. The basin has experienced severe flood inundation events caused by extreme short-term rainfall events. The backwater phenomenon integrated inland flooding, which has caused serious damage in the past, was observed. When the water level increases at the confluence point, the backwater phenomenon can occur in this basin. Furthermore, flood inundation is more severe when the time difference is shorter.

Therefore, considering the dangerous impacts of the backwater phenomenon on flood inundation risk in the Chitose River basin, the differences between the time of peak discharge at the reference station in the Chitose River basin and that of peak water level at the confluence point intersecting the Ishikari River was investigated using the RRI model. Figure 4.15 shows the frequency of the time differences in the Chitose River basin for the top 20 past and top 36 future rainfall events. The results reveal that the time difference has a large range from 0 to 50 h in the future, whereas the time difference from the historical simulation has a range from 0 to 30 h in the target basin. However, it can be observed that the short time difference from 0 to 10 h is projected to significantly increase in the future. This result indicates that the flood inundation risk due to the backwater phenomenon is likely to be more severe in the future in the Chitose River basin. In addition, the results indicate that the time difference from 10 to 20 h does not change in the future, whereas the time difference from 20 to 30 h is predicted to increase remarkably in the future. These results will help policymakers enact proactive measurements to mitigate flood inundation damages in vulnerable areas in the target basin.

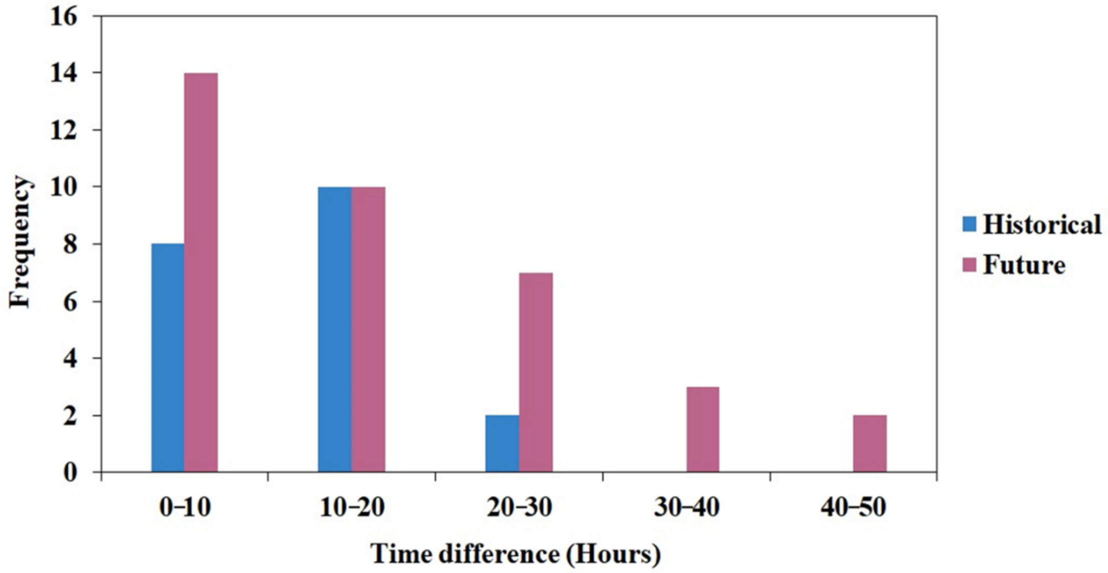

Figure 4.15. Frequency of time difference in the Chitose River basin for the top 20 rainfall events (historical simulation) and top 36 rainfall events (future simulation).

4.3.5. Discussions

This study investigated the impact of climate change on potential river flood hazards along the Ishikari River basin, and in particular flood inundation risk in the Chitose River basin, a tributary of the Ishikari River, using a large-ensemble rainfall dataset with a high resolution of 5 km d4PDF as input data to the RRI model. The RRI model performance was examined by a comparison between the simulated and observed river discharges for four large-scale flood events in the Ishikari River basin. In addition, although the flood inundation depth data were not available in the Chitose River basin, an attempt was made to reproduce the greatest historical flood event of August 1981 in this basin. In addition to appropriate river discharge simulation results, the simulated inundation results also indicated that the flood inundation area was similar to the observed inundation area for this flood event. In addition, the simulated results were close to the calculated flood inundation areas estimated by Oki et al. (2017) [50]. Therefore, this study indicated that the RRI model could provide reasonable results not only for river discharge along the Ishikari River basin but also flood inundation along the Chitose River basin.

The prediction results of future river floods from this study clearly indicated that the river discharge in the Ishikari River basin was significantly affected by climate change impacts. The extreme river flood is expected to increase significantly by 21–24% along the Ishikari River basin. This result is in close agreement with several studies conducted on the Ishikari River basin. In a result of chapter 3, the river peak discharge was evaluated in the Ishikari River basin, as well as in its main sub-basins using the IFAS model. The river peak discharge is expected to increase by 33.3% in the entire of this basin. Duan et al. (2017) [57] evaluated the impacts of climate change on the hydroclimatology of the upper Ishikari River basin using the downscaled large-scale Hadley Centre Climate Model 3 Global Circulation Model A2 and B2 scenarios data. They found out that the annual mean river discharge is predicted to increase for all three periods (2020–2039), (2050–2069), and (2080–2099), except the 2090s under the A2a scenario, and the largest increase is approximately 7.56%. However, a study by Sato et al. [29] evaluated the impacts of climate change on river discharge in several major river basins in Japan using the super high-resolution atmospheric general circulation model (AGCM) with a resolution of 20 km for the present climate (1980–1999) and future climate (2080–2099). The results showed that although the high temperature is projected to increase in the Ishikari River basin, the monthly river discharge will not change significantly.

The Chitose River basin is the main tributary located in the downstream low-lying area of Ishikari River. Hence, this river basin is considered to be a flood-prone area of the Ishikari River basin. In the past, the Chitose River basin has experienced severe flood inundation events due to short-term heavy rainfall and caused serious damage. Therefore, assessment of flood inundation risk in this basin is a crucial target for flood damage mitigation. To the best of our knowledge, there have been no studies evaluating the impacts of climate changes on flood inundation hazards in this basin area. As a result, this study can be considered a pioneering work to comprehensively assess the impacts of climate changes on flood inundation risk in the Chitose River basin. According to the simulation results, the flood inundation magnitude would be more severe in the Chitose River basin in the future compared to the historical climate simulations. The inundation magnitude is expected to increase significantly by 24.5, 46.5, and 13.8% for the inundation area, inundation volume, and peak inundation depth, respectively. In addition to the investigation changes in the inundation area, inundation volume, and peak inundation depth in this area, the inundation frequency, and inundation duration were assessed for the historical and future simulations. The results indicate that the area with the high inundation frequency corresponds to a long inundation duration and vice versa in the target basin. The downstream area of this basin with low-lying characteristics is the most flood-prone area and should be specially considered to reduce flood damages in the future.

In addition, compared to the results of chapter 3, chapter 4 is conducted to improve the predicted time difference between the time of peak discharge at the reference station in the Chitose River basin and that of peak water level at the confluence point intersecting the Ishikari River using the RRI model. The RRI model uses a 1D diffusive wave for the river channel and a 2D diffusive wave for the slope, which provides more reliable time difference results in the Chitose River basin. The result indicated that the short time difference from 0 to 10 h is predicted to increase significantly in this area. Hence, the flood inundation risk due to the backwater phenomenon is likely to be more severe in the future.

4.4. Conclusions

This chapter presents the impacts of climate change on severe river discharges along the Ishikari River basin and in particular the flood inundation in the Chitose River basin, a tributary of the Ishikari River, considering the extreme rainfall impacts and topographic vulnerability. We used a large-ensemble rainfall dataset with a high resolution of 5 km (d4PDF) as the input rainfall data for the RRI model. The following results were found:

- Extreme river flooding in the Ishikari River basin is significantly affected by climate changes. River discharge is expected to increase by 21–24% in this basin. The greatest increase was observed in the middle of the Ishikari River.
- The flood inundation is expected to be severe and higher in the Chitose River basin, with increments of 24.5, 46.5, and 13.8% for the inundation area, inundation volume, and peak inundation depth, respectively. The downstream area of this basin with low-lying characteristics is the most flood-prone area and should be specially considered for minimizing flood damages in the future. This area is also likely to experience flood inundation with a frequency of 90–100% in the future. The inundation duration is expected to increase by approximately 5–10 h. In addition, the results indicate that

the area with high inundation frequency corresponds to long inundation durations and vice versa in the Chitose River basin.

- The predicted time difference is improved in the Chitose River basin using the RRI model compared to that of the previous study. The short time difference from 0 to 10 h is predicted to increase significantly in this basin, which indicates that the flood inundation risk due to the backwater phenomenon is likely to be more severe in the future in this basin.

Overall, these results are expected to provide useful information for river basin management, particularly for climate change adaptation and flood damage mitigation in floodplain areas.

However, there still remains considerable uncertainty in this study. We focused on assessing the changes in natural flood inundation risk in the target basin considering extreme rainfall impacts and topographic vulnerability. Therefore, existing flood control facilities such as dam operations, pump stations, and retarding basins were not implemented. Furthermore, land-use activities as well as the socio-economic rapid development were not considered. The impacts of these factors should be considered along the target basin in future studies as the rapid development would cause uncertainty in the flood inundation prediction. In addition, the effectiveness of flood control facilities should also be considered for flood inundation hazards in the Ishikari River basin as well as in the Chitose River basin to obtain more reliable projections. This study was conducted to assess changes in the future flood inundation hazards using the top 20 past and top 36 future rainfall events (corresponding to return periods equal to or larger than 150 years) [23] as input rainfall data for the RRI model. Therefore, assessing the future flood inundation risk based on yearly rainfall data for 3000 historical and 5400 future climate change scenarios extracted from the d4PDF dataset would provide more reliable future projections in the target basin.

4.5. References

1. Intergovermental Panel on Climate Change (IPCC). *Climate Change 2013: The Physical Science Basis. Contribution of Working Group I to the Fifth Assessment Report of the Intergovernmental Panel on Climate Change*; Stocker, T.F., Qin, D., Plattner, G.-K., Tignor, M.M.B., Allen, S.K.; Boschung, J.; Nauels, A.; Xia, Y.; Bex, V.,Midgley, P.M., Eds.; Cambridge University Press: Cambridge, UK; New York, NY, USA, 2013; Volume 3, pp. 154–196.
2. Wu, F.; Wang, X.; Cat, Y.; Li, C. Spatiotemporal analysis of precipitation trends under climate change in the upper reach of Mekong River basin. *Quat. Int.* **2013**, *392*, 137–146. DOI:10.1016/j.quaint.2013.05.049.
3. Willems, P.; Vrac, M. Statistical precipitation downscaling for small-scale hydrological impact investigations of climate change. *J. Hydrol.* **2011**, *402*, 193–205. DOI:10.1016/j.jhydrol.2011.02.030.
4. Ongdas, N.; Akiyanova, F.; Karakulov, Y.; Muratbayeva, A.; Zinabdin, N. Application of HEC-RAS (2D) for Flood Hazard Maps Generation for Yesil (Ishim) River in Kazakhstan. *Water **2020**, 12, 2672*. DOI:10.3390/w12102672.
5. Hirabayashi, Y.; Kanae, S.; Emori, S.; Oki, T.; Kimoto, M. Global projections of changing risks of floods and droughts in a changing climate. *Hydrol. Sci. J.* **2008**, *53*, 754–772. DOI:10.1623/hysj.53.4.754.
6. Zenkoji, S.; Oda, S.; Tebakari, T.; Archevarahuprok, B. Spatial characteristics of flooded areas in the Mun and Chi River basins in Northeastern Thailand. *J. Disaster Res.* **2019**, *14*, 1337–1345. DOI:10.20965/jdr.2019.p1337.
7. Shrestha, B.; Okazumi, T.; Miyamoto, M.; Nabesaka, S.; Tanaka, S.; Sugiura, A. Fundamental analysis for flood risk management in the selected river basins of Southeast Asia. *J. Disaster Res.* **2014**, *9*, 858–869. DOI:10.20965/jdr.2014.p0858.
8. Doocy, S.; Daniels, A.; Murray, S.; Kirsch, T.D. The human impact of floods: A historical review of events 1980-2009 and systematic literature review. *PLoS Curr.* **2013**, *5*. DOI:10.1371/currents.dis.f4deb457904936b07c09daa98ee8171a.
9. Jonkman, S.N. Global perpectives on loss of human life caused by floods. *Nat. Hazards*. **2005**, *34*, 151–175. DOI:10.1007/s11069-004-8891-3.
10. Try, S.; Tanaka, S.; Tanaka, K.; Sayama, T.; Lee, G.; Oeurng, C. Assessing the effects of climate change on flood inundation in the lower Mekong Basin using high-resolution AGCM outputs. *Prog. Earth Planet. Sci.* **2020**, *7*, 34. DOI:10.1186/s40645-020-00353-z.
11. Yamamoto, K.; Sayama, T. Impact of climate change on flood inundation in a tropical river basin in Indonesia. *Prog. Earth Planet. Sci.* **2021**, *8*, 5. DOI:10.1186/s40645-020-00386-4.
12. Ashgar, M.; Ushiyama, T.; Riaz, M.; Miyamoto, M. Flood and inundation forecasting in the sparsely gauged transboundary Chenab River basin using satellite rain and

coupling meteorological and hydrological models. *J. Hydrometeorol.* **2019**, *20*, 2315–2330. DOI:10.1175/JHM-D-18-0226.1.
13. Annis, A.; Nardi, F.; Petroselli, A.; Apollonio, C.; Arcangeletti, E.; Tauro, F.; Belli, C.; Bianconi, R.; Grimaldi, S. UAV-DEMs for Small-Scale Flood Hazard Mapping. *Water.* **2020**, *12*, 1717. DOI:10.3390/w12061717.
14. Młyński, D.; Wałęga, A.; Ozga-Zielinski, B.; Ciupak, M.; Petroselli, A. New approach for determining the quantiles of maximum annual flows in ungauged catchments using the EBA4SUB model. *J. Hydrol.* **2020**, *589*, 125198. DOI:10.1016/j.jhydrol.2020.125198.
15. Grimaldi, S.; Nardi, F.; Piscopia, R.; Petroselli, A.; Apollonio, C. Continuous hydrologic modelling for design simulation in small and ungauged basins: A step forward and some tests for its practical use. *J. Hydrol.* **2020**, 125664. DOI:10.1016/j.jhydrol.2020.125664.
16. Kumar, N.; Kumar, M.; Sherring, A.; Suryavanshi, S.; Ahmad, A.; Lal, D. Applicability of HEC-RAS 2D and GFMS for flood extent mapping: A case study of Sangam area, Prayagraj, India. *Model Earth Syst. Environ.* **2020**, *6*, 397–405. DOI:10.1007/s40808-019-00687-8.
17. Yamada, T.J. Adaptation Measures for Extreme Floods Using Huge Ensemble of High-Resolution Climate Model Simulation in Japan, Summary Report on the Eleventh Meeting of the Research Dialogue. United Nations Framework Convention on Climate Change (UNFCCC), Bonn, Germany 2019, 28–29. Available online: https://unfccc.int/sites/default/files/resource/RD11SummaryReport.pdf (accessed on 8 April 2020).
18. Japan Meteorological Agency. Climate Change Monitoring Report 2017. Available online: https://www.jma.go.jp/jma/en/NMHS/ccmr/ccmr2017_high.pdf (accessed on 20 December 2020).
19. Shakti, P.; Nakatani, T.; Misumi, R. Hydrological simulation of small river basins in Northern Kyushu, Japan, during the extreme rainfall event of July 5–6, 2017. *J. Disaster Res.* **2018**, *13*, 396–409. DOI:10.20965/jdr.2018.p0396.
20. River Council for Social Infrastructure Development. Flood Risk Management for Wide-Area and Long-Lasting Rainfall–Multi-Layered Countermeasures for Complex Disasters 2018. Available online: https://www.mlit.go.jp/river/mizubousaivision/toushin_e/1812_flood_risk_management_e.pdf (accessed on 20 December 2020).
21. Japan Society of Civil Engineers (JSCE). *Onsite Field Investigation Team, Site–Investigation Report for the Hokkaido Heavy Rainfall Disasters in August 2016*; Title was translated by N. Kimura; JSCE Report; JSCE: Tokyo, Japan, 2017**.** (In Japanese).
22. Shakti, P.; Hirano, K.; Iizuka, S. Flood inundation mapping of the Hitachi region in the Kuji River basin, Japan, during the October 11–13, 2019 extreme rainfal event. *J. Disaster Res.* **2020**, *15*, 712–725. DOI:10.20965/jdr.2020.p0712.

23. Nguyen, T.T.; Nakatsugawa, M.; Yamada, T.J.; Hoshino, T. Assessing climate change impacts on extreme rainfall and severe flooding during the summer monsoon season in the Ishikari River basin, Japan. *Hydrol. Res. Lett.* **2020**, *14*, 155–161. DOI:10.3178/hrl.14.155.
24. Tachikawa, Y.; Miyawaki, K.; Tanaka, T.; Yorozu, K.; Kato, M.; Ichikawa, Y.; Kim, S. Future change analysis of extreme floods using large ensemble climate simulation data. *J. Jpn. Soc. Civ. Eng. Ser. B1 (Hydraul. Eng.)* **2017**, *73*, 77–90. DOI:10.2208/jscejhe.73.77 (In Japanese).
25. Tanaka, T.; Tachikawa, Y.; Ichikawa, Y.; Yorozu, K. Impact assessment of upstream flooding on extreme flood frequency analysis by incorporating a flood-inundation model for flood risk assessment. *J. Hydrol.* **2017**, *554*, 370–382. DOI:10.1016/j.jhydrol.2017.09.012.
26. Sakaguchi, S.; Nakayama, K.; Kobayashi, K.; Komai, K. Inundation analysis using coupling storage function model with a distributed hydrological model in Kushiro Marsh, Japan. *Hydrol. Res. Lett.* **2020**, *14*, 75–80. DOI:10.3178/hrl.14.75.
27. Bates, B.C.; Kundzewicz, Z.W.; Wu, S.; Palutikof, J.P. *Climate Change and Water*; IPCC Technical Paper IV; Intergovernmental Panel on Climate Change: Geneva, Switzerland, 2008.
28. Li, G.; Zhang, X.; Zwiers, F.; Wen, Q.H. Quantification of uncertainty in high-resolution temperature scenarios for North America. *J. Clim.* **2012**, *25*, 3373–3389. DOI:10.1175/JCLI-D-11-00217.1.
29. Sato, Y.; Kojiri, T.; Michihiro, Y.; Suzuki, Y.; Nakakita, E. Estimates of climate change impact on river discharge in Japan based on a super-high-resolution climate model. *Terr. Atmos. Ocean. Sci.* **2012**, *23*, 527–540. DOI:10.3319/TAO.2012.05.03.02(WMH).
30. Yamada, T.J.; Hoshino, T.; Masuya, S.; Uemura, F.; Yoshida, T.; Omura, N.; Yamamoto, T.; Chiba, M.; Tomura, S.; Tokioka, S.; et al. The influence of climate change on flood risk in Hokkaido. *Adv. River Eng.* **2018**, *24*, 391–396. (In Japanese).
31. Sasaki, H.; Murada, A.; Hanafusa, M.; Oh'izumi, M.; Kurihara, K. Reproducibility of present climate in a non-hydrostatic regional climate model nested within an atmosphere general circulation model. *SOLA.* **2011**, *7*, 173–176. DOI:10.2151/sola.2011-044.
32. Scharffenberg, W. *Hydrological Modeling System HEC-HMS*; User's Manual; Publication of US Army Corps of Engineers: Davis, CA, USA, 2016.
33. International Centre for Water Hazard and Risk Management (ICHARM). IFAS ver 2.0 Technical Manual 2014. Available online: http://www.icharm.pwri.go.jp/research/ifas/ifas_2.0_top.html (accessed on 20 October 2018).
34. Beven, K.J.; Lamb, R.; Quinn, P.F.; Romanowics, R.; Freer, J. Top model. In *Computer Models of Watershed Hydrology*; Singh, V.P., Ed.; Water Resources Publications: Littleton, CO, USA, 1995; pp. 627–668.

35. Arnold, J.G.; Srinivasan, R.; Muttiah, R.S.; Williams, J.R. Large area hydrologic modeling and assessment part I: Model development. *JAWRA J. Am. Water Resour. Assoc.* **1998**, *34*, 73–89. DOI:10.1111/j 1752-1688.1998.tb05961.x.
36. Brunner, G. *HEC-RAS River Analysis System: Hydraulic Reference Manual, Version 5.0.*; US Army Corps of Engineers Hydrologic Engineering Center (HEC): Davis, CA, USA, **2016**; pp. 1–538.
37. FLO-2D Software Incorporated. *FLO-2D Reference Manual*; FLO-2D Software Incorporated: Nutrioso, AZ, USA, 2009.
38. DHI. *User Manual. MIKE 21 Flow Model*; DHI: Hørsholm, Denmark, 2016; pp. 12–14.
39. Deltares. *User Manual. SOBEK. Hydrodynamics, Rainfall-Runoff and Real-Time Control, 1D/2D Modelling Suite for Integrated Water Solutions*; Deltares: Delft, The Netherlands, 2019; pp 1–3.
40. Sayama, T.; Fukami, K.; Tanaka, S.; Takeuchi, K. Rainfall-runoff-inundation analysis for flood risk assessment at the regional scale. In Proceedings of the 5th Conference of Asia Pacific Association of Hydrology and Water Resources (AHPW), Hanoi, Vietnam, 8–10 November 2010; pp. 568–576.
41. Sayama, T.; Ozama, G.; Kawakami, T.; Nabesaka, S.; Fukami, K. Rainfall-runoff-inundation analysis of the 2010 Pakistan flood in the Kabul River basin. *Hydro. Sci. J.* **2012**, *57*, 298–312. DOI:10.1080/02626667.2011.644245.
42. Sayama, T.; Tatebe, Y.; Iwami, Y.; Tanaka, S. Hydrologic sensitivity of flood runoff and inundation: 2011 Thailand floods in the Chao Phraya River basin. *Nat. Hazards Earth Syst. Sci.* **2015**, *15*, 1617–1630. DOI:10.5194/nhess-15-1617-2015.
43. San, Z.; Zin, W.; Kawasaki, A.; Acierto, R.; Oo, T. Developing flood inundation map using RRI and SOBEK models: A case study of the Bago River basin, Myanmar. *J. Disaster Res.* **2020**, *15*, 277–287. DOI:10.20965/jdr.2020.p0277.
44. Try, S.; Lee, G.; Yu, W.; Oeurng, C.; Jang, C. Large-scale flood-inundation modeling in the Mekong River basin. *J. Hydrol. Eng.* **2018**, *23*, 05018011. DOI:10.1061/(ASCE) HE.1943-5584.0001664.
45. Try, S.; Tanaka, S.; Tanaka, K.; Sayama, T.; Oeurng, C.; Uk, S.; Tanaka, K.; Hu, M.; Han, D. Comparison of various gridded precipitation datasets for rainfall-runoff and inundation modeling in the Mekong River basin. *PLoS ONE* **2020**, *15*, e0226814. DOI:10.1371/journal.pone.0226814.
46. Try, S.; Tanaka, S.; Tanaka, K.; Sayama, T.; Hu, M.; Sok, T.; Oeurng, C. Projection of extreme flood inundation in the Mekong River basin under 4 K increasing scenario using large ensemble climate data. *Hydrol. Process.* **2020**, *34*, 4350–4364. DOI:10.1002/hyp.13859.
47. Shrestha, B.; Kawasaki, A. Quantitative assessment of flood risk with evaluation of the effectiveness of dam operation for flood control: A case of the Bago River basin of Myanmar. *Int. J. Disaster Risk Reduct.* **2020**, *50*, 101707. DOI:10.1016/j.ijdrr.2020.101707.

48. Shakti, P.C.; Kamimera, H.; Misumi, R. Inundation analysis of the Oda River basin in Japan during the flood event of 6-7 July 2018 utilizing local and global hydrographic data. *Water* **2020**, *12*, 1005. DOI:10.3390/w12041005.
49. Japan River Association. The Ishikari River 2003. Available online: http://www.japanriver.or.jp/EnglishDocument/DB/file/002%20Hokkaido%2003.pdf (accessed on 20 May 2019).
50. Oki, T.; Nakatsugawa, M. A flood analysis model for rivers in low-lying areas that integrates inland water and backwater. In Proceedings of the 37th IAHR World Congress, Kuala Lumpur, Malaysia, 13–18 August 2017.
51. Hunter, N.M.; Bates, P.D.; Horritt, M.S.;Wilson, M.D. Simple spatially-distributed models for predicting flood inundation: A review. *Geomorphology* **2007**, *90*, 208–225.
52. Khaing, Z.M.; Zhang, K.; Sawano, H.; Shrestha, B.B.; Sayama, T.; Nakamura, K. Flood hazard mapping and assessment in data-scarce Nyaungdon area, Myanmar. *PLoS ONE* **2019**, *14*. DOI:10.1371/journal.pone.0224558.
53. Lehner, B.; Verdin, K.; Jarvis, A. New Global Hydrography Derived From Spaceborne Elevation Data. *Eos. Trans. Agu* **2008**, *89*, 93–94. DOI:10.1029/2008EO100001.
54. Ministry of Land, Infrastructure, Transport, and Tourism in Japan (MLIT Japan). Water Information System. Available online: http://www1.river.go.jp/ (accessed on 21 October 2020).
55. Mizuta, R.; Murata, A.; Ishii, M.; Shiogama, H.; Hibino, K.; Mori, N.; Arakawa, O.; Imada, Y.; Yoshida, K.; Aoyagi, T.; et al. Over 5000 years of ensemble future climate simulations by 60-km global and 20-km regional atmospheric models. *Bull. Am. Meteorol. Soc.* **2016**, *98*, 1383–1398. DOI:10.1175/BAMS-D-16-0099.1.
56. Taylor, K.E.; Stouffer, R.J.; Meehl, G.A. Overview of CMIP5 and the Experimental Design. *Bull. Am. Meteorol. Soc.* **2012**, *93*, 485–498.
57. Duan, W.; He, B.; Takara, K.; Luo, P.; Nover, D.; Hu, M. Impacts of climate change on the hydro-climatology of the upper Ishikari river basin, Japan. *Environ. Earth Sci.* **2017**, *76*, 490. DOI:10.1007/s12665-017-6805-4.

Chapter 5

Conclusions and Suggestions

Chapter 5

5.1. Introduction

This chapter presents the findings obtained from this study and some suggestions for further study.

5.2. Summarize of the study findings

Recently, river flooding due to short-term extreme rainfall has occurred frequently in Japan, and Hokkaido island located in the Northern part of Japan is not an exception. In recent years, Hokkaido has been continuously exposed to many typhoons and extreme rainfall caused severe floods. For example, the severe flood disaster in August 2016. Serious damage was recorded for this severe flood event in Hokkaido, Japan. These disasters are considered to be related to the impacts of climate change. Therefore, adaptation to climate change impacts, as well as minimize severe flood damage should be considered in this region. This study aims to investigate the impact of climate change in extreme rainfall, as well as severe river floodings for the Ishikari River basin, the most socioeconomically important basin in Hokkaido, Japan. In addition, the climate change impacts on severe flood inundation were assessed in the Chitose River basin, the downstream lowland area of the Ishikari River basin. This basin is considered to be the most flood-prone in the Ishikari River basin. Owing to the topographical characteristics of its low-lying area, the Chitose River basin is frequently affected by the backwater from the Ishikari River and experiences severe flood inundation. This study is conducted using the IFAS model, the RRI model, and the rainfall data with a super high resolution of 5 km as input data to these models. The remarkable point of this study is to use the large-ensemble and super high-resolution climate simulations for extreme rainfall and severe floods assessment. It could predict extreme rainfall as well as severe flood events with return periods equal to or larger than 100 years or more. In addition, simulation with large ensemble members could reduce the uncertainty in the estimation of the probability of extreme events. The following results were found:

- Following validation, the IFAS model can provide reasonable simulations of river discharges in the Ishikari River basin.
- Severe rainfall and river flooding events are expected to increase significantly in the Ishikari River basin and in its main sub-basins in the future. Additionally, the river

flooding resulting from extreme rainfall would increase to a greater extent than the increase in extreme rainfall in the Ishikari River basin and in its main sub-basins. The effect of climate change is significant in the sub-basins located in the southern part of the Ishikari River basin, where extreme rainfall is expected to increase by 29%-35%, whereas the river discharge is likely to increase drastically by 37%-56%. The difference between the time of peak discharge at the reference station and the time of peak water level at the confluence point in the main river is expected to decrease by 1.02 h to 2.14 h in these regions.

- Special attention should be paid to the Chitose River basin, as it is located in a lowland area of the Ishikari River basin that is prone to flood damage.
- Extreme river flooding in the IRB is significantly affected by climate changes. River discharge is expected to increase by 21–24% in the Ishikari River basin. The greatest increase was observed in the middle of the Ishikari River.
- The flood inundation is expected to be severe and higher in the Chitose River basin, with increments of 24.5, 46.5, and 13.8% for the inundation area, inundation volume, and peak inundation depth, respectively. The downstream area of the Chitose River basin with low-lying characteristics is the most flood-prone area and should be specially considered for minimizing flood damages in the future. This area is also likely to experience flood inundation with a frequency of 90–100% in the future. The inundation duration is expected to increase by approximately 5–10 h. In addition, the results indicate that the area with high inundation frequency corresponds to long inundation durations and vice versa in the Chitose River basin.
- The short time difference from 0 to 10 h is predicted to increase significantly in the Chitose River basin, which indicates that the flood inundation risk due to the backwater phenomenon is likely to be more severe in the future in this basin.
- Using large-ensemble and high-resolution climate simulations could reduce the uncertainty in the estimation of extreme weather events caused by climate change impacts. Therefore, this method could be applied for assessing extreme rainfall and flood inundation for other river basins, in particularly in floodplain areas in the world to mitigate flood damage.

Overall, these results are expected to provide useful information for river basin management, particularly for climate change adaptation and flood damage mitigation in floodplain areas.

However, there still remains considerable uncertainty in this study. We focused on assessing the changes in natural flood inundation risk in the target basin considering extreme rainfall impacts and topographic vulnerability. Therefore, existing flood control facilities such as dam operations, pump stations, and retarding basins were not implemented. Furthermore, land-use activities as well as the socio-economic rapid development were not considered. The impacts of these factors should be considered along the target basin in future studies as the rapid development would cause uncertainty in the flood inundation prediction. In addition, the effectiveness of flood control facilities should also be considered for flood inundation hazards in the Ishikari River basin as well as in the Chitose River basin to obtain more reliable projections. This study was conducted to assess changes in the future flood inundation hazards using the top 20 past and top 36 future rainfall events (corresponding to return periods equal to or larger than 150 years) as input rainfall data for the RRI model. Therefore, assessing the future flood inundation risk based on yearly rainfall data for 3000 historical and 5400 future climate change scenarios extracted from the d4PDF dataset would provide more reliable future projections in the target basin.

5.3. Proposing flood mitigation measures

The flood disaster control measures include the “Structural measures” and “Non-structural measures”. The structural measures such as dam, diversion channel, drainage pump. And the non-structural measures such as human activities and awareness, early flood warning system, legal regulations. This study evaluated change in extreme rainfall and severe floods considering climate change impacts for the return period equal to or higher than 150 years, high-risk disasters. The construction of structural measures like dams, diversion channels will take a long time to complete. Therefore, to minimize flood damage effectively and comprehensively in the future in the target basin, this study proposes non-structural measures combined with suitable structural measures. These measures is also suitable for other floodplain areas, especially for agricutural areas. Some of our proposals were presented as below:

Structural measures:

- Maintaining and improving the function of retarding basin, levee, and other flood control facilities to ensure its best efficiency to mitigate flood risk in the future.
- Land treatment

Hokkaido island is the largest agricultual field in Japan. Therefore, this method can be used to mitigate flood risk in the future. The agricultural areas can keep more water during the flood season. Moreover, this method could help purify water, protect the natural environment.

Besides the agricutural field, the other public works like parks, building, square, car park and road, we could develop the plant system to help more water infiltrated to soil when the flood season happens. This method is combined to urban landscape. We believe that this method will be useful and suitable not only in the target basin but also entire Hokkaido island.

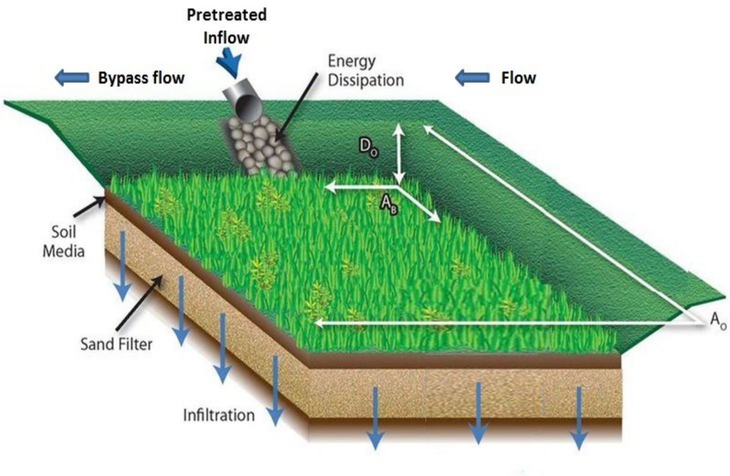

Figure 5.1. Land treatment for agricultural areas

Figure 5.2. Structural measures for mitigation flood damage in public works combined to urban landscape

- In addition, there are many available dams not only in the target basin but also entire Hokkaido. Figure 5.3 shows the available dams in Hokkaido, and in the Ishikari River basin. We believe that improving the function of dams, especially the function of flood control for all available dams is the most effective method to redure flood damage in the target basin in the future.

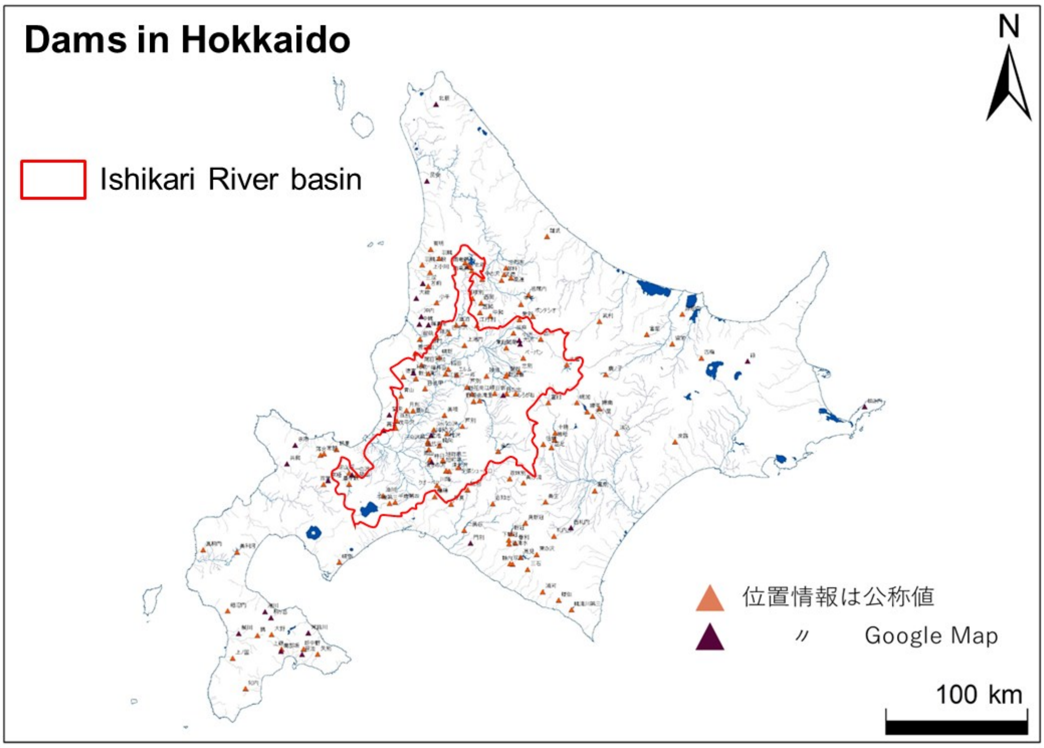

Figure 5.3. Dams in Hokkaido island

Non-structural measures:

- Raising community awareness in flood prevention.
- Based on the future prediction results, developing the early flood warning system.
- The residents located in vulnerable areas with high-risk floods need to be relocated to more safe areas.
- Developing national regulations prohibiting living in severe flood-prone areas.
- Developing national flood insurance programs.
- Promote researches on rare extreme weather events for future climate change adaptation.
- Developing flood hazard mapping.

These measures could be considered for implementation to mitigate flood damage in vulnerable areas considering climate change impacts in the future.

5.4. Suggestions for future researches

For future studies, we will evaluate the impacts of climate change on severe floods considering some aspects below to obtain reliable prediction results in the target basin.

- Change in land-use activities should be considered along the target basin in future studies as the rapid development of land-use change would cause uncertainty in the flood inundation prediction.
- The effectiveness of existing flood control facilities such as dam operations, pump stations, and retarding basins should also be considered for flood inundation hazards in the target basin to obtain more reliable projections.
- In addition, the important task is to assess the future flood inundation risk based on yearly rainfall data for 3,000 historical and 5,400 future climate change scenarios extracted from the d4PDF dataset would provide more reliable future projections in the Ishikari River basin as well as in the Chitose River basin.

Appendix

Journals

[1] Nguyen, T.T.; Nakatsugawa, M.; Yamada, T.J.; Hoshino, T. Assessing climate change impacts on extreme rainfall and severe flooding during the summer monsoon season in the Ishikari River basin. Japan. Hydrol. Res. Lett. 2020, 14, 155-161, DOI: 10.3178/hrl.14.155.

[2] Nguyen, T.T.; Nakatsugawa, M.; Yamada, T.J.; Hoshino, T. Flood inundation assessment in the low-lying river basin considering extreme rainfall impacts and topographic vulnerability. Water. 2021, 13, 896-908. DOI: 10.3390/w13070896

Proceedings and Conferences

[1] Nguyen, T.T.; Nakatsugawa, M.; Yamada, T.J.; Hoshino, T. Flood risk analysis for the Ishikari River considering rainfall patterns using downscaled d4PDF data. Proceedings of the 22nd IAHR-APD Congress 2020, Sapporo, Japan.